QUANTIFICATION OF GREENHOUSE GAS FLUXES AND DERIVATION OF MAIZE CROPPING CALENDAR IN CROPLANDS UNDER RAINFALL VARIABILITY IN KENYA

Joseph Maina Macharia
(BSc. Env. Sc., M. Env. Sc.)
C82/26405/2013

A Thesis Submitted in Fulfilment of the Requirements for the Award of the Degree of Doctor of Philosophy in Geography in the School of Humanities and Social Sciences of Kenyatta University

April 2019

DECLARATION

This thesis is my original work and has not been presented for a degree in any other university or any other award. No part of this thesis may be reproduced without prior permission from the author and /or Kenyatta University.

---------- ----------

Joseph Maina Macharia **Date**

DECLARATION BY SUPERVISORS

We confirm that the work reported in this thesis was carried out by the candidate under our supervision.

---------- ----------

Prof Chris A. Shisanya **Date**
Department of Geography
Kenyatta University

---------- ----------

Dr Felix Ngetich Kipchirchir **Date**
Department of Land and Water Management
University of Embu

DEDICATION

This work is dedicated to my lovely wife Rahab and our children: Joy, Jayden and Janice.

ACKNOWLEDGEMENTS

I thank the Australian Government for offering me a PhD fellowship through the System for Land-Based Emissions Estimation in Kenya (SLEEK) program, which was administered through the Government of Kenya's Ministry of Environment and Forestry, Clinton Foundation-Clinton Climate Initiative (CCI) and Kenyatta University. I appreciate the Consultative Group for International Agricultural Research (CGIAR), Research Program on Climate Change, Agriculture and Food Security (CCAFS) and the Climate Food and Farming (CLIFF) network for offering me a grant to support my research. I equally appreciate the Kenyan government for providing me with a research grant through the National Research Fund (NRF) to complete my research.

I sincerely thank my supervisors Prof Chris Shisanya and Dr Felix Ngetich for their support throughout my study. Your critical incites, patience and your unfailing guidance are much appreciated. I also appreciate the International Livestock Research Institute (ILRI) scientists; Dr Lutz Merbold and Dr David Pelster for their critical guidance in the field of greenhouse gases and for hosting me at Mazingira Institute-Nairobi during my lab work. I also thank Prof Daniel Mugendi, Dr Monica Mucheru-Muna and the University of Embu, for allowing me to set up my research trial alongside their on-going research project in Machang'a, Embu County, Kenya.

I appreciate my student colleagues: Anne Karanja, Milka Kiboi and Phillip Sagero, whom we walked through this journey together. Your encouragement and insistence on maintaining focus is deeply appreciated. Special thanks go to Silas Kiragu, the Machang'a site technician, for his assistance in running the field trial and in data collection. I sincerely thank ILRI technicians: Victor Lameck, George Wanyama, Paul Mutuo and Francis Njenga for their assistance during laboratory work at the Mazingira Centre. Your guidance and assistance in the laboratory made it bearable for me to carry on.

I am grateful to my family; my wife and children, my siblings and my parents. Your immense patience, support, encouragement and particularly understanding my absence in family occasions/gatherings during this period of study is well appreciated.

Completion of this work has been made possible through the support and assistance of the above mentioned individuals and institutions. You are all appreciated and may the almighty God bless you abundantly.

TABLE OF CONTENTS

LIST OF TABLES

LIST OF FIGURES

LIST OF PLATES

LIST OF ABBREVIATIONS AND ACRONYMS

ABG	-	Above Ground Biomass
AEZ	-	Agro-Ecological zones
AFOLU	-	Agriculture, Forestry and Other Land Uses
ANOVA	-	Analysis of Variance
ASALS	-	Arid and Semiarid lands
ASL	-	Above Sea Level
C	-	Carbon
CC	-	Correlation Coefficient
CH_4	-	Methane
CHIRPS	-	Climate Hazards Group InfraRed Precipitation with Stations
CHK	-	Central Highlands of Kenya
CO_2	-	Carbon dioxide
DNDC	-	DeNitrification DeComposition
DOC	-	Dissolved Organic Carbon
ECD	-	Electron Capture Detector
EF	-	Emission Factor
ETo	-	Reference Evapotranspiration [mm day^{-1}]
FAO	-	Food and Agriculture Organization
FID	-	Flame Ionisation Detector
GHG	-	Greenhouse Gases
GoK	-	Government of Kenya
GPCC	-	Global Precipitation Climatology Centre
IDW	-	Inverse Distance Weighing
IPCC	-	Intergovernmental Panel on Climate Change
IR	-	Infrared
ITCZ	-	Inter-Tropical Convergence Zones
JAXA	-	Japan Aerospace Exploration Agency
KCL	-	Potassium Chloride
KDM	-	Kenya Meteorological Department
LAI	-	Leaf Area Index
LM	-	Lower Midland
LR	-	Long Rains
MAE	-	Mean Absolute Error
MAM	-	March April May
MC	-	Moisture Content
ME	-	Mean Error
MSE	-	Mean Square Error
MV	-	Microwave
N	-	Nitrogen
N_2O	-	Nitrous oxide
NASA	-	National Aeronautics and Space Administration
NEMA	-	National Environment Management Authority
NH_3^-	-	Nitrate
NH_4^+	-	Ammonia

OND	-	October November December
PERSIANN	-	Precipitation Estimation from Remotely Sensed Information using Artificial Neural Networks
POWER	-	Prediction of Worldwide Energy Resource
RMSE	-	Root Mean Square Error
RRMSE	-	Relative Root Mean Square Error
SOC	-	Soil organic carbon
SOM	-	Soil organic matter
SR	-	Short Rain
SSA	-	Sub-Saharan Africa
TCA	-	Tropical cool arid
TCH	-	Tropical coo humid
TCSA	-	Tropical cool semi-arid
TCSH	-	Tropical cool sub-humid
TRMM	-	Tropical Rainfall Measuring Mission
TWA	-	Tropical warm arid
TWH	-	Tropical warm humid
TWSA	-	Tropical warm semi-arid
TWSH	-	Tropical warm sub-humid
UM	-	Upper Midland
UNFCCC	-	United Nations Framework Convention on Climate Change
UTM	-	Universal Transverse Mercator
WGS	-	World Geodetic System
YSE	-	Yield-scaled emission

ABSTRACT

Increase in global atmospheric greenhouse gases (GHG) has led to an increase in the radiative forcing resulting in climate variability. The objective of this study was to identify the best management practice which ensures high maize productivity while emitting as little GHG fluxes as possible under the influence of rainfall variability. The study was carried out in three major parts of Kenya, that is, Kenya as a whole, the agricultural potential zones and central highlands of Kenya. The accuracy of the satellite precipitation products was determined based on data obtained between 1983 and 2013 from Climate Hazards Group InfraRed Precipitation with Station (CHIRPS), Global Precipitation Climatology Center (GPCC), National Aeronautics and Space Administration-Prediction Of Worldwide Energy Resource (NASA-POWER) and Tropical Rainfall Measuring Mission - Multi-satellite Precipitation Analysis 3B42 version 7 (TRMM). The satellite data were compared with observed data from Kenya meteorological department. The soil GHG fluxes were quantified from maize production experiment in Mbeere South sub-county for one year using static GHG chambers. The DeNitrification-DeComposition (DNDC) model was parameterised using experimental data and used to simulate GHG fluxes. The length of the cropping season, onset and cessation date in the agricultural zones of Kenya were determined using daily satellite data from NASA-POWER between 1983-2017 using RAIN software. Results show that all satellite products either overestimated or underestimated rainfall amounts on a pixel to pixel comparison. The TRMM product best estimated rainfall in the tropical cool humid (r^2=0.64), tropical warm humid (r^2=0.58) and tropical cool sub-humid (r^2=0.39), GPCC product in the tropical warm semiarid (r^2=0.46) and tropical warm sub-humid (r^2=0.21), NASA- POWER product in tropical cool arid (r^2=0.97) and tropical cool semiarid (r^2=0.53) while CHIRPS product best estimated rainfall in the tropical warm arid (r^2=0.33). Cumulative annual GHG fluxes ranged from -0.05 to -0.65 kg CH_4-C ha^{-1} yr^{-1}, 1.31 to 3.39 Mg CO_2-C ha^{-1} yr^{-1} and 0.12 to 1.15 kg N_2O-N ha^{-1} yr^{-1} for the four different treatments respectively. Animal manure produced the highest amounts of CO_2 emissions ($P<0.001$) and N_2O fluxes ($P<0.001$) and the lowest yield-scaled emission (0.5 g N_2O–N kg^{-1} N). Animal manure + inorganic fertilisers produced the highest amounts of CH_4 fluxes ($P<0.001$) and the highest YSE (2.2 g N_2O–N kg^{-1} N). The DNDC simulated GHGs followed seasonality with peaks recorded immediately after the onset of rains which coincided with fertilisation. The DNDC simulated CO_2 was slightly higher than observed while the N_2O were slightly lower than observed though not significantly different at P=0.05. Results on cropping calendar demonstrate two key regions in Kenya, one with two seasons namely; the Long rains (LR) and Short rains (SR) and the other one with one season in a year. The LR onset is experienced in March and cessation in July; the SR onset in September and cessation in November while the one season onset in March and cessation in October. The LR and SR length of growing season ranges between 23-90 days while that of one season ranges between 192-259 days of sufficient rainfall. These results demonstrate the promising potential of the satellite data in complementing the unreliable data in Kenya. Animal manure has the ability to increase maize yields while simultaneously reducing yield-scaled GHG emissions. The DNDC model provides an accurate and cheaper alternatives for quantifying GHG for national GHG inventories and reporting to the UNFCCC. The results also derive a cropping calendar crucial for the planning of agricultural farming activities which will ultimately reduce losses and improve rainfed agricultural production.

CHAPTER ONE

INTRODUCTION

1.1 Background of the study

Climate variability has been on the rise in many parts of the world (Rezaei et al., 2015) posing a significant food security challenge to millions of people especially in the fragile rainfed agricultural systems in tropical environments (Rojas-Downing et al., 2017; Tesfaye et al., 2017). Global climate change is primarily caused by increased greenhouse gas (GHG) emissions (carbon dioxide - CO_2, Methane - CH_4 and Nitrous Oxide - N_2O) that result in warming of the atmosphere (IPCC, 2014; Oertel et al., 2016) and manifests itself through increased variation in weather, including temperature, precipitation and wind (Ali & Erenstein, 2017). The three primary GHGs (CO_2, CH_4 and N_2O) contribute about 80% of the current radiative forcing (Myhre et al., 2013).

Agriculture significantly contribute towards global greenhouse gas (GHG) emissions (Vetter et al., 2017; Sommer et al., 2018) contributing between 14 - 17% to the global anthropogenic GHG emissions (Smith et al., 2014). Separated by gas species, agriculture contributes approximately 13% towards the global CO_2 emissions majorly from land-use and land-use changes (LULUC) and about 60% of global N_2O emissions majorly from N fertilisers application (Smith et al., 2014). Net soil GHG fluxes are the result of complex soil processes involving many different biogeochemical reactions (Eugster & Merbold, 2015). Net soil CO_2 flux is an outcome of both autotrophic respirations from plant roots and associated mycorrhizal fungi and heterotrophic respirations from soil CO_2 produced through the oxidation of soil organic matter (Jovani-Sancho et al., 2017). Nitrous oxide is mainly a result of a

microbial production process in soils under oxygen (O_2) limiting environmental conditions (Butterbach-Bahl et al., 2013) and as a by-product of nitrification, an aerobic process requiring NH_4 (Bateman & Baggs, 2005). Greenhouse gas fluxes from agricultural systems may considerably differ based on the climatic conditions, soil properties and land management (Pelster et al., 2012; Masaka et al., 2014; Rosenstock et al., 2016). Therefore, accurate quantification of soil GHG fluxes from croplands is critical in determining whether a farming system is a net sink or source of GHGs (Shaojuna et al., 2011; Kirschke et al., 2013) and to arrive at valuable mitigation and adaptation measures.

In Sub-Saharan Africa, smallholder farmers face numerous risks to agricultural production; both climate and non-climate related (Harvey et al., 2014) making it difficult to eradicate poverty and achieve food security (McDowell & Hess, 2012). According to Rockström et al. (2010), more than 95% of the cropland in Sub-Saharan Africa (SSA), Kenya included, is rainfed with limited adaptive capacities (Waongo et al., 2015) making the smallholder farmers more vulnerable (Osman-Elasha, 2007). The overdependence on rainfed agriculture has led to a strong relationship between rainfall amounts, yields and food shortages (Funk et al., 2008; Campbell et al., 2016). Rainfall is a key factor influencing amounts of soil moisture, surface and groundwater thus influencing agricultural productivity (Amekudzi et al., 2015). Climate variability influences rainfed agricultural production mainly through rainfall variability (Olayide et al., 2016). Rainfall variability substantially influences food security, health, livelihood, and major socio-economic activities (Clarke et al., 2012; Priyan, 2015; Baidu et al., 2017) through regulation of available water for commercial and domestic use.

Therefore, understanding rainfall characteristics provides a platform for improving the socio-economic well-being of smallholder farmers resulting to optimal agricultural productivity (Kisaka et al., 2015). Understanding the rainfall spatial-temporal variability, in particular, can lead to improved agricultural productivity, contribute towards managing risks associated with climate variability (Montazerolghaem et al., 2016) and provide information regarding adaptation mechanisms that support food security and livelihoods (IPCC, 2014; Baidu et al., 2017). This is because the water available to crops mainly relies upon the onset, cessation and length of the growing season and which determines the failure or success of a cropping season (Ngetich et al., 2014). According to Amekudzi et al. (2015), rainfall variability inform of onset and cessation dates is a major factor influencing agricultural productivity, food security and human health in developing countries. Moreso, the cropping calendar (rainfall onset and cessation dates) ensures successful agricultural production through proper timing of agricultural activities such as land preparations, planting and harvesting is paramont (Amekudzi et al., 2015).

The rainfall onset and cessation dates are critical factors influencing changes in agricultural calendar and seasonal cycles (Boyard-Micheau et al., 2013). The existence of a link between rainfall onset and cessation, length of the season and onset and length of the season and cessation dates is very pertinent in agricultural planning (Mugalavai et al., 2008). Changing farming activity dates, particularly the planting date, due to climate variability has been reported in adaptation studies as a key way in maximising agricultural returns (Yegbemey et al., 2014). Therefore, derivation of a cropping calendar (prediction of length of the cropping season, onset and cessation dates) would go a long way in maximising returns from rainfed agriculture

(Byakatonda et al., 2018) as it would equip farmers in better managing risks associated with climate variability (MacLeod, 2018).

However, in Kenya, like many agricultural regions of the world, high quality measured weather data (MWD) are not available due to the sparse rain gauge coverage (Dinku et al., 2011; Satgé et al., 2016; Mourtzinis et al., 2017) and due to most weather stations having a short lifespan in recording historical data (Zambrano et al., 2017). In situ-based rainfall data has previously been used in determining the historical understanding of spatial-temporal rainfall variability and the amounts, but information on the length of recording, numbers of stations and their geographical distribution has generally been missing in many countries (Ouatiki et al., 2017; Zambrano et al., 2017). According to Satgé et al. (2016), the process of data collection and digitising introduces possible errors in the datasets. Therefore, the Kenyan MWD like in many other countries may be unreliable for use in agricultural applications (Mourtzinis et al., 2017) consequently the need for evaluating alternative sources of reliable spatial-temporal rainfall data.

To complement the weather data from the sparsely distributed rainfall stations, information about rain parameters may be obtained from satellite sensors (Ioannidou et al., 2016; Satgé et al., 2016). Satellite datasets have increasingly become essential in filling the spatial-temporal data gaps for climate-based studies in areas where measured weather data are missing (As-syakur et al., 2016; Shrestha et al., 2017; Zambrano et al., 2017; Bai et al., 2018). Satellite-based precipitation products have advantages over ground-based observations in terms of spatial and temporal resolution and areal coverage, providing a potential alternative data source for data-sparse or ungauged areas (Li et al., 2010; Meng et al., 2014). Satellite estimates are

however limited since none of the satellites' sensors predicts rainfall directly but uses one or several proxy variables to predict the relationship between observations and precipitation (Toté et al., 2015). Algorithms to estimate rainfall from satellite observations are based either on thermal infrared (TIR) bands (from which cloud-top temperature can be inferred) or on passive microwave (PMW) sensors (Paredes Trejo et al., 2016). Satellite recording of precipitation is one of the impending ways in attainig spatial-temporal data over a large area (As-syakur et al., 2016). There exists several global remotely sensed datasets (Funk et al., 2015), some which have historical recordings of over 18 years while others have long-term recording of over 30 years and which have provided reliable precipitation in several parts of the globe (Zambrano et al., 2017). This calls for evaluation of their accuracy in predicting precipitation for improved agricultural advisory services and other applications in Kenya.

Biogeochemical models are very resourceful tools for improving agricultural advisory services and management (Yu et al., 2014; Guest et al., 2017). They are tools with a capacity to evaluate the responses of crops towards changing environmental conditions and farm management practices (Lenz-Wiedemann et al., 2012). Process-based models have been used to predict crop yields and explain the influences of environmental changes at the farm, regional, national and global scales (Rui et al., 2017). Modelling provides an in depth analysis of Nitrogen (N) and Carbon (C) dynamics (Lenz-Wiedemann et al., 2012). Crop growth models simulate biomass yields based on three situations: (1) potential growth, (2) water-limited growth and (3) actual growth (Rui et al., 2017). According to Yu et al. (2014), crop models predict crop yields based on the crop physiological processes during crop growth. These

models provide information from complex biogeochemical systems at a broad spatial-temporal spectrum where it would otherwise be very costly and impractical to acquire data from (Gaillard et al., 2017). There is therefore the need to evaluate the accuracy of DeNitrification DeComposition (DNDC) model, which is cheap and popularly used, in simulating GHG from different management inputs in the maize fields under ASAL conditions in Kenya.

According to FAO (2009), Maize (*Zea mays L.)* ranks second, after wheat, in the order of importance among the world cereal crops. It is one of the most fundamental source of food and cash crops for both commercial purposes and subsistence in many rural families in Africa (Midega et al., 2018). In SSA, and more so in East Africa, maize is the most important food and cash crop for millions of rural households (Adamtey et al., 2016; Midega et al., 2016) and is the primary staple food in Kenya (Schroeder et al., 2013).

1.2 Statement of the problem and justification

Agricultural productivity from the smallholder farming systems in Kenya has been on the decline resulting in low yields, increased hunger and poverty due to increased food insecurity. To counter these impacts, several soil fertility interventions have been developed, tested and widely adopted resulting in both improved soil fertility and overall soil health as well as crop yields. However, their contribution towards the national GHG budget largely remains unknown, thus leaving a significant data gap on GHG inventories to be filled. Direct measurements of GHG for national inventories are impractical and very expensive to establish since it would require establishment of several experiments spread across the country for a long period of time. To overcome these challenges, process-based models have been developed, validated and

found reliable to provide supplementary information on large spatial-temporal scales from areas with which it would have been too costly and impractical to acquire. However, the accuracy of these process-based models in simulating GHG in Kenya largely remains unknown. Rainfall variability has been on the rise, immensely contributing towards the current status of food insecurity. However, reliable measured weather data (MWD) is generally lacking, particularly precipitation, due to the sparse rain gauge distribution in Kenya. To complement the lack of reliable precipitation data, several satellite products have been developed and evaluated in various parts of the world. However, very few studies have attempted to assess the accuracy of these satellite precipitation products with independent measurements, as an alternative source of rainfall data in Kenya. Similarly, a few studies in Kenya have attempted to determine the cropping calendar based on rainfall onset, cessation and length of growing season, as a result of rainfall variability and thus remaining mostly unknown. This study, therefore, sought to assess the accuracy of long-term satellite precipitation products, quantify GHG fluxes from different soil fertility interventions, evaluate the accuracy of DNDC model in simulating soil GHG fluxes and derive a cropping calendar over the agricultural potential zones of Kenya.

1.3 Research questions

The study sought to answer the following questions;

i) How accurate are the long-term satellite-derived precipitation products compared to observed data over Kenya for a period between 1998 and 2013?

ii) How much soil GHG (CO_2, CH_4 and N_2O) fluxes are produced or sequestered under different crop management practices in a maize field in the semiarid lands of central highlands of Kenya?

iii) How accurate is the DNDC model in simulating field measured soil GHG fluxes across different management practices in a maize field in the semiarid lands of central highlands of Kenya?

iv) What is the mean length of growing season, rainfall onset and cessation dates for Kenya's agricultural potential zones?

1.4 General objective of the study

To identify the best management practice which ensures high productivity of maize while emitting as little GHG fluxes as possible under the influence of rainfall variability

1.4.1 Specific objectives of the study

To achieve the broad objective, the study was guided by the following specific objectives:

i) To evaluate the accuracy of long-term satellite-derived precipitation products compared to observed data over Kenya for a period between 1998 and 2013.

ii) To quantify the soil GHG fluxes under different crop management practices in a maize field in the semiarid lands of central highlands of Kenya.

iii) To evaluate the ability of DNDC model to simulate field measured greenhouse gas fluxes under different management practices in a maize field in the semiarid lands of central highlands of Kenya.

iv) To derive the mean length of growing season, rainfall onset and cessation dates in the agricultural potential zones of Kenya.

1.5 Study hypotheses

The following hypotheses guided the study:

i) The long-term satellite-derived precipitation is inaccurately compared to observed rainfall for a period between 1998 and 2013.
ii) Animal manure emits highest amounts of CO_2, animal manure combined with inorganic fertilisers emits the highest amounts of N_2O while inorganic fertilisers have the highest uptake of CH_4 fluxes.
iii) The DNDC model doesn't accurately simulate soil GHG fluxes across different management practices in the semi-arid parts of central highlands of Kenya.

1.6 Significance of the study

The findings of this study provides details on the soil fertility treatment that produces the highest yields and lowest emissions as well as various emission factors based on individual soil fertility technologies. These findings fills in the gap on greenhouse gases from selected soil fertility inputs from maize files in the semiarid lands of central highlands of Kenya. These findings contributes to the development of a System for Land-Based Emissions Estimation in Kenya (SLEEK), a Tier III system which will enable the Kenyan government to accurately track and report GHG fluxes from the agricultural land sector. Besides supporting the SLEEK, this study will play a role in the smallholder farming systems as a decision support tool for subsistence farmers as they make decisions on when to prepare the land, mobilise inputs, equipment. The use of the derived cropping calendar as a decision support tool will likely reduce the hazards associated with too late or too early planting. This will ultimately minimise risks related to climate change/variability and hence improve agricultural production.

1.7 Operational definition of key terms as used in this thesis

Accuracy - the degree of measure of the extent to which the simulated data agrees or disagrees with the observed data

Climate variability - yearly climate fluctuations above or below a long-term average value

Cropping calendar - This is an agricultural decision support tool which describes in details the onset, cessation and length of growing season

Derivation - This is the identification/ determination of the rainfall onset, cessation and length of growing season

Greenhouse fluxes - it's the total emissions comprising of production (emission) and consumption (sequestration)

Modelling - all the activities aimed at making a particular part or feature of the world or system easier to understand, define, quantify, visualise, or simulate by referencing it to existing and usually commonly accepted knowledge

GHG quantification - The process in which the three GHG (CO_2, CH_4 and N_2O) are measured from the soil over a period of 1 year comprising of two seasons

Radiative forcing - the capacity of a gas to influence the energy balance in the atmosphere

CHAPTER TWO

LITERATURE REVIEW

2.1 Overview

This chapter highlights the key aspects related to climate variability, and their impacts on agricultural production. More specifically, the chapter presents review of the literature in comprehensive consideration of the major factors that relate to rainfall variability, inadequacies of rainfall data and long term-satellite precipitation products as an alternative source of rainfall data in Kenya. It also deals with the quantification of soil greenhouse gas fluxes (GHG) as well as biogeochemical simulation of soil GHGs as an alternative approach. This chapter also addresses the application of satellite products in deriving the cropping calendar based on the length of cropping season, onset and cessation dates in the agricultural potential zones of Kenya. The chapter also provides a summary of the research gaps addressed in this study and the conceptual framework.

2.2 Climate variability and agricultural production

Climate variability has adverse effects on agricultural productivity (Dourte et al., 2015; Mugi-Ngenga et al., 2016). African smallholder farmers have been termed as among those key individuals adversely affected by climate variability (IPCC, 2007) and have been considered to have low knowledge on adaptation towards climate variability. Climate variability influences agriculture by aggravating the frequency and distribution of weather conditions, reducing water supplies hence limiting irrigation and exacerbating soil erosion (IPCC, 2007). Recent trends in abrupt weather changes continue to pose a challenge to agricultural production in SSA, where smallholder farmers are consistently vulnerable, making them more socio-

economically miserable (Kolawole et al., 2014). Considering a "business as usual" scenario, agricultural productivity would decline at a rate of between 10 to 25 percent by year 2080, whereby some countries would experience an estimated 50 percent decrease in agricultural productivity (IFAD, 2008). Climate change and climate variability have been viewed as one of the leading environmental problems of the 21st century (Reidsma et al., 2010).

2.3 Long-term satellite-derived precipitation products for improved agricultural advisory services

Rainfall is a crucial driver of many economic activities including agriculture, transport, health, industry and tourism, directly influencing socio-economic capacities of majority of the populations that directly depend on rain-fed agriculture. Rainfall also plays a crucial role in climatology and particularly in climate change and variability related studies as one of the vital climatic variables that affect both the spatial and temporal patterns of water availability (Hossain et al., 2014; Taxak et al., 2014; Satgé et al., 2016; Sharma & Singh, 2017; Wan et al., 2017; Zambrano et al., 2017). To achieve all these applications, accurate rainfall estimation is paramount globally (Sungmin et al., 2016). However, in Kenya like many other regions of Sub-Saharan Africa, there is general lack of reliable data due to the scarcity of weather stations and where available are mostly located in the urban centres with short incomplete historical records (Dinku et al., 2011; Satgé et al., 2016; Mourtzinis et al., 2017). To complement this scarcity of reliable observed rainfall data, satellite products have become increasingly utilised to fill in the data gaps for climate-related applications (Zambrano et al., 2017).

According to Duan et al. (2016), several gridded precipitation products have been generated and made available at different spatial-temporal resolutions, at quasi-global

or global scale. They have broadly been categorised into four classes. The first category being the gauge-only products which are based on observations from rain gauge stations only, based on different interpolation methods. They have widely been used for various applications including the Global Precipitation Climatology Centre (GPCC) monthly precipitation product (Schneider et al., 2014), the Climate Prediction Center (CPC) unified gauge-based analysis of global daily precipitation (Chen et al., 2008) and the Climatic Research Unit (CRU) monthly precipitation (Harris et al., 2014). These products are available at a coarser spatial resolution than 0.5° x 0.5° (Duan et al., 2016). The second category of precipitation products uses atmospheric models that combine satellite and in-situ observations of various atmospheric properties as inputs. These products include National Centers for Environmental Prediction-National Center for Atmospheric Research (NCEP–NCAR) (Kalnay et al., 1996) and European Centre for Medium-Range Weather Forecasts (ECMWF) (Balsamo et al., 2015).

The third category of precipitation product uses satellite-only products based either on the infrared (IR) information frequently measured from geostationary satellites, the microwave (MV) information less frequently measured from low earth orbiting satellites, or a combination of IR and MV information (Duan et al., 2016). The fourth category of precipitation products are the satellite-gauge products that combine two individual (gauge-only and satellite-only) products through different bias correction or blending procedures. They include TRMM (Tropical Rainfall Measuring Mission) multi-satellite precipitation analysis (TMPA) (Huffman et al., 2007), the CMORPH (CPC MORPhing technique) (Joyce et al., 2004), PERSIANN (Precipitation Estimation from Remotely Sensed Information using Artificial Neural Networks)

(Hsu et al., 1997) available at a spatial resolution of 0.25° or finer and the recently released “satellite-gauge” type CHIRPS product (Climate Hazards Group InfraRed Precipitation with Station data) provides precipitation at the finest spatial resolution of 0.05° (Funk et al., 2015).

These precipitation products have been evaluated for their accuracy at a global or quasi-global level (Yong et al., 2015; Sun et al., 2017); at continental level (Africa (Awange et al., 2016), South America (Salio et al., 2015), Maritime Continent (As-syakur et al., 2016), Tropical South American and African Continents (Negrón Juárez et al., 2009)); at country level (Bolivia (Blacutt et al., 2015), Brazil (Nogueira et al., 2018), Chile (Zambrano et al., 2017), China (Chen et al., 2014; Bai et al., 2018; Zhao et al., 2018), Colombia (Dinku et al., 2010), Cyprus (Katsanos et al., 2016), Ghana (Baidu et al., 2017), Greece (Nastos et al., 2015), Ethiopia (Duan & Bastiaanssen, 2013), India (Sunilkumar et al., 2015; Prakash et al., 2016), USA (Tian et al., 2007; Mourtzinis et al., 2017), Iran (Katiraie-Boroujerdy et al., 2013; Moazami et al., 2016), Malaysia (Tan et al., 2015), Morocco (Ouatiki et al., 2017), Mozambique (Toté et al., 2015); Nepal (Krakauer et al., 2015; Shrestha et al., 2017) and Saudi Arabia (Tippett et al., 2015)); at basin level (Southern Amazon-Brazil (Zulkafli et al., 2014; Arvor et al., 2017), Santo Antônio county (Goiás, Brazil) (Quirino et al., 2017), slopes of the subtropical Andes (Hobouchian et al., 2017), Pacific–Andean region of Ecuador and Peru (Ochoa et al., 2014), Upper Blue Nile Basin-Ethiopia (Rientjes et al., 2012; Tesfaye et al., 2017), Ganzi River Basin of the Tibetan Plateau (Alazzy et al., 2017), Island of Sicilia in southern Italy (Conti et al., 2014), part of East Africa (Shukla et al., 2014) and Mekong River basin in China (He et al., 2017)).

Based on previous evaluations of accuracy on the available satellite precipitation products, it is evident that the available products have global (or quasi-global) alignment, and their performance vary from one region to another and from one product to the other. Therefore, evaluating the accuracy of these data with reliable measured weather data before use is of inevitable importance (Duan et al., 2016). Hence, the need to evaluate the accuracy of four selected monthly long-term satellite-based precipitation products, compared to observed data over Kenya for a period between 1998 and 2013, as a potential alternative source of weather variable/indicator for agricultural advisory.

2.4 Greenhouse gas (GHG) fluxes

Previous research in Sub-Saharan Africa (SSA) has demonstrated that soil fertility decline is a major challenge affecting agricultural productivity and environmental welfares (Place et al., 2003; Mugwe et al., 2009; Mucheru-Muna et al., 2014). As a result, several soil fertility management interventions have been developed and found to have a significant capacity to improve both soil fertility and crop yields (Vanlauwe et al., 2014). In the central highlands of Kenya (CHK), like other livestock-arable farming systems in SSA, animal manure is one of the most widely used inputs being used by approximately 80% of households (Macharia et al., 2014). Use of inorganic fertilisers to replenish soil nutrients is a significant way of counterbalancing the low soil fertility, though the nutrients applied in mineral fertilisers by the smallholder farmers in CHK although they remain relatively low due to high costs of fertilisers (Mugwe et al., 2009). The integration of mineral fertilisers with organics has also been identified to improve the agronomic efficiency of the external inputs used, reduce the risks of acidification and provide a more balanced supply of nutrients (Mugwe et al.,

2009). However, none of the studies conducted in the CHK has quantified soil GHG fluxes from the various soil fertility management practices from maize production.

Due to a lack of observational data from typical farming systems in sub-Saharan Africa (SSA), in particular from smallholder systems (Pelster et al., 2017), a complete and accurate inventory of GHG fluxes is not available for the region (Valentini et al., 2014). According to Valentini et al. (2014), the available information on GHG emissions from SSA is limited, unreliable and fails to underscore whether the African continent acts as a GHG source or a sink. Notably, the limitation in data availability on GHG emissions from African agricultural soils hinders the understanding of continental GHG emissions (Ciais et al., 2011; Hickman et al., 2014) and leaves a significant data gap that needs to be addressed (Pelster et al., 2017). Also, the lack of data makes it impossible for developing countries like Kenya to accurately assess and report to the UNFCCC the current GHG emissions from the agriculture, forestry and other land use (AFOLU) sector (Pelster et al., 2017).

Kenya has compiled and reported to UNFCCC the national circumstances and responses to climate change in its Second National Communication (NEMA, 2015). From this report, agriculture is the most significant contributing sector (41%) towards Kenyan GHG emission with an annual increase rate of 2.2%. Regarding individual GHG, CO_2 was the highest contributor (52%) towards Kenya's GHG inventory and majorly from land use changes. These estimates were calculated based on the default IPCC Tier 1 emission factors (EFs) rather than measured GHG emissions (NEMA, 2015). According to Richards et al. (2016), the 'GHG calculators' used in Tier 1estimations tend to over-estimate GHG emissions in tropical developing countries. This translates to inflated national GHG inventories that may result in incorrect

targeting and inefficient mitigation measures (Pelster et al., 2017). Therefore, there is a need to establish further empirical studies to provide country-specific EFs which will improve the accuracy in the assessment and reporting of emissions from agricultural soils.

2.5 Biogeochemical DeNitrification-DeComposition (DNDC) modelling

Greenhouse gases are primarily the cause of global climate change that results in warming in the atmosphere (IPCC, 2014). Greenhouse gas (GHG) concentrations have significantly increased leading to an increase in average global surface temperatures (IPCC, 2014; Oertel et al., 2016). The current increase in atmospheric GHG and the consequent global warming can be offset not only by lowering anthropogenic GHG emissions but also through ways of sequestering GHG emissions over extended time periods (Martinez et al., 2016). Croplands have been pointed out as a potential part of the ecosystem which has the capacity to sequester the GHG emissions through various biological processes such as photosynthesis (Nyćkowiak et al., 2018) thus indirectly reducing GHG emission from the atmosphere (Venhari et al., 2017). Croplands functions as GHG sinks depending on soil types, weather conditions, crop species and farm management practices (Chi et al., 2016). However, understanding the amounts GHG fluxes from crop lands remains a major challenge.

Direct measurements of greenhouse gases and biomass (through destructive sampling) for national inventories are impractical and very expensive to establish (Giltrap et al., 2010). Therefore, most countries and mainly developing countries cannot afford to establish these empirical studies and hence rely heavily on the IPCC default emission factors (EF) which were determined from a limited number of studies assuming uniformity in the soil types, environmental conditions and management

practices. However, process-based models have been developed, validated and found capable of providing information at large spatial-temporal location. More so, the development of a process-based model not only provides information at site, regional, national and global levels but also provides an avenue for exploration of potential mitigation strategies (Giltrap et al., 2010).

In this study, DeNitrification-DeComposition (DNDC) model which is one of the prominent biogeochemical models for studying GHG emissions was used. The model has been developed to simulate the biogeochemical processes such as hydrogen, carbon, phosphorus, nitrogen, oxygen and cycles in agroecosystems (Yu et al., 2014). The DNDC model has been adopted worldwide in the last three decades to study crop biomass and yields from a variety of major crops, such as rice, maize and wheat, under a broad spectrum of farm management activities (Zhang et al., 2002; Kröbel et al., 2011; Sansoulet et al., 2014; Zhang et al., 2015; Dutta et al., 2017; Rui et al., 2017; Jarecki et al., 2018; Zhang et al., 2018). The DNDC model has also been used to predict soil GHG fluxes (Wang et al., 2011; Chen et al., 2015; Uzoma et al., 2015; Deng et al., 2016; Li et al., 2017) under different cop management. There is, however, no literature which demonstrates the use of the DNDC model in the simulation of GHG from Kenya and East Africa at large. Therefore, this study could be the first attempt to use the DNDC model for simulating GHG fluxes in Kenya for improved accuracy in the national GHG inventories. As such, there is need to assess the ability of DNDC model to simulate field measured GHG fluxes (CO_2 and N_2O) across various management practices in the semiarid parts of central highlands of Kenya.

2.6 Agricultural cropping calendar

An agricultural cropping calendar is a crucial tool that provide timely information on cropping activities including land preparation, planting and harvesting periods. It contains information on the production of locally adapted crops in specific agro-ecological zones (FAO, 2010). Crop calendar heavily relies on environmental conditions including rainfall, solar radiation and temperature, since these factors regulate plant growth (Oyoshi et al., 2013). Alterations of farming activities including land preparation and planting dates have been reported in the adaptation studies (Nhemachena & Hassan. 2007; Yegbemey et al., 2013). These changes in cropping activities have been adopted and viewed as a critical strategy in adapting towards climate variability. Since the cropping activities in a season are dependent upon planting dates, farmers tend to adjust the cropping calendar either forward or backward depending on previous cropping calendar (Yegbemey et al., 2014). The farming calendar changes are about varying dates of various cropping activities in a cropping season (Yegbemey et al., 2013). Although changing planting dates are crucial in the management of the cropping calendar in the SSA, information on these farming activity dates is generally missing and so is the cropping calendar (Sari et al., 2013; Waongo et al., 2015).

To minimise the adverse impacts of climate variability on agriculture, adaptation is considered one of the alternative approaches (Kassie et al., 2013; Khatri-Chhetri et al., 2017; Bieber et al., 2018) towards achieving food security. Shifting agricultural cropping calendar; particularly sowing dates and length of growing season has been documented as a critical way of adapting to changing weather conditions (Rötter et al., 2011; Teixeira et al., 2011; Kassie et al., 2013; Shiferaw et al., 2014; Yegbemey

et al., 2014). As other studies have reported, selection and adjustment of cropping calendars has been the key to successful production in hot regions where short duration cultivars have facilitated a change of cropping calendars (Wassmann et al., 2009). According to Njenga et al. (2014), in a study on adaptation mechanisms, shifting of planting seasons was the most adopted measure by small-scale farmers in North Kinangop, Kenya, though the least effective measure since it is usually based on previous year's weather events and indigenous knowledge. The scarcity of planting date information in many regions over SSA can partly be explained by the fact that farmers use indigenous knowledge, mainly non-climatic reasons for sowing (Waongo et al., 2015). This has led to farmers miscalculating the seasons resulting in loss of sowed seeds due to delayed onset of rains or washout by high-intensity rains (Njenga et al., 2014). Due to farmers' lack of capacity as well as high onset of rainy season variability in SSA, advances to better approximate the onset of growing season for planting crops might be valuable options as crop management strategies (Waongo et al., 2015). This, in turn, affects the germination and following phenological stages of crop development (Njenga et al., 2014).

Typical sowing dates differ depending on region of the country, and actual sowing dates vary inter-annually with occurrence of rains (Gourdji et al., 2015). In Kenya, where agriculture is majorly rainfed, climate variability is exacerbated by an unspecified cropping calendar (Mulianga et al., 2013). A study by Mugalavai et al. (2008) analysed onset and cessation of rainfall in Kenya and linked their variation to atmospheric, oceanic and local conditions (topography, water bodies, winds, vegetation cover). Previous studies have also investigated within-season dry spell and their impact on planting dates and crop yields (Mzezewa et al., 2010). The main

findings of these studies include variations in dates of onset, a small proportion of rainy days supplying a high percentage of rainfall and occurrence of dry spells that disrupt crop development and lower yield in SSA (Recha et al., 2012). Since rainfall in SSA is mostly seasonal, it is therefore vital that a meaningful analysis of the impact of rains on crop yield be based on seasonal and not annual rainfall (Recha et al., 2012). According to Yegbemey et al. (2013), seasons and agro-ecological zone are shifting as a result of climate change though there is no investigation on how the farmers are adjusting the whole cropping calendar as an adaptive measure to climate variability.

However, as much as the length of the growing season, rainfall onset and cessation dates have previously been determined in some parts of Kenya (Mugalavai et al., 2008; Recha et al., 2012; Ngetich et al., 2014; Kisaka et al., 2015; Dunning et al., 2016; MacLeod, 2018), there is general lack of robust information to guide progression of the Kenyan agricultural calendar towards climate variability adaptation. Therefore, this study envisaged to establish and determine the length of growing season, rainfall onset and cessation dates in the agricultural potential zones of Kenya, as a guide to inform smallholder farmers' agricultural crops, calendar and a precursor to climate variability adaptation.

2.7 Research Gaps

From the literature reviewed,

1. It was noted that in Kenya there is a general lack of reliable rainfall data, besides the poor distribution network of rainfall stations. This is because the weather stations are mostly located in urban centres leaving most of the agricultural parts uncovered, have inconsistent and short historical records and whose recording is manual which introduces errors in the available data. This

calls for an alternative source of rainfall data for agricultural advisory and weather-related studies. As such, satellite products come in handy to provide long-term spatial-temporal data over Kenya. However, these products need validation with observed rainfall data before they are used.

2. The impacts of climate change and variability have been felt across the country with detrimental effects especially on agriculture which is mainly rainfed. The cause of this escalating climate variability has been attributed to an increase in GHG (CH_4, CO_2 and N_2O) emissions to the atmosphere and which anthropogenic activities have a significant contribution. However, the current Kenyan status on the national GHG inventories as reported to the UNFCCC has been based on IPCC default emission factors (Tier 1) and which overestimates the emissions thus introducing an error in the choice of adaptation and mitigation measures. This calls for more empirical studies which would produce site-specific or region-specific EFs and which would reduce the uncertainties in the national GHG inventories.
3. Similarly, conducting empirical studies across the country for generating country-specific EFs could be very expensive to establish for a developing country like Kenya. However, process-based biogeochemical models have been developed and validated with observed data in various parts of the world and which have been found to correctly simulate GHG based on multiple soil fertility management practices. In Kenya, however, only a few studies have been established to determine the accuracy of the GHG models for use in simulating EFs for national GHG inventories. There is, therefore, need to parameterise, validate and simulate GHG emissions using DNDC model that

has not been used in East Africa, one of the most prominent models in the field of GHG simulation, in comparison with observed GHG data.

4. Climate variability affects agricultural production mostly through alteration of weather patterns and mainly through rainfall variability. As a result, smallholder farmers need to adapt to the changing weather patterns. Agricultural cropping calendar is a very relevant tool for farmers since it guides all the farming activities including land preparations, sowing and harvesting. However, the current status on the cropping calendar for the agricultural potential zones of Kenya is not clear and generally unavailable, and therefore there is a need to derive it. As such, this study strived to determine the length of the growing season, rainfall onset and cessation based on long-term satellite precipitation products between 1983 and 2017.

2.8 Conceptual framework

Increase in atmospheric GHGs from various sources, including agricultural production, leads to an increase in radiative forcing which in turn bring about climate change and variability. Climate variability have a direct negative impact on agricultural production resulting in increased food insecurity and its associated problems of hunger and poverty. Adaptation to climate change is imperative in ensuring survival of smallholder farmers who primarily depend on rainfed agricultural production. To adapt to climate change and variability, several steps must come into place, as proposed in this study (Figure 2.1). The first step is to determine the accuracy of the long-term satellite precipitation products (Objective 1). This ensures that the freely available satellite products which cover more considerable spatial-temporal extent are validated for use as an alternative source of rainfall data for understanding

rainfall variability, an essential element influencing agricultural production. Secondly, to reduce the amounts of GHGs in the atmosphere and understand the contribution of soil fertility amendments towards national GHG inventories, and the treatment which produces high yields and low GHG emissions simultaneously, quantification of GHG fluxes from different soil fertility technologies is established (Objective 2). This is followed by the third step of utilising the data from observed soil fertility technologies to validate, parameterise and simulate GHG emissions using DNDC model, which is a cheaper way of obtaining data for a larger area relevant to the national GHG inventories (Objective 3). Lastly, (step 4) to understand current status of agricultural calendar for the agricultural potential zones of Kenya, the length of growing season, rainfall onset and cessation were derived (Objective 4). This provided mean dates of agricultural activities based on long-term satellite observations (Figure 2.1).

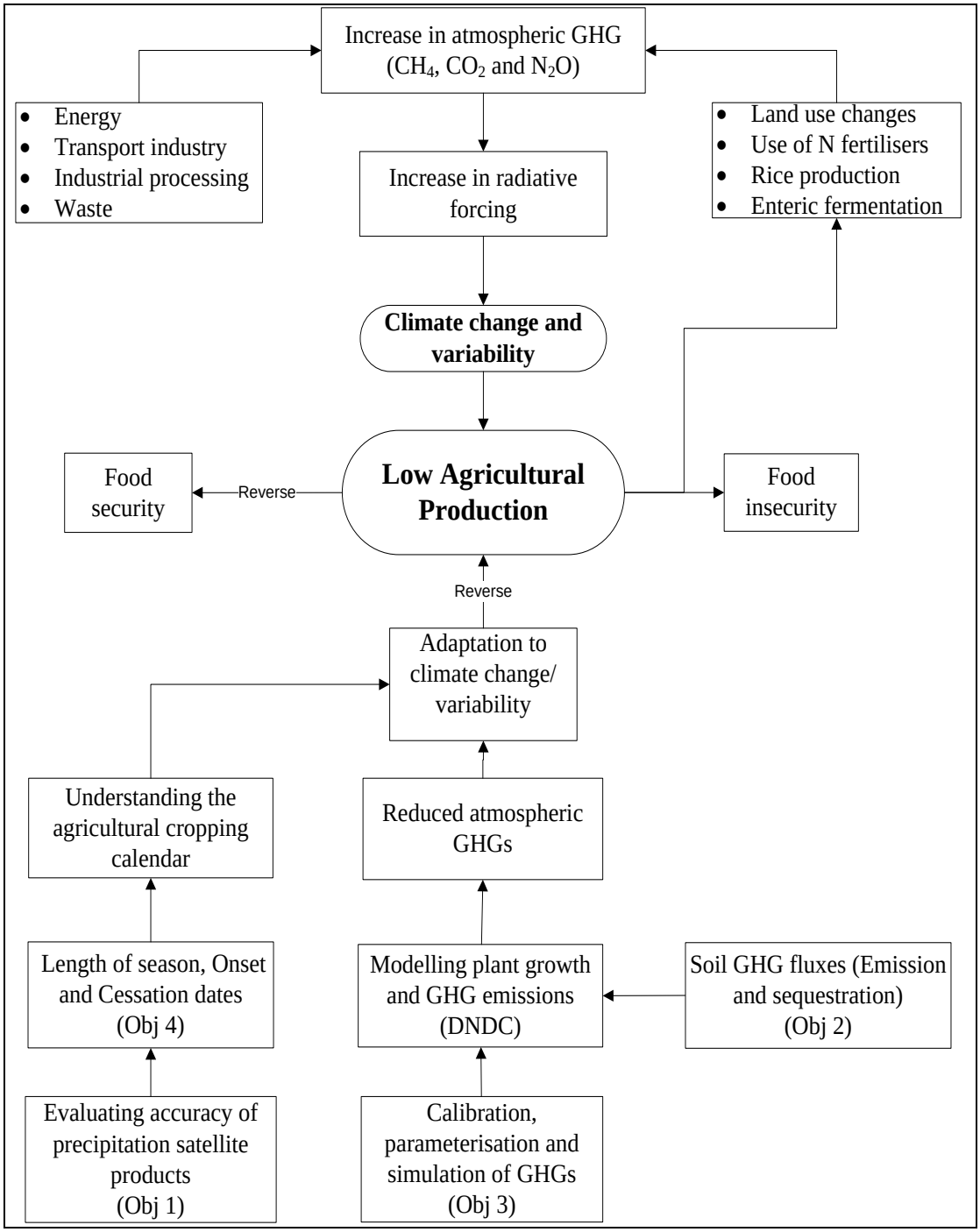

Figure 2.1: Conceptual framework showing the linkages between the study objectives (Source: Literature synthesis, 2018)

CHAPTER THREE

MATERIALS AND METHODS

3.1 Overview

This chapter presents the methodology used in the quantification of soil greenhouse gas fluxes, DNDC model simulation of GHG emissions, evaluation of satellite precipitation products for improved agricultural advisory services and productivity in Kenya. It also describes the process followed in the derivation of maize cropping calendar (rainfall onset, cessation and length of growing season) in croplands under climate variability in Kenya.

3.2 Long-term satellite-derived precipitation products for improved agricultural productivity in Kenya

3.2.1 Study area

Kenya lies along the equator in East Africa (Figure 3.1) covering an estimated area of 582, 646 km^2, of which water covers about 2% of the land mass, and 80% is arid to semi-arid (ASALs) zones. Approximately 17% of the Kenyan land is considered as high potential agricultural land. This agricultural potential land sustains about 75% of the Kenyan population (Huho & Mugalavai, 2010). Kenya lies between longitudes 34° E to 42° E, and latitudes 5° N to 5.5° S and borders Uganda to the west, Somalia to the east, Ethiopia and Sudan to the North and Tanzania to the south (Figure 3.1). Kenya is subdivided into 47 counties administratively, lying at an altitude of between sea level and the peak of Mt Kenya at 5,199 m above sea level.

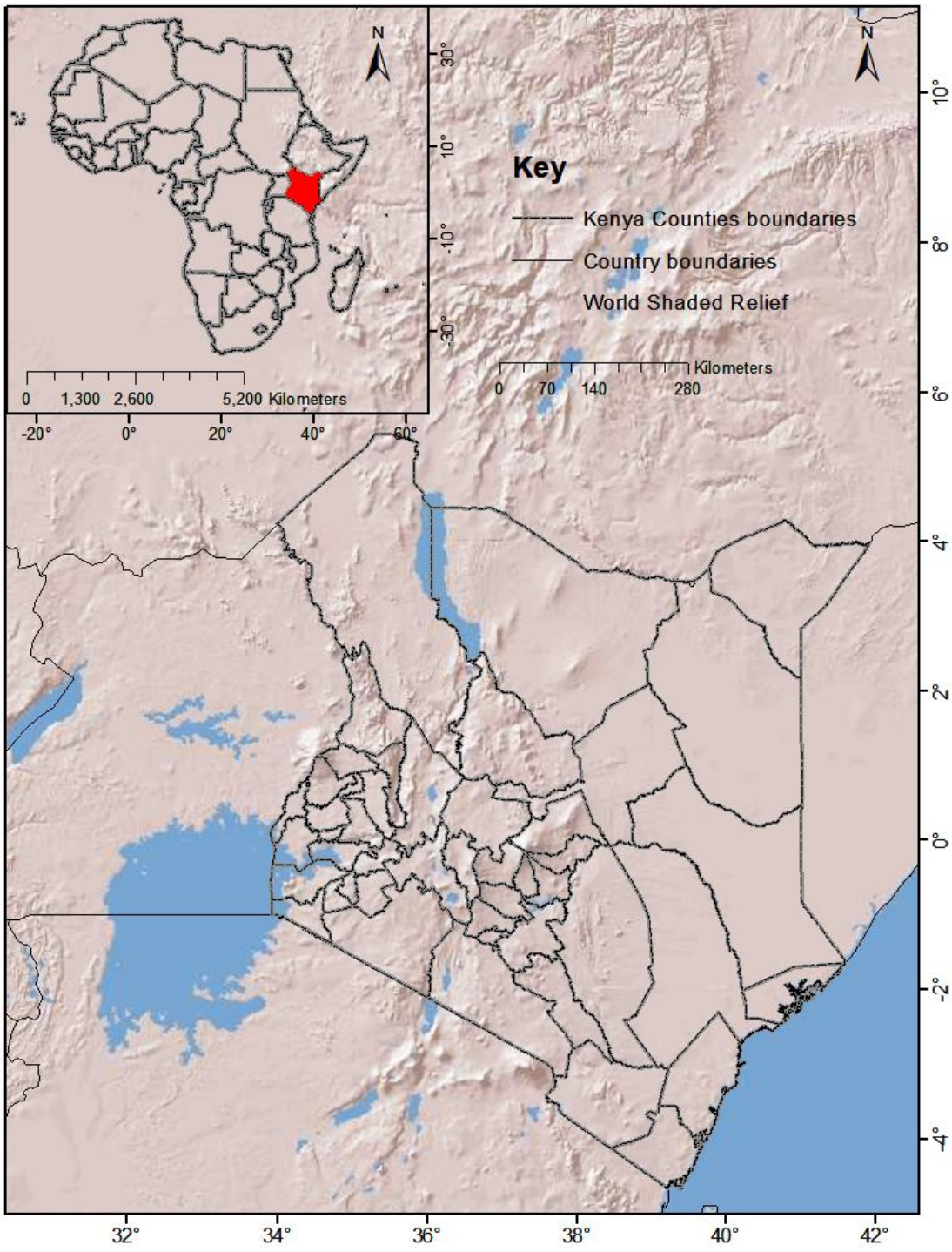

Figure 3.1: Map of Africa showing the geographical position of Kenya (Source: ESRI, 2018)

Kenya is classified into eight major agro-ecological zones (AEZ) (FAO, 1996). The zones are; tropical cool arid (TCA), tropical cool humid (TCH), tropical cool semiarid (TCSA), tropical cool sub-humid (TCSH), tropical warm arid (TWA), tropical warm humid (TWH), tropical warm semiarid (TWSA) and tropical warm sub-humid

(TWSH) (Figure 3.2). These zones are associated with corresponding temperature variations ranging from freezing temperatures -8°C to 40°C (Otolo & Wakhungu, 2013).

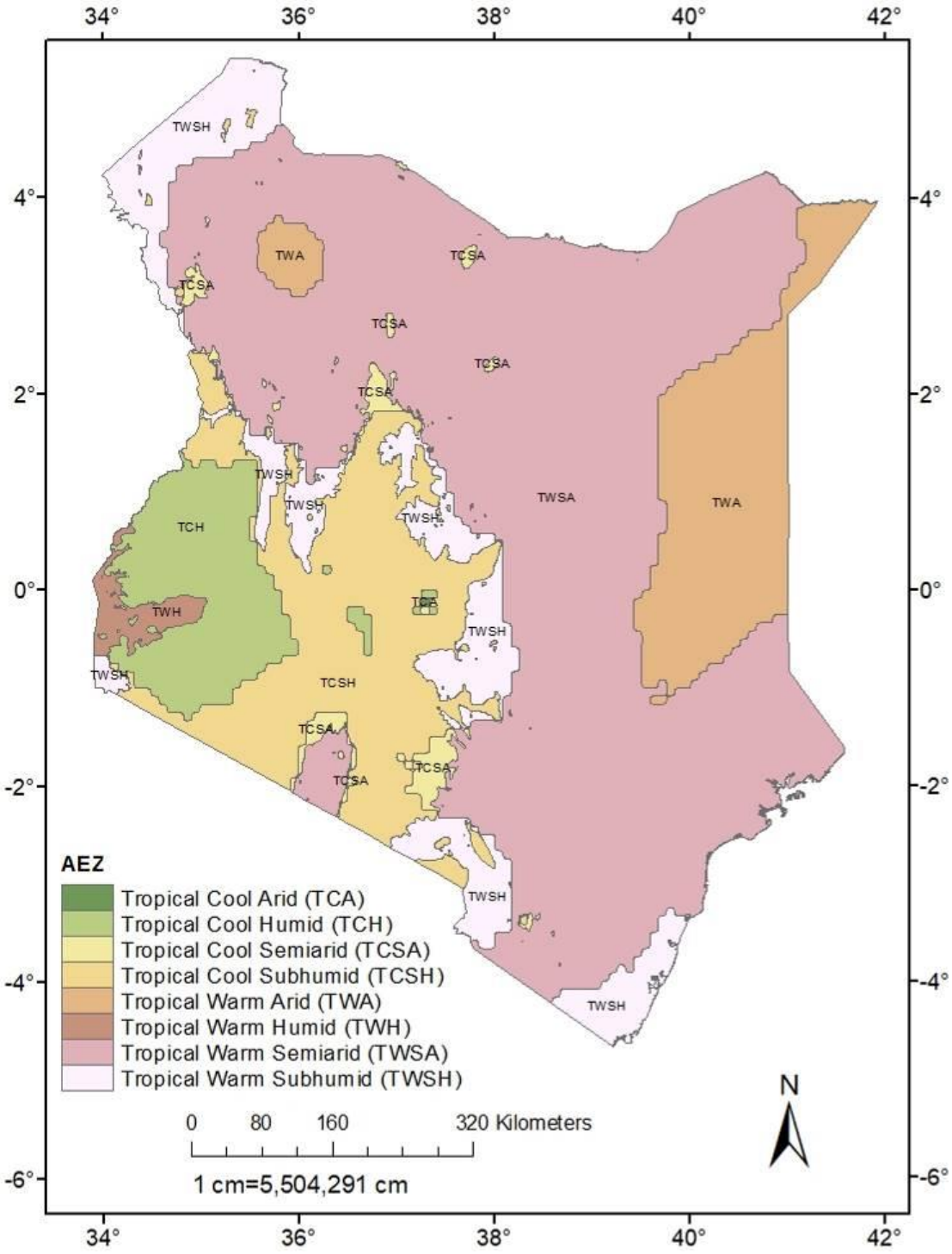

Figure 3.2: Kenya Agro ecological zones (AEZ) (Source: ESRI, 2016)

Most parts of the country experience bimodal rainfall regime with the “long rains” season being experienced from March to May (MAM) while the “short rains” occurring from October to December (OND) (Yang et al., 2014). According to Anyah and Semazzi (2006), these rainy seasons particularly coincide with periods of the year when the Inter-tropical convergence zone (ITCZ) is overhead the equator. The average annual rainfall is 680 mm with a variation from less than 250 mm in northern Kenya to over 2,000 mm in Western Kenya. The climate is influenced by the ITCZ and relief and ranges from permanent snow above 4,600 metres on top of Mt. Kenya to the driest parts like the Chalbi desert in the Marsabit county in the northern part of the country.

Soil types across the country vary depending on soil forming factors like parent material, amount of rainfall and topography. Soils in Western Kenya are mainly acrisols, and cambisols, which are highly weathered. Nitosols and andosols, which are of volcanic origin, are the predominant soil types in the Central parts of Kenya. Soils in the ASALs are majorly gleysols, phaeozems and vertisols, with characteristic features of salinity, sodicity, low soil fertility and high vulnerability to erosion. Coastal soils are mostly acrisols, luvisols and arenosols, which are coarse textured and low in organic matter (FAO, 1996).

3.2.2 Dataset sources, acquisition and processing

Monthly precipitation (mm month $^{-1}$) estimates from four satellite products namely; TRMM-TMPA 3B42 V7, CHIRPS 2.0, GPCC and NASA LARC-POWER, and the ground-based KMD monthly precipitation data, between 1998 and 2013, were acquired. The first product was daily rainfall data from NASA LARC Prediction of Worldwide Energy Resource (POWER) at 0.25° x 0.25° spatial resolution (Rienecker

et al., 2011) from 1st January 1998 to 31st December 2013, were extracted over Kenya. They were converted to monthly time series (mm month^{-1}) before comparison and analysis.

The second product was TRMM-TMPA product 3B42 version 7 at 0.25° by 0.25° spatial resolution (Huffman et al., 2007). The TRMM 3B42 product is one type of the TMPA (TRMM Multi-satellite Precipitation Analysis) products (Huffman et al., 2007). TRMM was the first satellite-based program mission dedicated to measuring tropical and sub-tropical rainfall (Chen et al., 2011; Abiola et al., 2012). The TRMM satellite runs in an orbit which is not synchronous to the Sun, and as a result, it comes to the same point at a different time and is proper to study the daily change of rainfalls (Chen et al., 2011). It is a joint mission between the National Aeronautics and Space Administration (NASA) and the Japan Aerospace Exploration Agency (JAXA) launched in 1997 with the aim of studying precipitation in the tropics (Shrivastava et al., 2014). The latest product Version 7 applies the TMPA algorithm. The TMPA algorithm combines precipitation estimates from microwave (MW) and infrared (IR) satellites, as well as the GPCC monthly gauge analysis (Duan et al., 2016).

The third satellite product was the GPCC at 0.5° by 0.5° spatial resolutions. The GPCC's database comprises precipitation data on a monthly basis from a variety of sources. GPCC has set up a portfolio of different precipitation analysis products to fulfil the different requirements of the user community (Schneider et al., 2014). The fourth satellite product was the Climate Hazards Group InfraRed Precipitation with Stations (CHIRPS) V2.0 at a 0.05° X 0.05° spatial resolution with the satellite data calibrated with in situ station data to create gridded rainfall time series (Funk et al., 2015). This latest product, released in February 2015, is relatively a new rainfall

product with highest temporal and spatial resolution based on multiple data sources (Paredes-Trejo et al., 2016). The CHIRPS product is a “satellite-gauge” based on integration of various datasets: the monthly precipitation climatology (CHPclim) that is created using rain gauge stations collected from FAO and GHCN, the Cold Cloud Duration (CCD) information based on thermal infrared data archived from CPC and NOAA National Climate Data Center (NCDC), the Version 7 TRMM 3B42 data, the Version 2 atmospheric model rainfall field from the NOAA Climate Forecast System (CFS), and the rain gauge stations data from multiple sources (Funk et al., 2015; Tuo et al., 2016).

Kenya Meteorological Department (KMD) is the national institution with a mandate to collect and store data in Kenya. The data is collected from a collaboration of the KMD and various institutions and volunteers (GoK, 2012). For this study, monthly data from 32 surface climate observing stations countrywide (Synoptic Stations, Annex 1) were used (Figure 3.3).

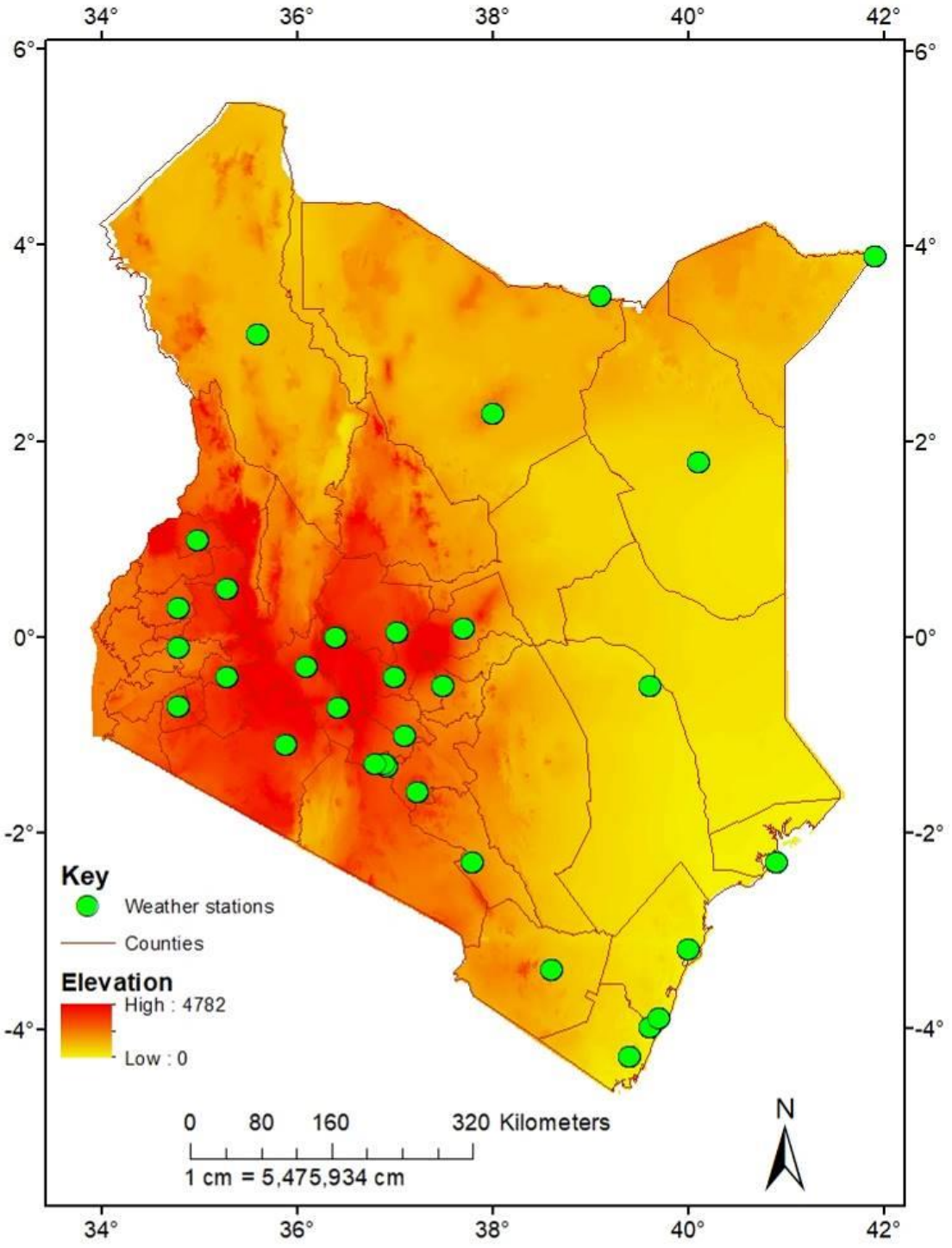

Figure 3.3: Kenya digital elevation map, the spatial distribution of weather stations and counties (Source: Author, 2018)

The KMD and NASA-LARC datasets were first assessed for completeness and where necessary corrective measures were taken. The datasets were managed in Ms Excel, saved as comma separated version (.csv) file and uploaded to ArcGIS 10.4 version 10.4.1.5686 where they were first projected as point data. The datasets were interpolated to raster files using inverse distance weighting (IDW) approach, at 0.0318° by 0.0318° spatial resolution for KMD and 0.036° x 0.036° for NASA LARC-POWER (Figure 3.4). The IDW was used due to its ease of interpretation and popularity in rainfall interpolation studies (Hu et al., 2014). The TMPA, GPCC and CHIRPS were already aggregated in monthly time-series and did not require additional temporal modifications before analysis.

3.2.3 Rainfall products standardisation

All the rainfall products (1 observed and four satellite products) were sourced at different spatial resolution. Before analysis, all the five products were projected to World Geodetic System (WGS) 1984, Universal Transverse Mercator (UTM) zone 37 N ensuring a similar processing extent for all products. They were further rescaled from their spatial resolutions to assume the lowest temporal resolution (0.0318° x 0.0318°) from the observed rainfall for uniformity in comparison. Lastly, they were reclassified following defined uniform intervals for ease of comparisons (Figure 3.4).

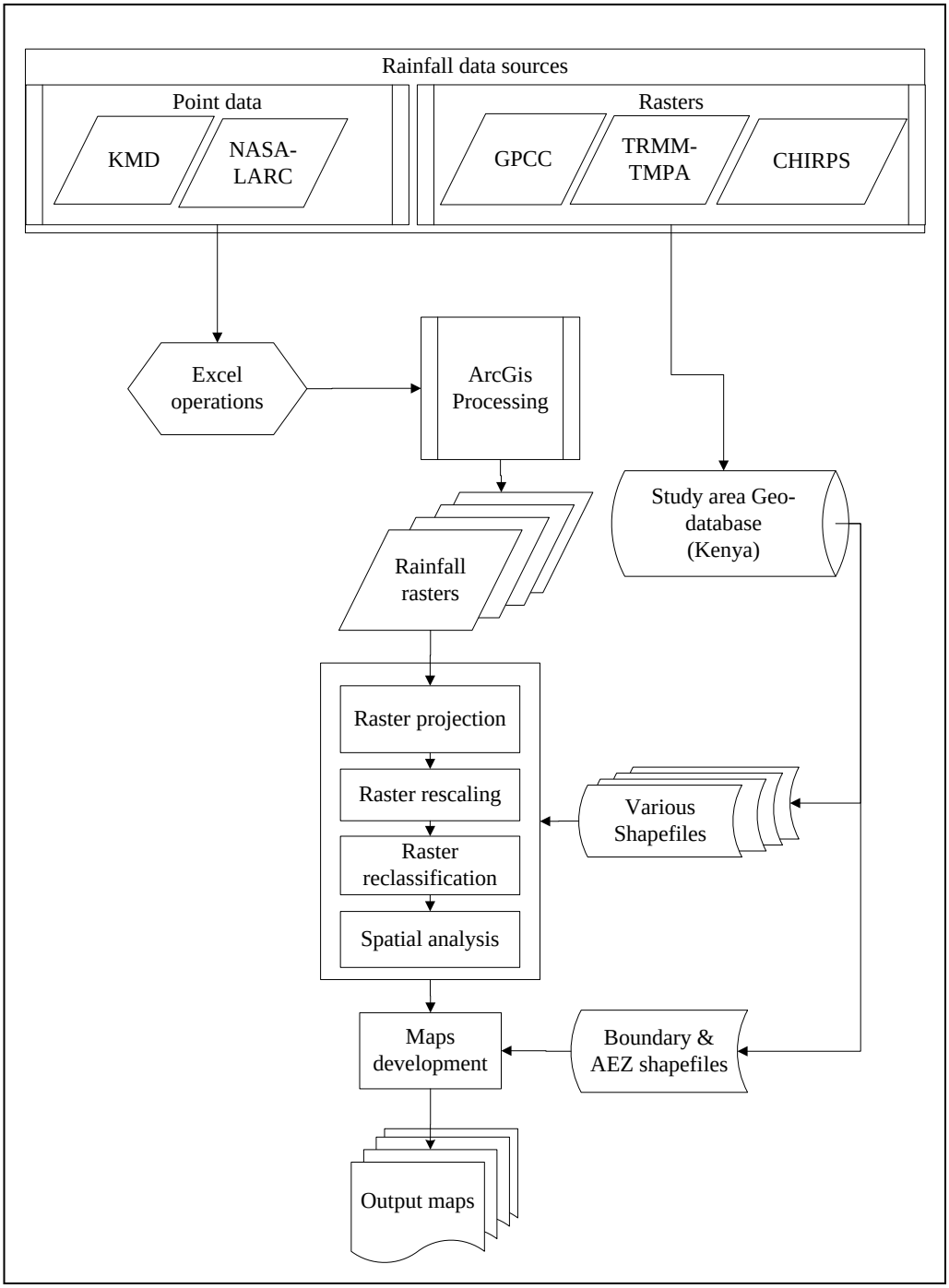

Figure 3.4: Flow chart showing the methodology followed in developing various maps (Source: Author, 2018)

3.2.4 Satellite products evaluation

Data from the time-series of the monthly precipitations were compared between satellite products and the KMD monthly data. Due to the uniqueness in topographical systems over Kenya, and to evaluate the potential regional variations in line with agricultural productivity, the country was divided into eight agricultural zones as classified by FAO (1996). Annual differences between satellite data and KMD interpolated data were calculated from the spatially aggregated data to determine the level of overestimation or underestimations among the datasets. For comparative evaluations, the datasets were subjected to nine statistics: Mean Error (ME) (Eq 1), Mean Absolute Error (MAE) (Eq 2), Mean Square Error (MSE) (Eq 3), Root Mean Square Error (RSME) (Eq 4), Relative Root Mean Square Error (RRMSE) (Eq 5), Multiplicable bias (Eq 6), Efficiency (Eq 7), Pearson's correlation coefficient (CC) (Eq 8), Spatial mean (Eq 9) (Table 3.1). Analysis of ME, MAE, MSE, RMSE, RRMSE, Multiplicable bias, Efficiency and spatial mean were pixel to pixel and carried out spatially. For correlation, the rasters were first extracted to eight agroecological zones and after that converted to point data and analysed using R Studio version 1.0.143.

Table 3.1: Statistical formulas of performance measures for the satellite products

Statistical metric	Equation	Optimal value
1. Mean error	$ME = \frac{1}{N}\sum_{i=1}^{N}(S_i - G_i)$	0
2. Mean absolute error	$\mathrm{MAE} = \frac{\frac{1}{N}\sum_{i=1}^{N}\lvert S_i - G_i\rvert}{\overline{G_i}}$	0
3. Mean squared error	$\mathrm{MSE} = \frac{\sum_{i=1}^{N}(S_i - G_i)^2}{n}$	0
4. Root mean square error	$RMSE = \sqrt{\frac{\frac{1}{N}\sum_{i=1}^{N}(S_i - G_i)^2}{G_i}}$	0
5. Relative root mean square error	$RRMSE = \sqrt{\frac{\frac{1}{N}\sum_{i=1}^{N}(S_i - G_i)^2}{(G_i)^2}}$	0
6. Multiplicable bias	$\mathrm{BIAS} = 1 - \frac{\sum S}{\sum G}$	1
7. Efficiency	$\mathrm{Eff} = 1 - \frac{\sum(S_i - G_i)^2}{\sum(G_i - S_i)^2}$	1
8. Coefficient of determination (r^2)	$r = \frac{\sum(G-\bar{G})(S-\bar{S})}{\sqrt{(G-\bar{G})^2}\sqrt{(S-\bar{S})^2}}$	-1 to 1
9. Spatial mean ($\bar{X}$)	$\bar{X} = \sum_{i=1}^{n} x_i$	None

Where *G* is gauge data, *S* is satellite data, x_i is the coordinate feature of i, and n is the total number of features.

3.3 Soil GHG fluxes from maize production in semi-arid lands of central highlands of Kenya

3.3.1 Study site

This study was carried out in Mbeere South sub-county in Embu County, Kenya (Figure 3.5), which lies in the Lower Midland (LM5) agro-ecological zone on the eastern slopes of Mount Kenya (FAO, 1996; Jaetzold et al., 2007) within the upper Tana river catchment. The trial was set up in 2004 at Machang'a secondary school (00° 47' 26.8"S; 37° 39' 45.3"E), located at 1030 m a.s.l. (Mucheru-Muna et al., 2009). The rainfall pattern in the study area is bimodal with long rains (LRs) lasting for approximately three months (mid-March to June) and short rains (SRs) occurring between (mid-October to December), thus supporting two cropping seasons per year. The climate is Tropical Savanna (Köppen climate classification) whose annual rainfall

ranges between 700 mm and 900 mm. The average rainfall over the long term for long rains season is 430 mm whereas that of the short rains season is 350 mm with a mean annual temperature of 21.6°C (Jaetzold et al., 2007).

The soils are predominantly sandy loam (Ngetich et al., 2014) less weathered, yellowish red, Xanthic Ferralsols (Jaetzold et al., 2007). The study site lies in a marginal area characteristic of low agricultural potential and very short cropping seasons (Jaetzold et al., 2007; Ngetich et al., 2014), but the zone is suitable for low-land hybrid maize (*Zea mays L.*), green grams (*Vigna radiata*), chickpeas (*Cicera rietinum*), common beans (*Phaseolus vulgaris*), sorghum (*Sorghum bicolour*) and cowpea (*Vigna unguiculata*) among others (Jaetzold et al., 2007). Typical cropping systems in the region are primarily maize-based (Okeyo et al., 2014) with common beans (*Phaseolus vulgaris*), as the most preferred legume for intercropping (Kiboi et al., 2017).

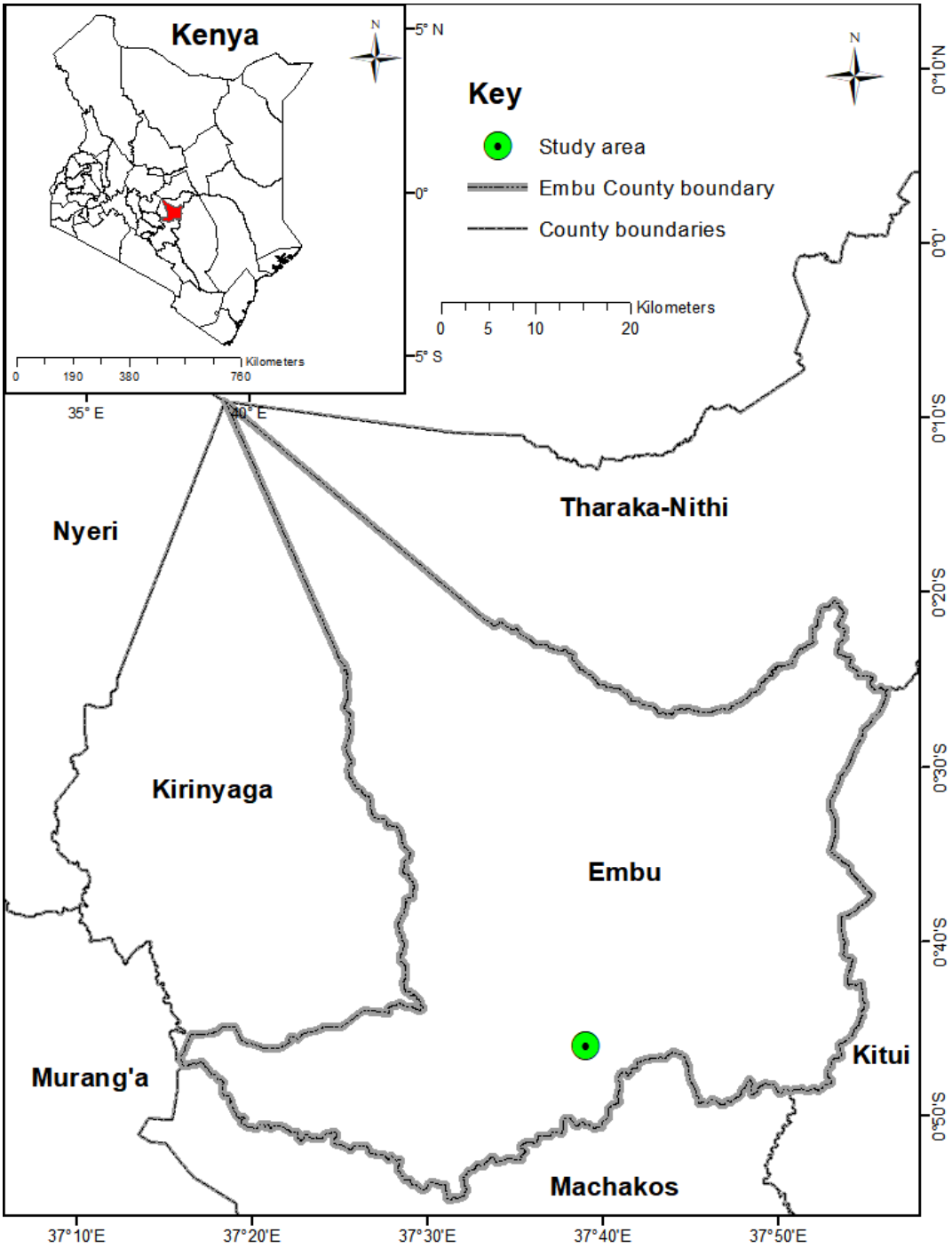

Figure 3.5: Map of the study area showing the location of the study site in Embu county (Source: Author, 2018)

3.3.2 Experimental design

The experiment was set up as a researcher designed and managed trial and laid out as a randomised complete block design replicated thrice. The details on trial establishment are explained in Mucheru-Muna et al. (2009). In brief, the full trial comprised of 12 treatments of different organic and inorganic inputs, different assorted combinations and a control (treatment with no external input of nutrients). For this study on soil GHG fluxes, however, only four treatments were selected: (i) no external input (control), (ii) inorganic fertiliser NPK at N=23%, P=23% and K=0% applied at the rate of 60 kg N ha^{-1}; (iii) animal (goat) manure applied at a rate of 60 kg N ha^{-1}; and (iv) animal (goat) manure applied at rate of 30 kg N ha^{-1} combined with inorganic fertiliser (NPK) applied at a rate of 30 kg N ha^{-1}. These treatments were selected based on their popularity and relatively high level of use by the smallholder farmers in the study area (Mugwe et al., 2009; Macharia et al., 2014). The experimental plots measured 6 m by 4.5 m with one meter as a border between plots and at least two meters between blocks (Plate 3.1).

Plate 3.1: Experimental field set with chamber bases installed (Source: Author, 2017)

The land was manually prepared with all aboveground fallow biomass removed from the plots at the beginning of each cropping season (February 2017 and August 2017). Animal manure was broadcast and immediately incorporated during land preparation, through hand ploughing, approximately one week before seeding. The amounts of goat manure applied were calculated based on 3 composite samples of manure analysed in the National Agricultural Research Laboratories (NARL-Nairobi). The manure had 2% N translating into 3 Mg dry matter ha^{-1} to supply 60 kg N ha^{-1}. The

dry matter was estimated to contain 40% C translating to approximately 1.2 Mg C ha^{-1}. The inorganic fertiliser was applied directly in the maize planting holes and thoroughly mixed with the soils before placing the seeds on top of the mixture during planting immediately, as is typically practised by local farmers, after the onset of the rains. Dry highland (DH 04) maize (*Zea mays L.*) variety was used as the test crop and planted at an interval of 0.90 m x 0.60 m, inter and intra-row distance, respectively. Three seeds were sown per hole and thinned to two plants three weeks after emergence. Weeds were controlled regularly using hand hoes with minimal soil disturbance.

3.3.3 GHG concentration measurements

The three greenhouse gases (CH_4, CO_2 and N_2O) were measured using vented manual static chambers. The chambers were made out of PVC plastic and consisted of a base (27 x 37.2 x 10 cm) and a lid (27 x 37.2 x 12.5 cm). Three chamber bases per plot were inserted into the soils to a depth of approximately 7 cm two weeks before the first sampling event (25th January 2017). The chamber bases were removed during land preparations, manure incorporation and planting at the beginning of long rains (LR) and short rains (SR) (4th March and 5th October 2017, respectively) and returned immediately after the activities. The chamber lids were equipped with a vent to equilibrate pressure difference between the headspace of the chambers and the ambient air pressure during closure; a fan to avoid concentration gradients in the chamber headspace; a digital probe thermometer (TFA thermometer, Zum Ottersberg, Wertheim, Germany) to record the internal chamber temperature; a sampling port sealed with a silicon septum; and a closed-cell foam gasket between the lid and the base to ensure airtight sealing between the two compartments. Chamber base and lid

were tightly clipped together with large metal binder clips. Sampling was done once a week. Chambers were closed for 30 minutes, and gas samples were taken four times (0, 10, 20 and 30 min) using syringes (60 mL propylene) fitted with Luer locks. The gas pooling technique was chosen, following Arias-Navarro et al. (2013) where a total sample of 20 mL from each of the three chambers in a plot was collected. The pooled gas was thoroughly mixed while still in the syringe and the first 40 mL of the content transferred to pre-evacuated glass vials ensuring overpressure to reduce chances of sample contamination with ambient air. The gas samples were packaged per plot (Plate 3.2) and transported to Mazingira Centre at the International Livestock Research Institute (Nairobi, Kenya) for analysis.

Plate 3.2: GHG gas sampling, transfer and packaging of vials (Source: Author, 2017)

Concentrations of CO_2, CH_4, and N_2O were determined using gas chromatography (8610C; SRI Instruments, Torrance, CA, USA) fitted with a ^{63}Ni-electron capture detector (ECD) for determining N_2O concentrations as well as a flame ionisation detector (FID) and a methaniser for CO_2 and CH_4 analysis. Nitrogen gas (N_2) was used as the carrier gas for both the ECD and FID channels at a flow rate of 20 mL min^{-1}. The gas samples' concentrations were determined using the peak area as obtained from gas chromatograph relative to peak areas of the standards (four calibration gases). A

linear regression approach was used to calculate CH_4 and CO_2 concentrations while a power function was used to calculate N_2O concentration based on the peak areas of the calibration gases.

3.3.4 GHG flux calculations and data quality control/quality assurance (QC/QA)

The instantaneous soil GHG emissions were determined based on the rate of change in concentration over time in the chamber headspace after chamber deployment (Rosenstock et al., 2016, Pelster et al., 2017). The calculation was based on the volume of the chamber, the soil area covered by the chamber, and included a correction for atmospheric pressure fluctuations as well as the internal chamber temperature using the ideal gas law as shown in equation (10).

$$F_{GHG} = (\partial c/\partial t) * (M/V_m) * (V/A), \quad (10)$$

where:

F_{GHG} is the flux of the GHG in question, $\partial c/\partial t$ is the change in concentration over time, M is the molar mass of the element in question (C for CO_2 and CH_4, and N_2 for N_2O), V_m is the molar volume of gas at the sampling temperature and atmospheric pressure, V is the volume of the chamber headspace, and A is the area covered by the chamber. Fluxes were calculated in mg C m^{-2} h^{-1} for CH_4, mg C m^{-2} h^{-1} for CO_2 and µg N m^{-2} h^{-1} for N_2O. These fluxes were later converted to kg CH_4-C ha^{-1} yr^{-1}, Mg CO_2-C ha^{-1} yr^{-1} and kg N_2O-N ha^{-1} yr^{-1} for CH_4, CO_2 and N_2O, respectively.

A linear regression of the simultaneous CO_2 concentration over time was fitted. Where the R^2 for the CO_2 concentration relation was less than 0.90, the three flux measurements were considered unreliable. This was based on the assumption that the chambers malfunctioned due to a possible non-closure or due to leaks and similar

problems. Where the R^2 value for CO_2 concentration was higher than 0.90, the three flux measurements were assumed reliable including those below the minimum detection limit calculated following (Parkin et al., 2012). The detection limits for the three GHG were on average 3.15±0.26 mg CO_2-C m^{-2} h^{-1} for CO_2 (100% of the samples were above the detection limit), 3.91±0.30 µg N_2O-N m^{-2} h^{-1} for N_2O (33% of the samples were above the detection limit) and ± 0.03±0.01 mg CH_4-C m^{-2} h^{-1} for CH_4 fluxes (14% of the samples were above the detection limit). Flux values below the minimum detection limit were still retained and used to calculate the cumulative fluxes of the three GHGs.

3.3.5 Soil and meteorological measurements

Soil properties were determined based on standard procedures and included the following. Bulk density for the top 5 cm of soils was determined for each plot using soil sample rings with a 100 cm^3 volume (Eijkelkamp Agrisearch Equipment, Giesbeek, The Netherlands). The bulk density samples were oven dried at 105°C for 24 hours (Stoof et al., 2015). A composite sample made of three soil cores per plot were collected to a depth of 0-20 cm using single gouge auger (Eijkelkamp Agrisearch Equipment, Giesbeek, The Netherlands). The soil samples were individually packed in labelled Ziplock bags. Any large clumps of soil were immediately crushed by hand before the samples were transported to the laboratory for further analysis. The soil samples were then oven-dried at 40°C for three days (72 hours) before grounding using a ball mill (Retsch ball mill, Haan, Germany) for further analysis. The ratio of soil: water (1:2) was used to determine the soil pH from the suspension using a glass probe pH meter (Crison Instruments, Barcelona, Spain). Total carbon (C) and nitrogen

(N) concentrations were determined on the powdered samples using a C/N analyser (Thermal Scientific, Flash 2000 Analyzer, Waltham, MA USA).

Determination of inorganic N (NO_3-N and NH_4-N) concentrations was conducted for the period between February-July 2017 and October 2017-February 2018, during the two cropping seasons, starting immediately after planting until physiological maturity at a sampling interval of two weeks. During sampling, a composite (one per plot) consisting of three sub-samples of undisturbed soils was collected to a depth of 20 cm using the single gouge auger described above. Soil samples were transported to the laboratory at Mazingira Centre, International Livestock Research Institute (Nairobi, Kenya), using a standard commercial cool box filled with ice packs. The fresh soils were extracted within a day of sampling by mixing 10 g of fresh soils with 50 mL of 2M KCL and shaking the slurry in an orbital shaker (Edmund Buhler model, Hechingen, Germany) for 1 hour at 100 shakes per minute. The samples were then centrifuged (Hettich Centrifuge, Tullingen, Germany) for 10 minutes at 3,000 revolutions per minute, after which the supernatant was passed through a 110 mm Whatman ™ filter (No. 42) enhanced with a vacuum pump. The extracted samples were frozen until further analysis. The analysis was performed using a photometric analyser (Aquakem200: Thermo Scientific, Wilmington, DE, US). A sample of composite fresh soil was oven dried at 105°C until a constant soil weight was obtained to determine soil moisture content. Conversion of inorganic N (IN) concentrations to soil mass was based on the soil moisture content determined as a percentage of the dry soil mass. Cumulative IN (NH_4^+-N + NO_3^--N) was determined through linear interpolation between sampling dates following Burton et al. (2008).

Core meteorological variables were collected at the site and included rainfall at 3.5 m above ground, air temperature at 3 m above ground, relative humidity at 1.5 m above ground and solar radiation at 3.7 m above ground using S-THB-M002, S-THB-M002 and S-LIB-M003 sensors, respectively. The data was averaged for 15 minutes and then uploaded to a HOBO U30 NRC station data logger (Onset Computer Corporation, Bourne, MA, USA) (Plate 3). The data was then downloaded after every three months. Also, soil water content and soil temperature measurements were carried out adjacent to each chamber every time during gas sampling using a Procheck (ProCheck GS3 Sensor, Decagon Devices Inc. Pullman, Washington, USA).

3.3.6 Biomass measurements

A sample of eight maize plants from four holes covering 2.16 m^2 (1.8 m × 1.2 m) near the middle of each plot (avoiding edge effects) was collected for biomass determination every season at harvest (6th July 2017 and 7th February 2018). The aboveground maize plant samples were separated into its components: leaves, stems and grains. To determine belowground biomass, the roots from the eight maize plants per plot were dug up, mixed with water and sieved with a 2-mm wire gauze to ensure the roots were free of soils. However, the dead and alive fine roots were not distinguished. The samples for the various plant components were weighed to measure their fresh weight and air dried for three weeks before weighing again to determine the dry weight and subsequent water content. The samples were then transported to the laboratory, dried for 48 hours at 60°C and weighed again. A subsample of the roots, leaves, grains and stems were ground using a hammer mill (IKA mills, MF 10.2, Willington, N.C., USA) and later analysed for C and N content using the same C/N analyser described above for soil analysis content. Maize grain

yields were determined from a 19.9 m^2 (3.9 m × 5.1 m) harvest area at physiological maturity. Leaf Area Index (LAI) was measured using a ceptometer (Decagon Devices, Inc., Pullman, Washington, USA) on a weekly basis from the time the maize crop formed a canopy (at the 6th leaf stage or approximately one foot above ground) till physiological maturity.

3.3.7 Nitrous oxide (N_2O) yield-scaled emissions (YSE) and emission factors (EF)

Yield-scaled N_2O emissions (g N_2O-N kg^{-1} emitted per kg N exported as grains) were determined for each plot for the year of study by dividing the cumulative N_2O emissions (g N_2O-N ha^{-1}) of the study period by the sum total of grain yields (kg ha^{-1}) for two seasons (LR 2017 and SR 2017) (van Groenigen et al., 2010; Pelster et al., 2011). Nitrous oxide emission factors (EF) were derived from N inputs and cumulative N_2O fluxes as shown in equation (11).

$$EF = ((N_2O\text{-}N_{fertilised}) - (N_2O_{unfertilised})) / N_{applied} \quad (11)$$

where "$N_2O\text{-}N_{fertilised}$" is the cumulative emission of N_2O (kg N_2O-N) from the individual treatment, "$N_2O\text{-}N_{unfertilised}$" is the cumulative emission from the control treatment, and "$N_{applied}$" is the inputs of N in the specific treatment (kg N) per year.

3.3.8 Global warming potential (GWP) and greenhouse gas intensity (GHGI)

Cumulative annual CH_4 and N_2O fluxes were converted to CO_2-equivalents using a global warming potential (GWP) of 298 for N_2O, and 34 for CH_4 (Myhre et al., 2013). Greenhouse gas intensity (GHGI) values were calculated per treatment by dividing the net global warming potential (CO_2+ N_2O + CH_4) by the annual grain yield production (Li et al., 2015) as shown in equation (12).

$$GHGI = \text{net GWP/maize grain yield (kg } CO_2 \text{ equivalent kg}^{-1}) \quad (12)$$

3.3.9 Statistical analyses

Seasonal cumulative GHG fluxes (the period between the two harvesting events) for long rains (LR 2017) and short rains (SR 2017) growing seasons as well as annual cumulative fluxes for the whole study period (Feb 2017 to Feb 2018) were determined for each plot based on linear interpolation between sampling dates. Before conducting any analysis, the data were subjected to a normality test using the Shapiro-Wilk test (Shapiro & Wilk, 1965) and log-transformed where necessary. The effects of treatments on the cumulative GHG fluxes were tested using ANOVA (AOV in RStudio version 1.0.143). Correlations between cumulative seasonal soil GHG fluxes and soil properties, biomass (below and above ground), and cumulative inorganic nitrogen were tested using Pearson's correlation.

3.4 Simulation of field measured GHG gas fluxes across various management practices in the semiarid parts of central highlands of Kenya

3.4.1 Study site

This study was carried out in Mbeere South sub-county in Embu County, Kenya as detailed in objective two above (Figure 3.5).

3.4.2 Experimental design

The experiment was set up as a researcher-managed trial and laid out as a randomised complete block design with three replicates as described in objective two above (Plate 3.1).

3.4.3 GHG concentration and other field measurements

The greenhouse gases were measured using vented manual static plastic chambers and gas chromatography for a whole year (Feb 2017 to Feb 2018) as detailed in objective two above.

3.4.4 The Denitrification-Decomposition (DNDC) model

The DeNitrification-DeComposition (DNDC) model version 9.5 was used in this study (Li et al., 1992). The DNDC model is a process-based model of carbon (C) and nitrogen (N) biogeochemistry in agricultural ecosystems. The DNDC model framework includes processes for soil, climate, crop production, C and N dynamics, and trace gas emissions reported at a daily time step (Jarecki et al., 2018). The DNDC model was initially developed for quantifying C sequestration and emissions of greenhouse gases (GHG). DNDC is a well-calibrated and validated model for studying carbon and nitrogen cycles in various ecosystems worldwide (Rui et al., 2017) and consists of two components. The first component contains sub-models for soil (bulk density, texture, soil hydraulic parameters, and SOC), climate (air temperature, precipitation, wind speed, solar radiation, and humidity), crop growth (crop type, potential yield, biomass fractions, C/N ratio, water demand, and optimal temperature), agricultural management (tillage, residue, irrigation, plant and harvest dates, and fertiliser) and decomposition (litter, labile humus, passive humus, and microbial biomass). The model converts primary drivers such as climate, soil, vegetation, and human activity into soil environmental factors such as soil temperature, humidity, pH, redox potential and concentration gradients of substrates (Zhang et al., 2018). The second component comprises sub-models for nitrification, denitrification, and fermentation and calculates nitrous oxide (N_2O) and methane (CH_4) production and consumption (Li, 2007).

3.4.5 DNDC model input parameters

Climate, soils, crop and land management parameters

Daily rainfall (cm), maximum and minimum air temperature (°C), wind speed (m s^{-1}), solar radiation MJ m^{-2} d^{-1} and relative humidity (%) data were collected using HOBO U30 NRC station data logger (Onset Computer Corporation, Bourne, MA, USA) from a weather station within the experimental site (Plate 3.3). The weather files for the above climate parameters for the year of study were prepared as described in the DNDC guide (version 9.5).

Plate 3.3: Automatic weather station at the study site (Source: Author, 2017)

Soil parameters

Soils were sampled from each of the plots before the beginning of the experiment (January 2017) and taken to the National Agricultural Research Laboratory (NARL-Nairobi) for analysis following standard laboratory procedures (Table 3.3). They were tested for bulk density, texture, soil organic carbon, mineral nitrogen and soil pH as described in section 3.3.5. Field capacity, slope, conductivity, wilting point and porosity had been earlier on been determined by Ngetich et al. (2014).

Table 3.2: Soil physicochemical properties of Machang'a, Embu county

Parameters	**Treatment**	**Values**
Soil texture		Sandy Loam
Clay content (%)		43
Field Capacity (WFPS)		0.60
Wilting point (WFPS)		0.28
Saturated hydraulic conductivity (m hr^{-1}		0.015
Slope		4 - 5^0
Porosity		0.426
Bulk density (g cm^{-3})	Control	1.40
	Fertiliser	1.39
	Manure	1.26
	Manure + Fertilisers	1.28
Soil pH	Control	5.9
	Fertiliser	6.1
	Manure	8.0
	Manure + Fertiliser	7.8
Soil Organic Carbon	Control	0.006
	Fertiliser	0.007
	Manure	0.015
	Manure + Fertiliser	0.012
NO_3^-N (mg N kg^{-1})	Control	0.44
	Fertiliser	1.17
	Manure	0.34
	Manure + Fertiliser	0.33
NH_4^+N (mg N kg^{-1})	Control	1.44
	Fertiliser	4.14
	Manure	13.57
	Manure + Fertiliser	12.57

Source: Field measurements

Crop management parameters

Cropping data (type of crop, planting and harvesting), tillage data (method of ploughing, day and month of land preparation, biomass fraction and biomass C/N ratio), fertilization (type, amount and method of fertiliser applied and the day and month of application) and manure amendments (type, amount, method of application and day and month applied were collected from the experiment (Table 3.4).

Table 3.3: Plant management practices in Machang'a, Embu county

Planting practices	**Season 1**	**Season 2**
Planting date	6th March 2017	23rd October 2017
Harvest date	6th July 2017	6th February 2018
Date of manure incorporation	3rd June 2017	10th September 2017
Date of fertiliser application	6th March 2017	23rd October 2017
Date of tillage	3rd June 2017	10th September 2017
Tillage practices	Ploughing - 5cm	Ploughing - 5cm
Maize variety	DH 04	DH 04
Fertilization (kg N ha $^{-1}$)	60	60
Fertiliser application	Manually in holes	Manually in holes
Manure amendment (kg N ha $^{-1}$)	60	60
Manure type	Farmyard manure	Farmyard manure
Manure C/N ratio	13	13
Manure application	Incorporation	Incorporation
C content in biomass		
Biomass fraction of grains		0.04
Biomass fraction of leaves		0.59
Biomass fraction of Stems		0.3
Biomass fraction of Roots		0.03
C: N ratio of grain		21.2
C: N ratio leaf		43.95
C:N ratio leaf + stem		46.82
C: N ratio roots		38.1

Source: Field data

3.4.6 Calibration, validating and evaluation of the DNDC model

Model calibration to observed data is an essential first step to determine the set of model parameter values that maximise model simulation of observed data as assessed statistically (Gaillard et al., 2017). Validation with independent data away from the

calibration data is crucial for evaluating the accuracy of the model in simulating different conditions (Zhou et al., 2010). In this study, calibration and validation were done by comparing the observed grain yields, biomass and leaf area index (LAI) from experimental treatments with simulated model values. The grain yield is expressed on an equivalent C basis, where 1 kg (maize) grain contains 0.4 kg C following the DNDC model user guide. It should be noted that during the calibration and validation of the model, all the crop and soil parameters were based on sample analysis in the laboratory. The few parameters which were not measured were filled using expert opinion. To ascertain the general performance of the model; bias (Eq. (13)), the root means square error (RMSE) (Eq. (14)), and the coefficient of determination (R^2) (Eq. (15)) were calculated between the model predicted values and field observed as follows (Table 3.2);

Table 3.4: Statistical evaluation of the DNDC's performance

	Statistical metric	**Equation**	**Optimal value**
13.	Multiplicable bias	$\mathrm{BIAS} = 1 - \frac{\sum \mathrm{p}}{\sum \mathrm{G}}$	1
14.	Root mean square error	$RMSE = \sqrt{\frac{\frac{1}{N}\sum_{i=1}^{N}(P_i - G_i)^2}{G_i}}$	0
15.	The coefficient of determination (r)	$\mathrm{r} = \frac{\sum(G-\bar{G})(P-\bar{P})}{\sqrt{(G-\bar{G})^2}\sqrt{(P-\bar{P})^2}}$	-1 to 1

Where *G* is field observed data, P is the DNDC modelled data.

3.5 Length of growing season, rainfall onset and cessation dates in the agricultural potential zones of Kenya

3.5.1 Study area

The study was carried out in the agricultural potential zones of Kenya as detailed in objective 1 and as illustrated in Figure 3.6 below.

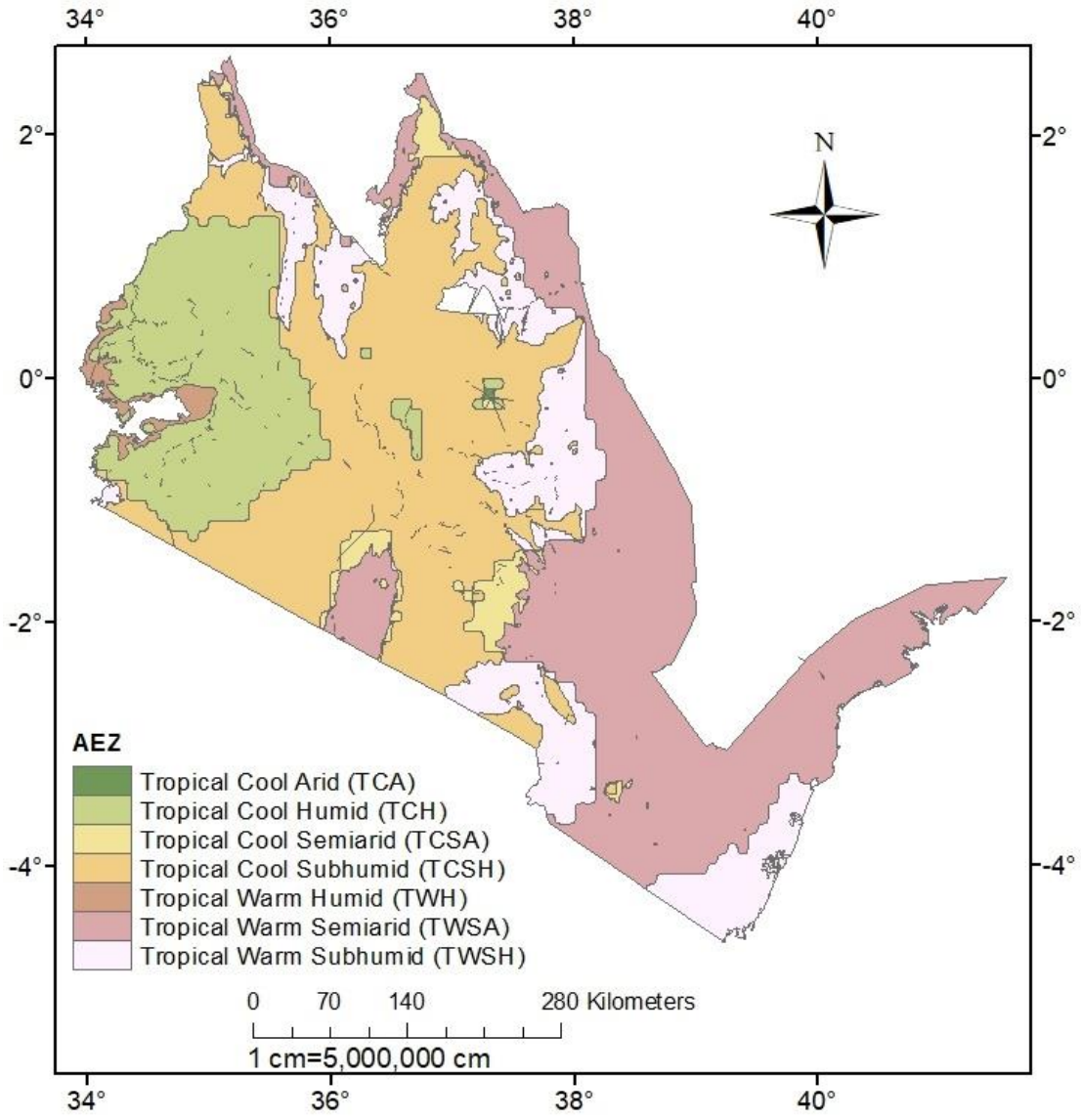

Figure 3.6: Map of the study area - potential agricultural zones of Kenya (Source: Author, 2018)

3.5.2 Data acquisition and processing

Determination of a crop calendar (length of growing season, rainfall onset and cessation dates) requires that both rainfall and temperature time series are available (Byakatonda et al., 2018). Weather data including daily rainfall, minimum and maximum temperature were extracted over Kenya from NASA-LARC Prediction of Worldwide Energy Resource (POWER) at 0.5^{o} x 0.5° spatial resolution (Rienecker et al., 2011) for the period between 1983 to 2017. Due to the limitation in downloading data for the whole country at once, based on the maximum area processed of 4.5^{o} x 4.5° degree (100 points), the country was subdivided into four equal sections, two on each side of the equator. The data was later combined and extracted further restricting the study area to the agriculturally potential areas of Kenya (134 data points) (Figure 3.6).

3.5.3 Identification of length of growing season, rainfall onset and cessation dates

Several studies have been carried out in predicting the rainfall onset and cessation dates and length of growing season using various methodological approaches (Mugalavai et al., 2008; Recha et al., 2012; Ngetich et al., 2014; Kisaka et al., 2015; Dunning et al., 2016; Byakatonda et al., 2018). As observed by Odekunle (2006), use of rainfall amount and rainy days do not have significant differences in determining mean onset and cessation. For this study, derivation of rainfall onset, cessation and length of growing season was done using RAIN software (Kipkorir, 2005) based on rainfall amounts. During the analysis, it was assumed that the onset of rains and the start of growing season were identical and were defined as receipt of sufficient rain for the survival of seedlings after sowing (Ngetich et al., 2014). The criterion followed in determining onset was based on various parameters. The rainfall threshold was set

at 1 mm while the lag time of the season was set at seven days after onset. Threshold-based measures are appropriate for local agronomic studies, as they are designed to take into account the availability of soil moisture (MacLeod, 2018). Onset was determined based on accumulated rainfall over a period of 4 days of at least 25 mm from new rains. For Cessation criterion, threshold water stress coefficient was set at 70% while relative yield threshold value was set at 35%. Cessation was quantified by considering the date on which the water stress in the root zone of a maize crop exceeds a threshold value (Mugalavai et al., 2008). The length of the rain season was computed as the number of days between onset and cessation dates (Byakatonda et al., 2018).

3.5.4 ETo calculation

Evapotranspiration (mm/day), a critical component in the determination of onset and cessation dates, was determined following the Blaney-Criddle method (Blaney & Criddle, 1962) (Equation 16).

$$ETo = p \times (0.46 \times T_{mean} + 8.13) \qquad \text{Equation 16}$$

Where p is the mean daily percentage of annual daytime hours for different latitudes. For this study, which lies between 4.75° South and 2° North, the mean daily percentage of annual daytime hours for the study area was set at 0.27.

3.5.5 Spatial presentation of the length of growing season, onset and cessation dates

The determined length of growing season, onset and cessation dates were uploaded and displayed as point data in ArcGIS software version 10.4 (version 10.4.1.5686). The data were interpolated using Spline method and later the raster files projected to World Geodetic System (WGS) 1984, Universal Transverse Mercator (UTM) zone 37 N and hence ensuring a similar processing extent. Extraction of the cropping maps

(length of growing season, onset and cessation dates) was done using pre-determined boundary shapes and masks (Figure 3.7) and presented as Julian days.

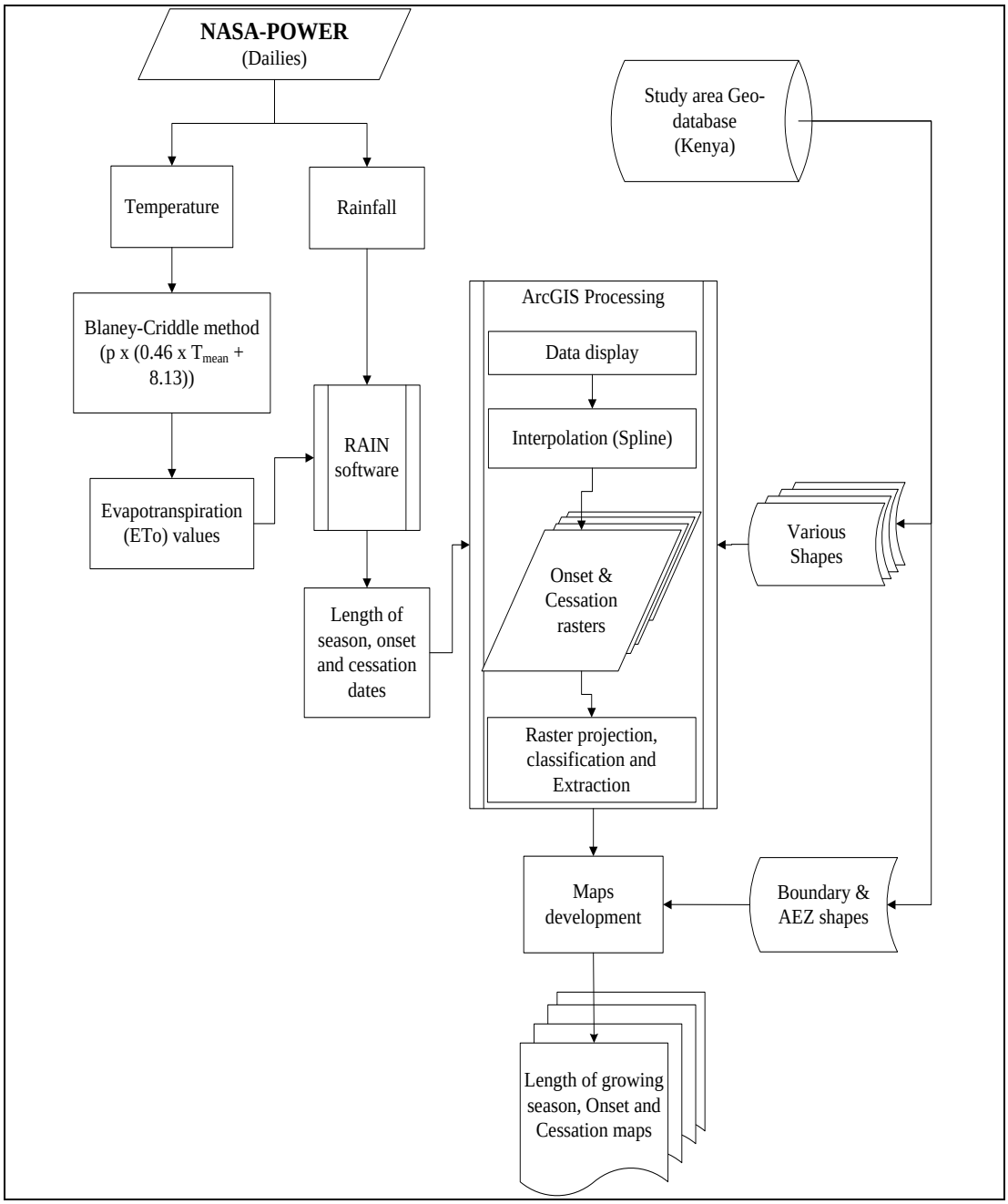

Figure 3.7: Flowchart showing the methodology followed in developing onset and cessation maps (Source: Author, 2018)

CHAPTER FOUR

RESULTS AND DISCUSSIONS

4.1 Overview

This chapter presents the findings of this study and the discussion following the studies objectives. In particular, the chapter contains results and discussions on (a) evaluation of accuracy of long-term precipitation products for improved agricultural productivity in Kenya, (b) quantification of soil greenhouse gases under different soil fertility treatments in semi-arid area of central highlands of Kenya, (c) calibration, validation and evaluation of the ability of DNDC model in simulating soil greenhouse gases based on different soil fertility treatments and (d) the length of growing season, onset and cessation dates as per derived cropping calendar for the agricultural potential zones of Kenya.

4.2 Long-term satellite-derived precipitation products for improved agricultural productivity in Kenya

4.2.1 Annual average rainfall based on monthly totals

From cell to cell summary of the five layers of data sources for the multi-year mean of monthly rainfall totals, using band collection analysis, it was established that Kenya meteorological data (gauge) recorded the highest minimum rainfall amount (19.4 mm) in a cell while the GPCC recorded the least minimum amount of data (4.0 mm). The TRMM product, on the other hand, recorded the highest amounts of maximum rainfall (217.9 mm) in a cell while LARC-POWER recorded the lowest amount of maximum rainfall (159.7 mm) in a cell. The average highest amounts recorded per cell was obtained from the gauge data (69.0 mm) while the lowest average recorded per cell was from the GPCC data source at 30.2 mm (Figure 4.1).

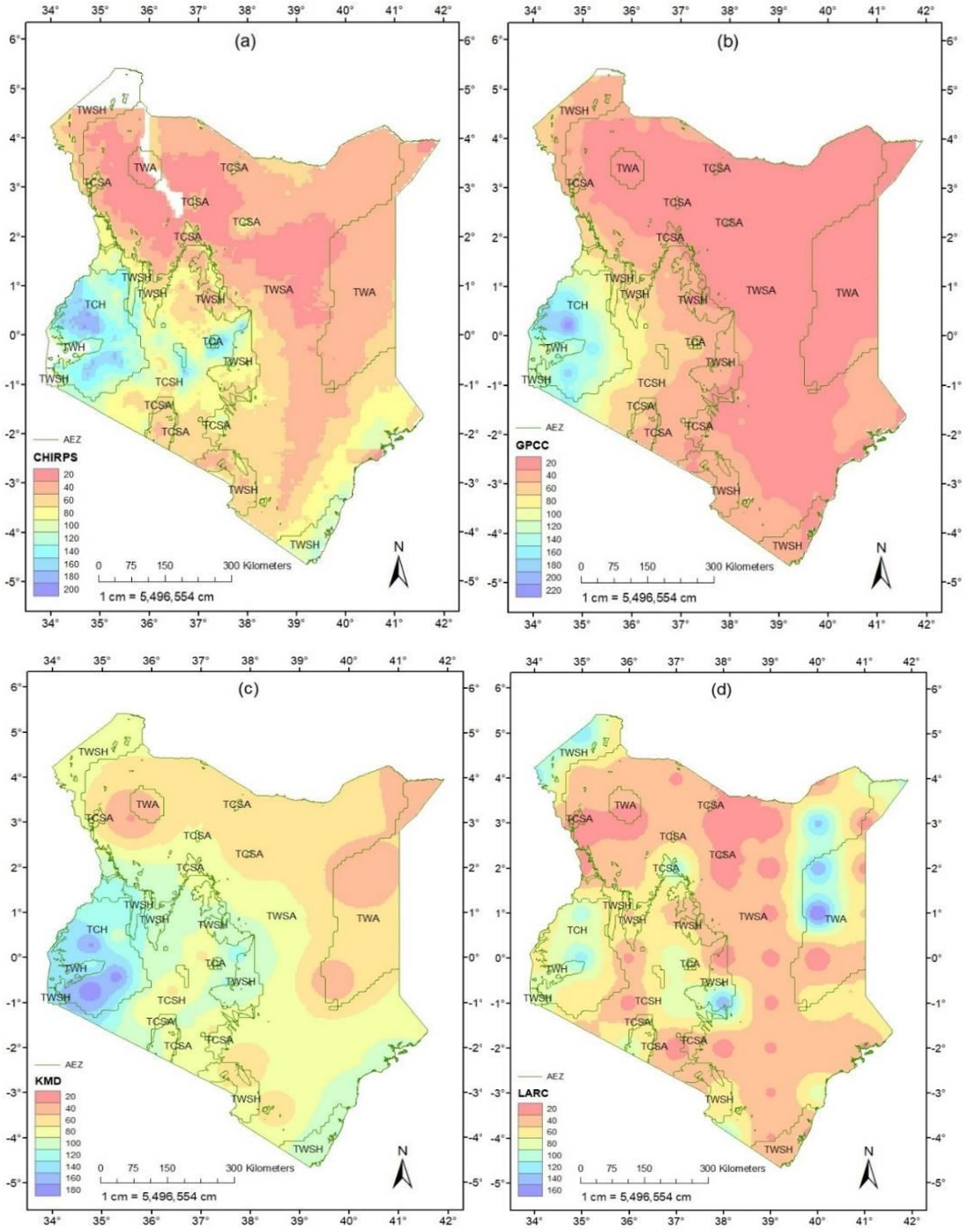
(a)
(b)
(c)
(d)
AEZ
CHIRPS
GPCC
KMD
LARC
20
40
60
80
100
120
140
160
180
200
220
0 75 150 300 Kilometers
1 cm = 5,496,554 cm
N
TWSH
TWA
TCSA
TWSA
TCH
TWH
TCA
TCSH

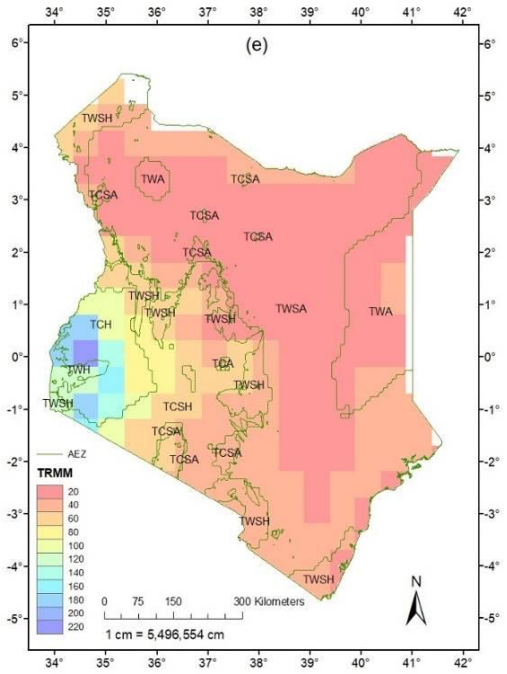

Figure 4.1: Comparison (Multi-year mean of monthly rainfall totals) of satellite products and Kenya meteorological data (gauge) from 1998-2013. In (a) CHIRPS 2.0; (b) GPCC; c) Kenya Meteorological (gauge); d) LARC-POWER; and e) TRMM data.

4.2.2 Statistical analysis between satellite-derived products and gauge data

Mean Error (ME)

Mean error was used to determine the level at which the satellite products tended to either overestimate or underestimate rainfall amounts across the agro-ecological zones of Kenya. It was established that all the satellite sources both overestimated and underestimated the rainfall amounts across the Kenyan agro-ecological zones. As indicated in figure 4.2 below, CHIRPS data source tended to overestimate rainfall amounts mainly in the tropical cool humid (TCH), tropical warm arid (TWA), tropical cool arid (TCA), tropical cool sub-humid (TCSH), and tropical cool sub-humid (TCSH) zones of Kenya. However, it tended to underestimate rainfall amounts in the tropical warm semiarid (TWSA) zone. The GPCC satellite product tended to overestimate rainfall amounts in the tropical warm humid (TWH), tropical cool humid (TCH) and tropical warm arid (TWA) but tended to underestimate rainfall amounts in

the tropical warm sub-humid (TWSH) and tropical warm semiarid (TWSA). The LARC-POWER satellite product tended to overestimate rainfall amounts in the tropical warm arid (TWA) and tropical warm semiarid (TWSA) (Figure 4.2). However, LARC-POWER products tended to underestimate rainfall amounts in the tropical cool humid (TCH), tropical warm sub-humid (TWSH), and tropical warm humid (TWH). The TRMM satellite product tended to overestimate rainfall amounts in the tropical cool humid (TCH), tropical warm humid (TWH) and tropical warm arid (TWA). It, however, tended to underestimate rainfall amounts in the tropical cool semiarid (TCSA), tropical warm sub-humid (TWSH) and tropical warm semiarid (TWSA) zones of Kenya (Figure 4.2).

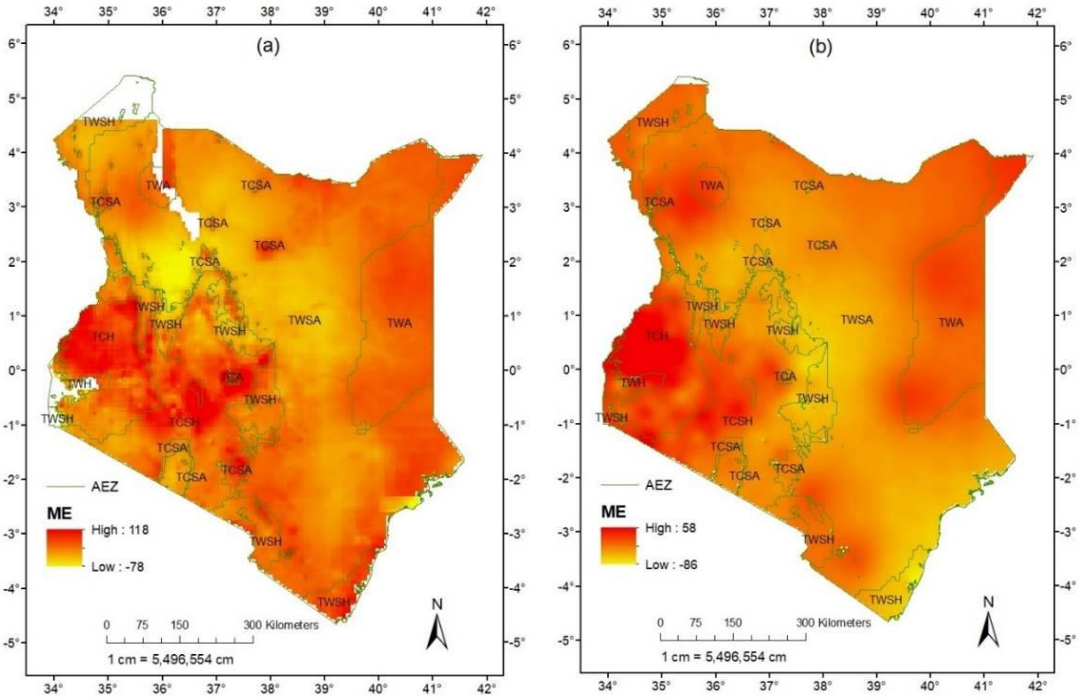

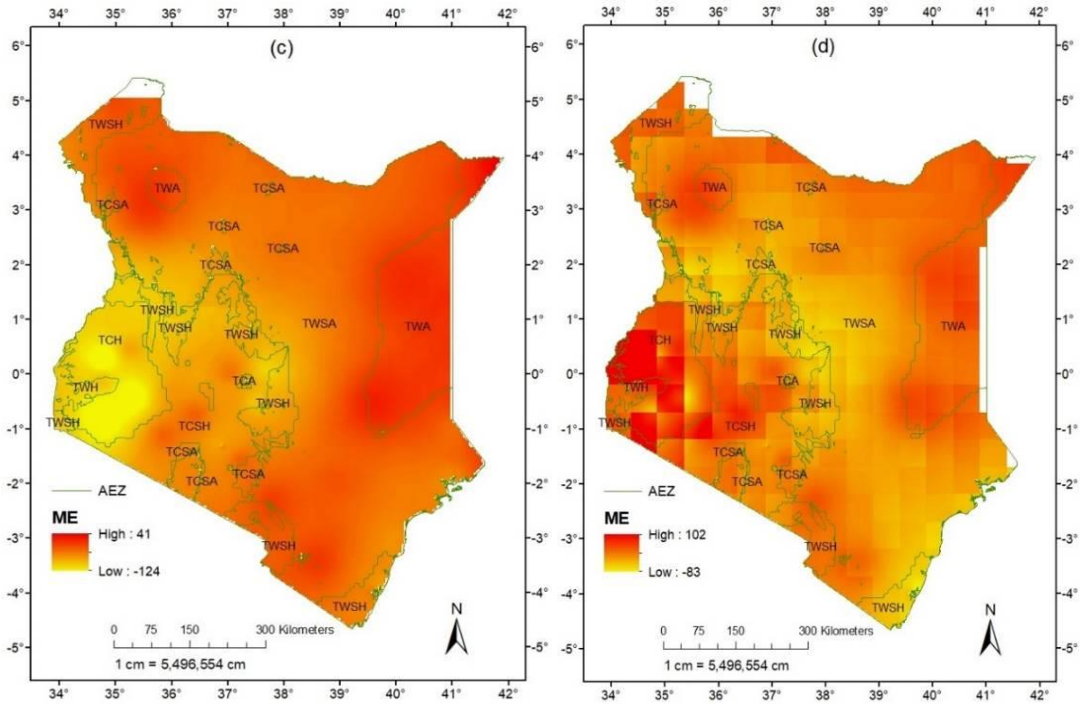

Figure 4.2: Comparison (Mean Error) of satellite products and Kenya meteorological data from 1998-2013. In (a) CHIRPS 2.0; (b) GPCC; c) LARC-POWER; and d) TRMM data.

Mean Squared Error (MSE)

In terms of variations in the differences, each product predicted the variations differently across the agro-ecological zones. For CHIRPS data, the variations were high in the tropical cool arid (TCA) but low in the tropical cool humid (TCH). The GPCC product exhibited the highest variations in the tropical warm semiarid (TWSA) but low variations in the tropical cool humid (TCH). The LARC-POWER product showed the highest variation in the tropical cool humid (TCH) and tropical warm humid (TWH) but less variations in the tropical cool arid (TCA). The TRMM product had the highest variation in the tropical warm sub-humid (TWSH) but less differences in the tropical cool humid (TCH) and tropical warm humid (TWH) (Figure 4.3).

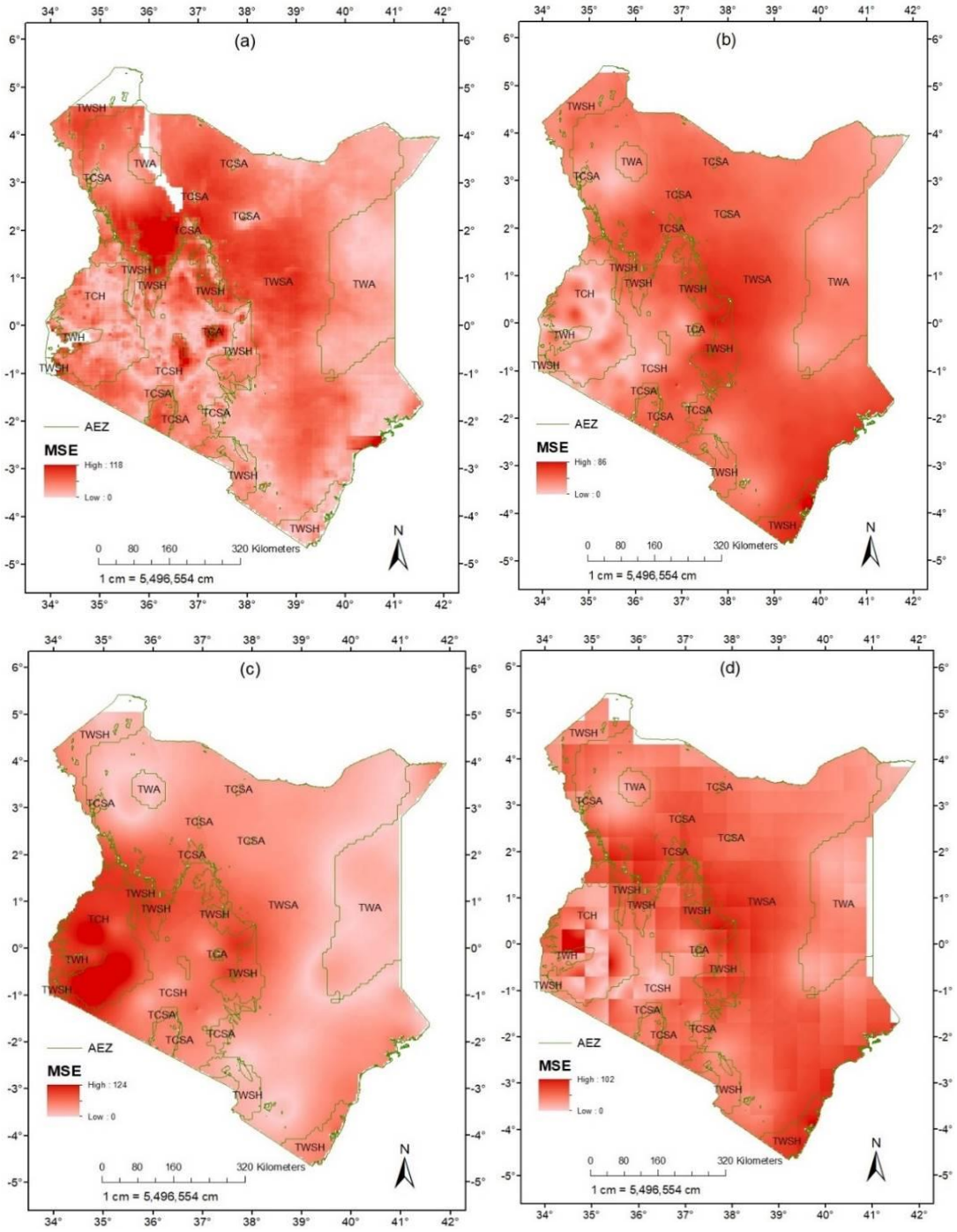

Figure 4.3: Comparison (Mean Squared Error) of satellite products and Kenya meteorological data from 1998-2013. In In (a) CHIRPS 2.0; (b) GPCC; c) LARC-POWER; and d) TRMM data.

Root Mean Square Error (RMSE)

The overall performance of the satellite products was assessed using the root mean square of error (RMSE). It was observed that the four products performed generally the same with RSME from CHIRPS data being in the range of 0-11 mm, GPCC ranged between 0-9 mm, LARC-POWER ranged between 0-11 mm, while TRMM had an RSME ranging between 0-10 mm across the Kenyan agro-ecological zones (Figure 4.4).

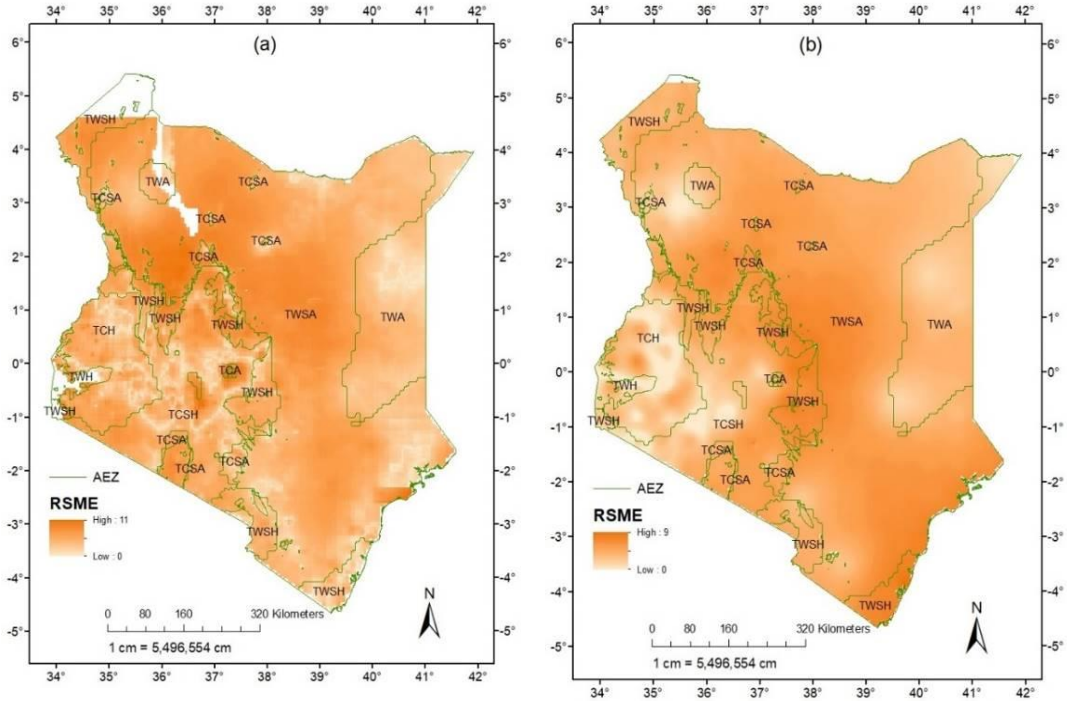

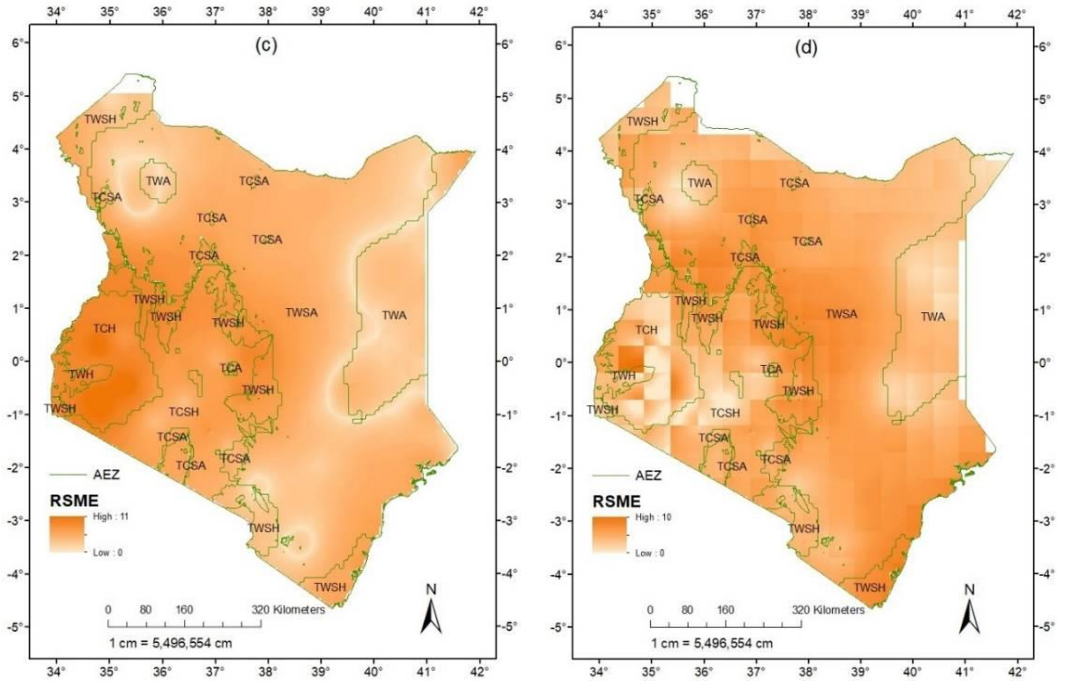

Figure 4.4: Comparison (Root Mean Square Error) of satellite products and Kenya meteorological data from 1998-2013. In (a) CHIRPS 2.0; (b) GPCC; c) LARC-POWER; and d) TRMM data.

Relative Root Mean Square Error (RRMSE)

To further confirm the reliability of the satellite data, relative root mean square error (RRMSE) which is the root mean squared error (RMSE) normalised by the arithmetic mean of the data was performed on the satellite products following Baidu et al. (2017). The results indicate very low RRMSE values of less than 0.4 mm identified in most cells over the country and which confirms a relatively good agreement between the observed gauge data and the satellite data. The TRMM data had the lowest RRMSE value of between 0 - 0.16 mm while LARC had the highest RRMSE value of 0 - 0.3 mm (Figure 4.5).

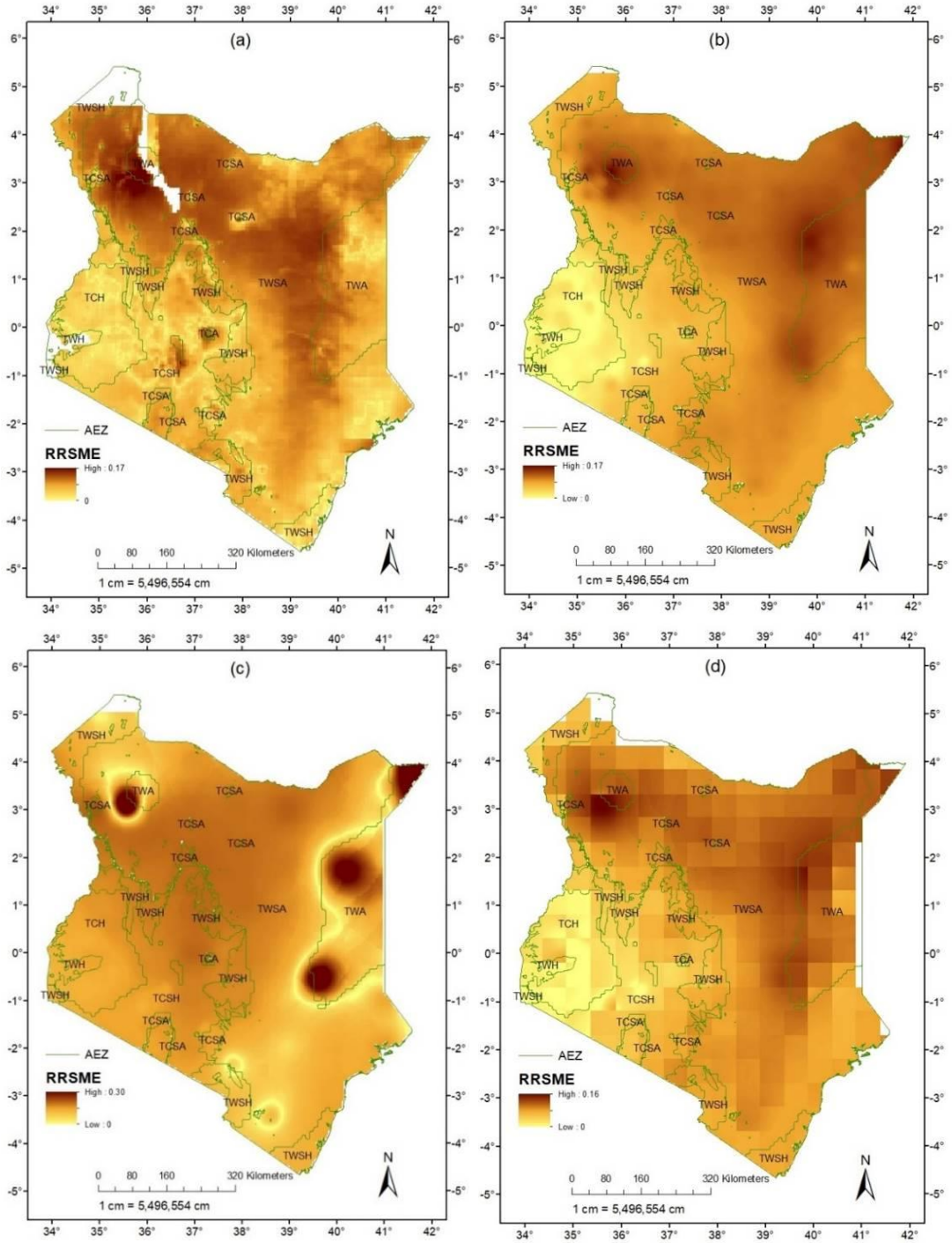

Figure 4.5: Comparison (Relative Root Mean Square Error) of satellite products and Kenya meteorological data from 1998-2013. In (a) CHIRPS 2.0; (b) GPCC; c) LARC-POWER; and d) TRMM data.

Mean Absolute Error (MAE)

To further understand the reliability of the satellite rainfall products, the satellite products were subjected to mean absolute error (MAE). The MAE avoids outlier compensation effects, whereby overestimation at one gauge may cancel out the underestimation at another (leading to underestimation of the true error) (Müller & Thompson, 2013). From the findings, LARC had the highest mean absolute error of 1.94, followed by CHIRPS at 1.65, followed by GPCC product with 0.93 error while TRMM had the lowest mean absolute error of 0.91 (Figure 4.6).

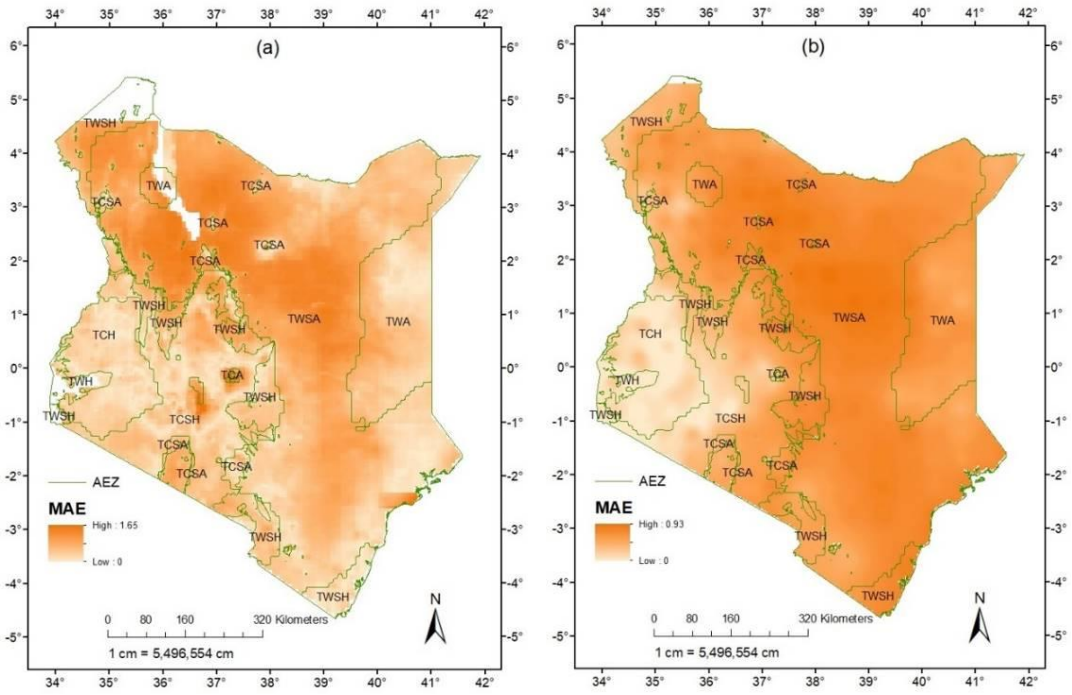

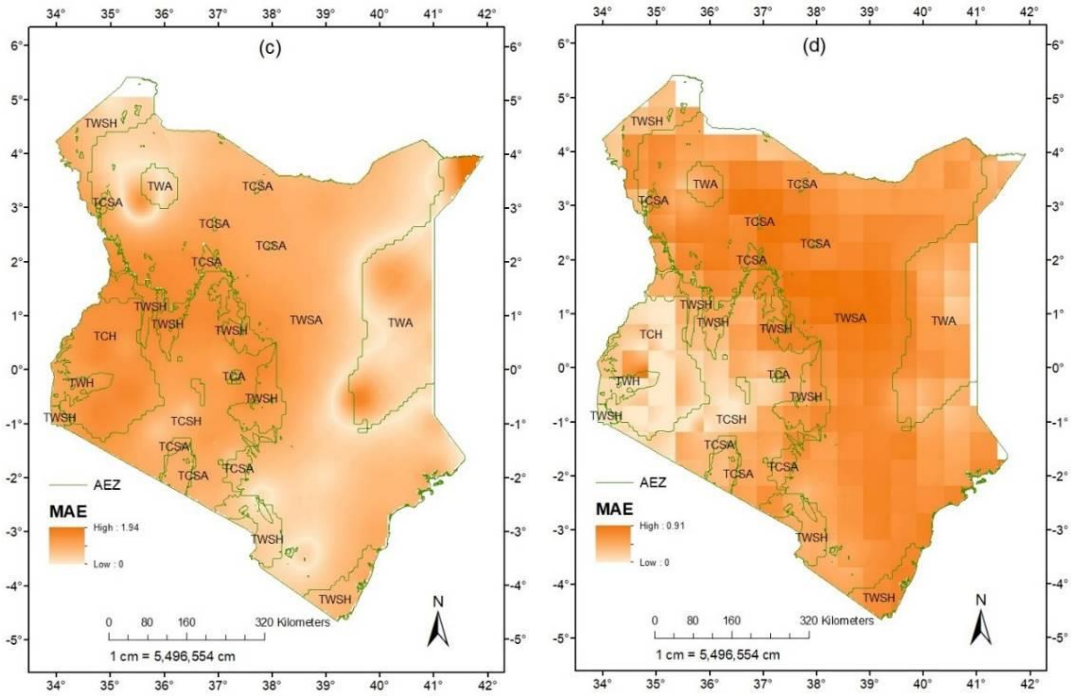

Figure 4.6: Comparison (Mean Absolute Error) of satellite products and Kenya meteorological data from 1998-2013. In (a) CHIRPS 2.0; (b) GPCC; c) LARC-POWER; and d) TRMM data.

Bias

The data was further analysed using multipliable bias. Results indicate that the satellite products had both positive and negative bias. They all scored relatively the same with a positive bias in the range of (0.91-0.93). However, in terms of the negative bias, the satellite products performed differently with the LARC-POWER having a bias of 3.55 while GPCC had a negative bias of 0.38 (Figure 4.7).

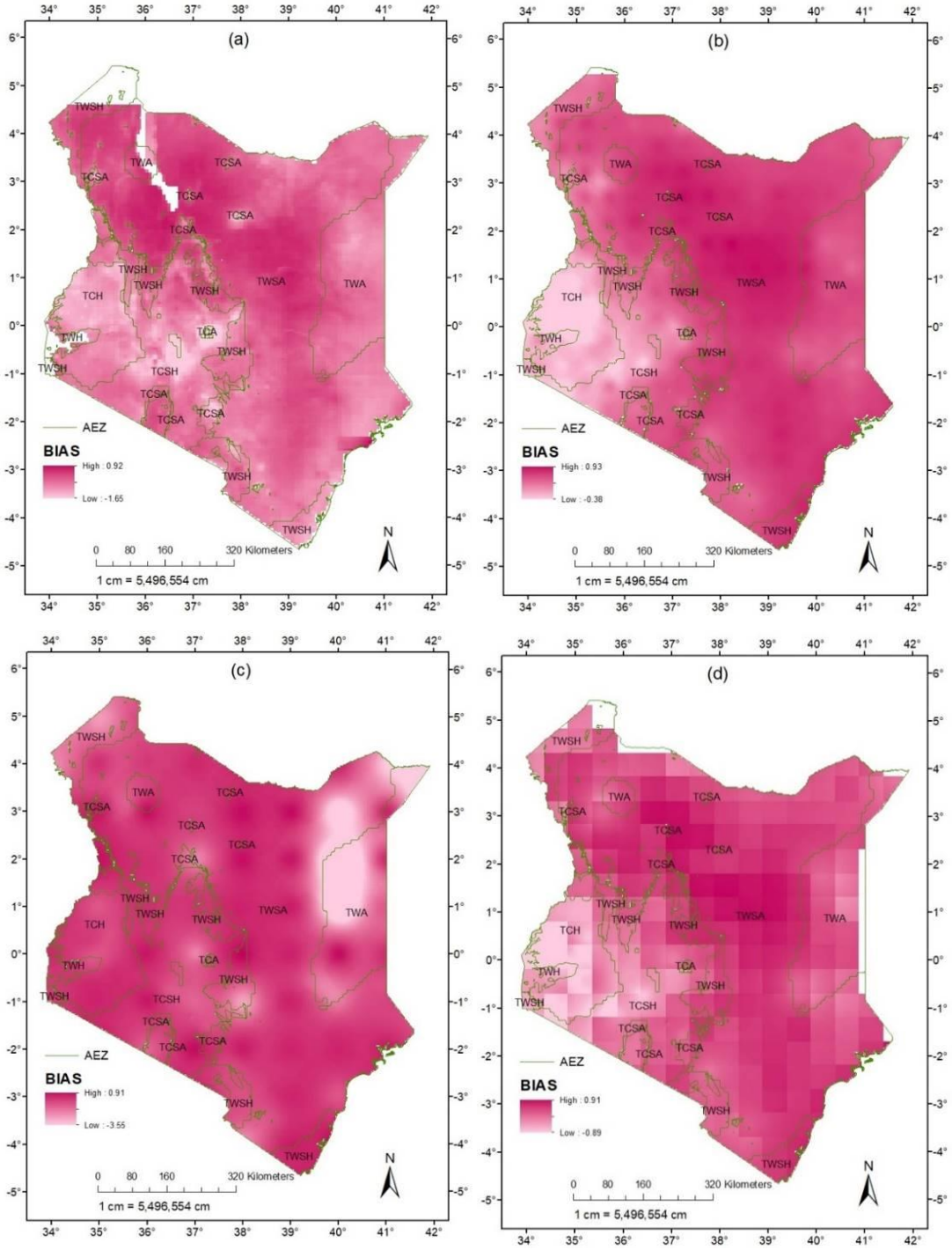

Figure 4.7: Comparison (Bias) of satellite products and Kenya meteorological data from 1998-2013**.** In (a) CHIRPS 2.0; (b) GPCC; c) LARC-POWER; and d) TRMM data.

Efficiency

The datasets were subjected to efficiency test to ascertain how efficient the satellite products were in predicting the rainfall over Kenya. From the results, all the

predictions from the satellite products were highly efficient ranging from 0.91 to 1 across the various agro-ecological zones of Kenya (Figure 4.8).

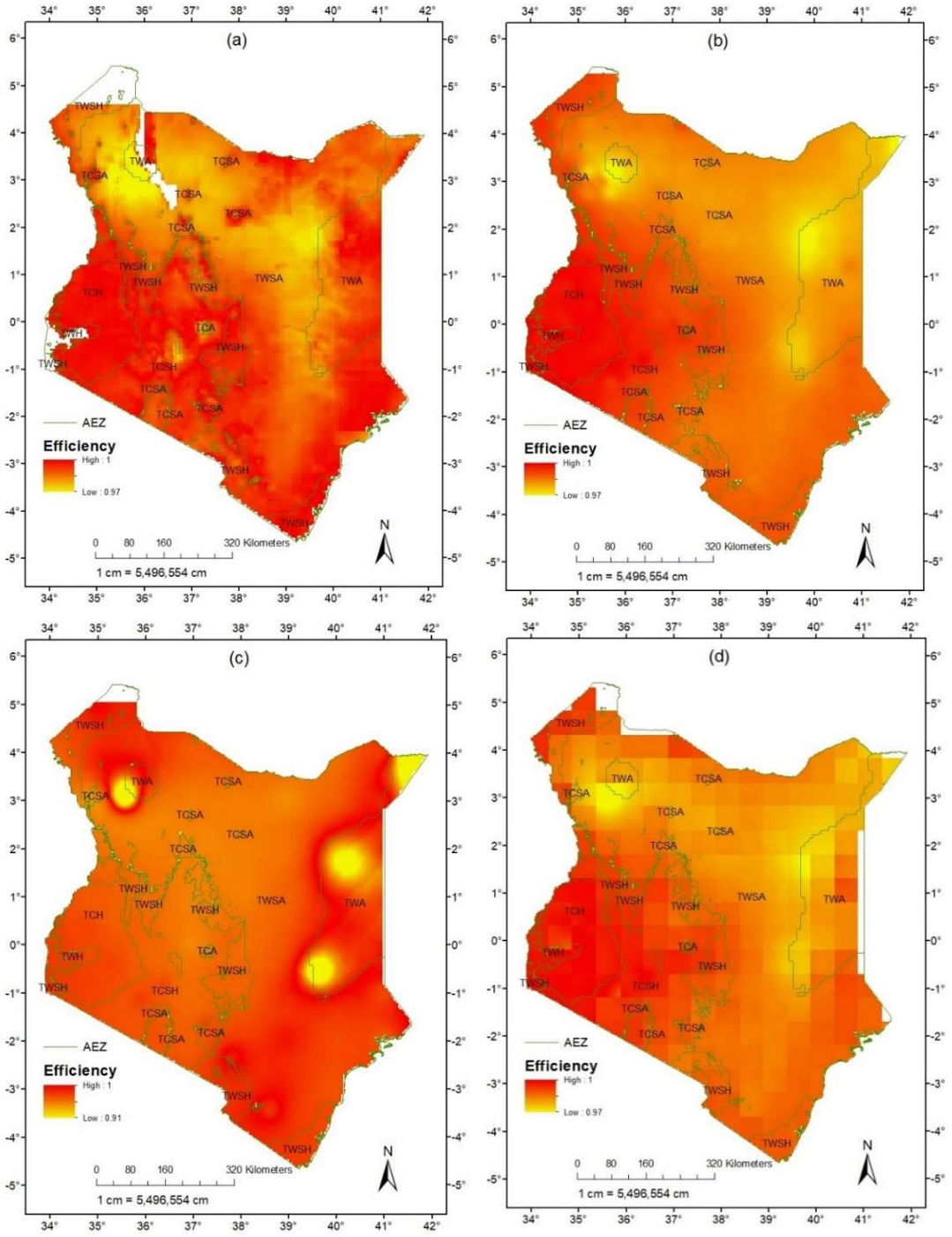

Figure 4.8: Comparison (Efficiency) of satellite products and Kenya meteorological data from 1998-2013. In (a) CHIRPS 2.0; (b) GPCC; c) LARC-POWER; and d) TRMM data.

Pearson's Correlation

Correlation analysis based on the various Kenyan agro-ecological zones reveals discrete differences among the satellite products. The CHIRPS 2.0 satellite product had the highest, though weak, correlation coefficient ($r^2 = 0.33$) in predicting rainfall in the tropical warm arid (TWA) which is the zone receiving the least amounts of rainfall in Kenya. The LARC-POWER satellite product had the highest correlation coefficient ($r^2 = 0.97$) in predicting rainfall in the tropical cool arid (TCA) zone, which is the highest altitude zone on the peak of Mt Kenya ($r^2 = 0.97$), as well as the tropical cool semiarid (TCSA) with a correlation coefficient of $r^2 = 0.53$. The GPCC products had the highest correlation coefficient for the tropical warm semiarid (TWSA) ($r^2 = 0.46$) and tropical warm sub-humid (TWSH) ($r^2 = 0.21$). The TRMM satellite product had the highest correlation coefficient in predicting rainfall in the tropical cool humid (TCH) ($r^2 = 0.64$), tropical cool sub-humid (TCSH) ($r^2 = 0.39$) and tropical warm humid (TWH) (0.58) (Table 4.1).

Table 4.1: Point to point Pearson's correlation coefficient (r) between Kenya meteorological data and satellite products across the various agroecosystems of Kenya between 1998 and 2013

	AEZ[1]	CHIRPS[2]	GPCC[3]	LARC-POWER[4]	TRMM[5]
1	TCA	0.04	0.52	0.97	*
2	TCH	0.40	0.61	0.05	0.64
3	TCSA	0.01	0.30	0.53	0.35
4	TCSH	0.15	0.25	0.01	0.39
5	TWA	0.33	0.28	0.22	0.15
6	TWH	0.08	0.31	0.38	0.58
7	TWSA	0.32	0.46	0.05	0.06
8	TWSH	0.05	0.21	0.16	0.08

*Could not be computed due to the similarity in the rainfall amounts in the point data under TRMM satellite product.

[1] AEZ (Agroecological zones): TCA = tropical cool arid, TCH = tropical cool humid, TCSA = tropical cool semiarid, TCSA = tropical cool subhumid, TWA = tropical

warm arid, TWH = tropical warm humid, TWSA = tropical warm semiarid, and TWSH = tropical warm subhumid

Mean performance of the rainfall products

The CHIRPS product generally performed better than the rest of the satellite in predicting rainfall across the agro-ecological zones of Kenya. It, however, overestimated rainfall in the tropical cool arid (TCA) zone and slightly in the tropical cool humid (TCH) zone but underestimated in the rest of the zones. The GPCC product generally underestimated rainfall in all agro-ecological zones of Kenya. The LARC-POWER product overestimated rainfall in the tropical warm arid (TWA) zone but underestimated in the rest of the zones. The TRMM product overestimated rainfall in tropical warm humid (TWH) zone while underestimating rainfall in the rest of the zones (Table 4.2).

Table 4.2: Mean (± standard deviation (SD)) performance of Kenya meteorological data and satellite products across the various agroecosystems of Kenya between 1998 and 2013

	AEZ[1]	KMD[2]	CHIRPS[3]	GPCC[4]	LARC-POWER[5]	TRMM[6]
1	TCA	76.98 ± 2.02	134.92 ± 3.71	44.38 ± 1.76	59.67 ± 1.59	35.97 ± 0.00
2	TCH	126.76 ± 21.75	127.65 ± 20.75	46.77 ± 31.34	61.52 ± 15.35	122.50 ± 44.40
3	TCSA	67.73 ± 10.19	54.39 ± 16.84	25.73 ± 9.62	39.08 ± 20.48	25.80 ± 11.54
4	TCSH	83.62 ±15.20	74.70 ± 23.09	46.77 ± 22.42	44.36 ± 16.10	48.17 ± 23.02
5	TWA	39.45 ± 7.82	29.49 ± 7.80	13.34 ± 3.21	56.56 ± 33.50	33.50 ± 4.63
6	TWH	130.86 ± 5.66	113.21 ± 16.70	123.48 ± 16.04	65.32 ± 13.39	136.17 ± 36.28
7	TWSA	60.48 ± 13.97	34.35 ± 17.26	15.92 ± 6.94	34.10 ± 17.76	17.87 ± 7.92
8	TWSH	79.44 ± 15.31	58.75 ± 16.48	32.35 ± 25.51	52.87 ± 16.19	33.81 ± 21.50

[1] AEZ (Agroecological zones): TCA = tropical cool arid, TCH = tropical cool humid, TCSA = tropical cool semiarid, TCSA = tropical cool sub-humid, TWA = tropical warm arid, TWH = tropical warm humid, TWSA = tropical warm semiarid, and TWSH = tropical warm sub-humid

[2] KMD = Kenya meteorological department

[3] CHIRPS = Climate Hazards Group InfraRed Precipitation with Station

[4] GPCC = Global Precipitation Climatology Center

[5] LARC-POWER = National Aeronautics and Space Administration-Prediction Of Worldwide Energy Resource

[6]TRMM = Tropical Rainfall Measuring Mission (TRMM) Multi-satellite Precipitation Analysis (TMPA) 3B42 version 7

4.2.3 Overall performance of satellite-derived precipitation products

Overall the four satellite products (CHIRPS, GPCC, TRMM and LARC-POWER) captured most of the Kenyan regional variations in terms of the rainfall distributions as reflected in the different agro-ecological zones. The rainfall estimates were reasonably comparable to the ground-based rainfall observations with instances of both underestimation and overestimations. The accuracy in estimating rainfall for most of the satellite products (apart from LARC-POWER which portrayed an inverse relationship), tended to be high in agro-ecological zones that received high amounts of rainfall as compared to the zones that generally received low amounts of rainfall. These agro-ecological zones that received the highest amounts of rainfall are the humid zones along the Lake Victoria basin (tropical cool humid (TCH) and tropical warm humid (TWH)). The agro-ecological zones that received low amounts of rainfall were the arid and semiarid zones including tropical warm arid (TWA), tropical warm semiarid (TWSA) and tropical cool semiarid (TCSA). These results agree with Zambrano et al. (2017) in a study in Chile who noted that the accuracy of satellite products was highly dependent on the amount of monthly rainfall with the best results found during winter seasons and in zones (Central to South) with higher amounts of precipitation. The results also agree with Paredes-Trejo et al. (2016) who noted that the coherence between satellite rainfall estimates and station observations is moderately high along the rainy season, but shows a marked underestimation during the driest period.

Generally in terms of performance, CHIRPS rainfall product underestimated rainfall in six (6) out of eight (8) agro-ecological zones, TRMM and LARC-POWER rainfall products underestimated rainfall in seven (7) out of eight (8) agro-ecological zones

while GPCC rainfall product underestimated rainfall in all (eight out of eight) agro-ecological zones of Kenya. However, based on point to point analysis, the four satellite products used for this study (CHIRPS, GPCC, TRMM and LARC-POWER) both overestimated and underestimated the rainfall amounts over Kenya. This discrepancies in estimations could be as a result of the satellite having errors between the observations and precipitation estimates. The satellite-based rainfall estimates have random errors and non-negligible bias due to lack of direct relation between observation and precipitation as well as due to inadequacy in sampling and algorithm imperfections (Toté et al., 2015; Rossi et al., 2017; Shrestha et al., 2017). It could also be attributed to errors during collecting and digitising gauge data, especially while using manual methods which introduce uncertainties in the observed data as was noted by Satgé et al. (2016).

It was observed that the zones at the peak of Mt. Kenya and Mt. Elgon (tropical cool arid (TCA)), as well as most of the low-lying arid and semiarid agro-ecological zones of Kenya, had the highest variation in terms of rainfall amounts. According to Ochoa et al. (2014), the critical challenges in the estimation of precipitation from satellites estimates arise from the processing scheme for a microwave (MV) and infrared (IR) data with the major problem with IR data processing being that the global algorithms do not consider the altitude of the agrometeor. The underestimation over the mountainous region is ascribed to the warm orographic rain process, while the overestimations over the dry regions may be because of sub-cloud evaporation (Dinku et al., 2011). The variations in rainfall estimations in the dry areas could also be attributed to rainfall suppression by desert aerosols and surface effects among other error sources that severely affect satellite rainfall estimation in drier parts of the

continent (Awange et al., 2016). However, as was observed by Tesfaye et al. (2017) CHIRPS is less affected by variation in elevation.

The CHIRPS product tended to overestimate the rainfall amounts mainly in the zones that generally received high amounts of rainfall both orographic, especially on the peak of Mt. Kenya (tropical cool arid (TCA)). The CHIRPS product tended to slightly overestimate rainfall in areas that received convectional rainfall, particularly the L. Victoria basin (tropical warm humid (TWH) and tropical cool humid (TCH)) zones. The CHIRPS data equally underestimated the rainfall amounts mainly in the zones that generally received low amounts of rainfall and whose climatic conditions are majorly arid to semiarid. The underestimation was more pronounced in the tropical warm semiarid zone (TWSA). These results disagree with a study carried out by Paredes-Trejo et al. (2016) in Venezuela using CHIRPS 2.0 data which noted that the CHIRPS data tended to overestimate the lower monthly rainfall values and underestimate higher rainfall values. The results, however, agree with Zambrano et al. (2017) and Bai et al. (2018) who identified that CHIRPS product has low capacity in estimating rainfall amounts in areas that receive low rainfall amounts. Analysis based on the spatial context show that the CHIRPS 2.0 data tended to inaccurately predict rainfall amounts in the high elevation to rugged mountainous zones (e.g., Mt. Kenya). It however accurately predicted the rainfall amounts in regions which are relatively low-lying to flat regions (e.g., Lake Victoria basin which majorly relies on conventional rainfall). This agrees with Paredes-Trejo et al. (2016) and Shrestha et al. (2017) who identified the accuracy of the CHIRPS 2.0 data being high in predicting rainfall in the flat low-lying to open flat region but weak in predicting rainfall in the

high-elevation regions. These are regions where synoptic weather stations are mainly dominated by the ITCZ activity and local convective systems.

The GPCC satellite product tended to accurately predict rainfall across the agro-ecological zones with a relatively high level of agreement (over 20% agreement) with the ground-based gauge observation across the zones. These results are consistent with other studies carried out using GPCC data and which identified a substantial agreement between GPCC satellite product and the observed gauge observation (Manzanas et al., 2014; Asfaw et al., 2017; Baidu et al., 2017). There was, however, a slight overestimation of the rainfall amounts in some sections of the tropical warm humid (TWH), though the average rainfall in the zone was lower than observed rainfall. These are areas around the Lake Victoria basin and which generally received high amounts of rainfall and portrayed a strong correlation with observed rainfall data. This agrees with Jury (2017) in a study carried out in the Upper Zambezi catchment and whose findings identified a strong correlation between GPCC satellite data and observed rainfall. The GPCC product, however, underestimated (slightly) the prediction of rainfall amounts in zones that generally received low amounts of rainfall. These underestimations were majorly in the areas categorised as arid and semi-arid zones including tropical warm arid (TWA), tropical warm semiarid (TWSA) and the tropical cool semiarid (TCSA) and of which forms 80% of the Kenyan agro-ecological zones (FAO, 1996). The slight disparities (cell-cell) agrees with Baidu et al. (2017) who identified that the GPCC data tended to underestimate rainfall amounts in most parts of Ghana generally. Spatially the GPCC data was not accurate in predicting the rainfall amounts in both the lowlands and the Kenyan highlands since it tended to underestimate the rainfall amounts in these zones.

The TRMM data accurately and qualitatively predicted rainfall over Kenya and relatively agreed with observed gauge data. The results concur with Meng et al. (2014) who noted that the monthly TRMM data have a much better linear relationship with the gauge rainfall data with a high determination coefficient. The TRMM data was however not as accurate in predicting rainfall amounts in areas that generally received high amounts of rainfall (e.g., Lake Victoria basin and particularly the tropical warm, humid (TWH) zone) since they tended to overestimate rainfall amounts in these agro-ecological zones. There was a strong correlation between the TRMM product and observed rainfall data in the tropical cool humid (TCH) which is a zone around Lake Victoria and generally received high amounts of rainfall. These results disagree with Katsanos et al. (2016) and Ouatiki et al. (2017) who identified TRMM product tending to, in general, overestimate rainfall in dry regions and underestimate rainfall in the humid areas, which are usually located at the highest elevations. However, according to Shrivastava et al. (2014), the TRMM data captures rainfall distribution qualitatively, but there exist differences in quantities of predicted rainfall with respect to ground observations. The TRMM satellite data tended to improve accuracy with increase in rainfall amounts particularly in tropical warm humid (TWH) and tropical cool humid (TCH); which are influenced by convective rainfall system around the Lake Victoria basin. These results are consistent with studies carried out by Robbins (2016) and Prakash et al. (2016) who noted an increase in performance with an increase in precipitation accumulation for the TRMM product.

Just like the GPCC data, the TRMM underestimated the prediction of rainfall amounts mainly in the arid and semiarid agro-ecological zones that received lower rainfall amounts and which forms 80% of the Kenyan agro-ecological zones (tropical warm

arid (TWA), tropical cool arid (TCA), tropical warm semiarid (TWSA), tropical cool semiarid (TCSH) and tropical warm sub-humid (TWSH)) (FAO, 1996). These results agree with Shrivastava et al. (2014), Meng et al. (2014) and Dhib et al. (2017) who identified that the TRMM prediction on rainfall was slightly lower (underestimates) than the observed gauge data in most parts of the study area. The TRMM data was found accurate in estimating rainfall in the lowlands zones of the Lake Victoria (tropical cool humid (TCH)) and which majorly receives convectional rainfall but could not accurately predict rainfall amounts in the Kenyan highlands/mountainous zones due to similarity in the data resulting from the coarse spatial resolution (0.5° x 0.5°), for the small area covered by the tropical cool arid (TCA) zone. According to Rossi et al. (2017), the TRMM data fails to accurately capture the rainfall amounts in the mountainous areas with a high level of underestimations.

The NASA LARC-POWER product tended to underestimate rainfall amounts in the regions such as Lake Victoria basin which generally received high rainfall amounts (tropical warm humid (TWH)). This observation is inverse to the predictions by the three other satellite products which had a high correlation in predicting rainfall in these zones that received high amounts of rainfall. The LARC-POWER data tended to overestimate rainfall amounts in zones characterised with arid and semiarid climatic conditions and particularly the tropical warm arid (TWA) zone where it predicted 44% higher than observed. The LARC-POWER data tended to closely predict rainfall amounts in the high elevation to rugged mountainous zones (e.g., Mt. Kenya) though it inaccurately predicted the rainfall amounts in regions which are relatively low-lying to flat regions (e.g., Lake Victoria basin and along the Kenyan coastal line). These results agree with White et al. (2008) who noted that LARC-POWER product

performs well in regions with a short distance of comparison and where coastal conditions are not involved due to the inherent local variability of weather data.

4.3 Soil GHG fluxes from maize production in semi-arid lands of central highlands of Kenya

4.3.1 Field meteorological and site observations

The total annual precipitation for the study period, between 6th February 2017 and 7th February 2018, was 704 mm. The total rainfall for season one (LR 2017 - February to July 2017), was 304 mm with 64% (194 mm) received in April coinciding with the onset of the long rains. For season two (SR 2017 - October 2017 to February 2018), total rainfall was 400 mm with 96% (384.5 mm) occurring during the first month (19th October to 18th November 2017) after the onset of short rains. Air temperature for the entire year ranged from 19.9 to 27.5 °C (mean= 23.4±0.14°C) (Figure 4.9 a), soil temperature ranged from 27.2 and 38.4°C (mean = 32.6±0.39°C) (Figure 4.9 a), relative humidity ranged from 41 to 90% (mean = 64±0.5%) (Figure 4.9 b) while solar radiation ranged from 50.7 and 345.9 Wm^{-2} (mean = 251.1±3.32 Wm^{-2}) (Figure 4.9 c).

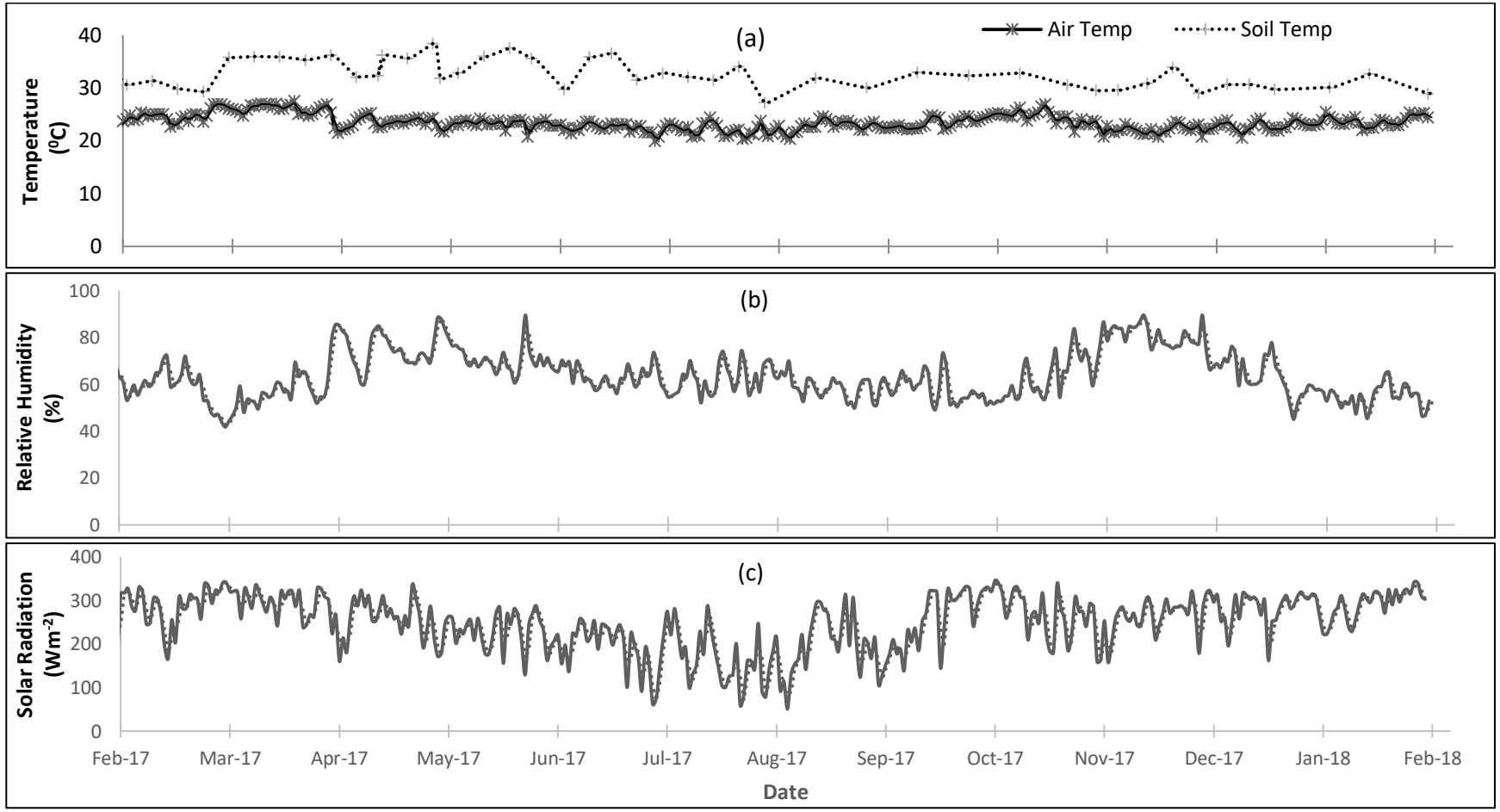

Figure 4.9: Field meteorological and site observations (a) Soil and air temperature (^{0}C), (b) relative humidity (%) and (c) solar radiation (Wm^{-2}) for the study site in Machang'a secondary in Embu County between February 2017 and February 2018

The soils were predominantly neutral with C concentrations ranging from 0.5 to 1.5% and N concentrations ranging from 0.09 to 0.14%, (Table 4.3). The C/N ratio ranged from 6.17 to 11.00 (mean = 8.3±0.55) while bulk density ranged from 1.26 to 1.40 g cm^{-3} (Table 4.3).

Table 4.3: Soil properties for 0 to 20 cm depth for different treatments in ASAL lands of Embu County, Kenya

Treatments[1]	**C content (%)**	**N content (%)**	**C/N ratio**	**pH in water**	**Bulk density (g cm^{-3})**
Control	0.54^{c} [2]±0.01	0.09^{b}±0.01	6.17^{c}±0.23	5.9^{b}±0.50	1.40^{a}±0.01
In. Fert.	0.71^{c}±0.03	0.09^{b}±0.01	7.89^{c}±0.29	6.1^{b}±0.11	1.39^{a}±0.03
Manure	1.54^{a}±0.39	0.14^{a}±0.03	11.00^{a}±0.96	8.0^{a}±0.15	1.26^{b}±0.03
Manure + In. Fert.	1.18^{b}±0.20	0.14^{a}±0.02	8.40^{ab}±0.69	7.8^{a}±0.65	1.28^{b}±0.02
P value	*0.003*	*0.003*	*<0.001*	*<0.001*	*<0.001*

[1] Treatment abbreviation: Control = no external input, In. Fert. = inorganic fertiliser (60 kg N ha^{-1} from NPK at N=23%, P=23% and K=0%); Manure = animal manure applied at 60 kg N ha^{-1}; Manure + In. Fert. = combination of animal manure at half rate (30 kg N ha^{-1}) and inorganic fertiliser at half rate (30 kg N ha^{-1})

[2] Same superscript letters in the same column denote no significant difference between the treatment means

The total grains' C, N and C/N did not significantly differ across treatments (Table 4.4). Total leaves' N (P<0.001) and C/N ratio (P=0.004) significantly differed across the treatments ranging between 0.9 and 1.67% (mean = 1.21±0.1) and 24.94 to 46.21 (mean = 41.07±2.7) respectively (Table 4.4). Total roots' N (P<0.027) and C/N ratio (P = 0.034) significantly differed across treatments and ranged between 0.95 and 1.42% (mean = 1.21±0.7), and 31.92 to 47.85 (mean = 38.36±3.1) respectively (Table 4.4). Total stems' C (P=0.023), N (P<0.007) and C/N (P = 0.001) ratio significantly differed across treatments ranging between 37.96 and 43.19% (mean = 40.94±0.2),

0.70 to 1.87% (mean = 1.29±0.7) and 21.44 to 60.51 (mean = 38.64±3.9) respectively (Table 4.4).

Table 4.4: Mean carbon and nitrogen content for maize plant components grown during the LR 2017 season under four different fertiliser treatments in Embu County, Kenya

Plant Component	Treatments[1]	C content (%)	N content (%)	C/N ratio
Grains	Control	43.41±0.23	2.05±0.08	21.20±0.98
	In. Fert.	43.37±0.10	2.26±0.00	19.21±0.09
	Manure	43.49±0.09	2.14±0.10	20.45±0.92
	Manure + In. Fert.	43.46±0.11	2.10±0.16	20.94±1.49
	P value[3]	*0.912*	*0.744*	*0.708*
Leaves	Control	41.15±0.56	0.96^{c}±0.11	43.95^{a}±4.95
	In. Fert.	40.89±0.42	0.90^{c}±0.06	46.21^{a}±3.87
	Manure	40.69±0.42	1.32^{b}±0.03	30.83^{ab}±0.66
	Manure + In. Fert.	41.53±0.39	1.67^{a}±0.08	24.94^{b}±1.36
	P value[3]	*0.606*	*<0.001*	*0.004*
Roots	Control	44.40±0.09	1.18^{b}±0.68	38.10^{a}±3.50
	In. Fert.	44.84±0.07	0.95^{b}±0.32	47.85^{a}±3.61
	Manure	44.88±0.06	1.27^{ab}±0.80	35.56^{a}±2.28
	Manure + In. Fert.	44.52±0.11	1.42^{a}±0.84	31.92^{ab}±2.92
	P value[3]	*0.947*	*0.027*	*0.034*
Stems	Control	43.19^{a}±0.19	0.99^{b}±0.47	46.82^{a}±7.73
	In. Fert.	41.93^{a}±0.04	0.70^{b}±0.52	60.51^{a}±2.97
	Manure	40.69^{a}±0.07	1.58^{ab}±0.09	25.80^{b}±1.21
	Manure + In. Fert.	37.96^{ab}±0.29	1.87^{a}±1.76	21.44^{b}±3.88
	P value[3]	*0.023*	*0.007*	*0.001*

[1] Treatment abbreviation: Control = no external input, In. Fert. = inorganic fertiliser (60 kg N ha^{-1} from NPK at N=23%, P=23% and K=0%); Manure = animal manure applied at 60 kg N ha^{-1}; Manure + In. Fert. = combination of animal manure at half rate (30 kg N ha^{-1}) and inorganic fertiliser at half rate (30 kg N ha^{-1})

[2] Same superscript letters in the same column denote no significant difference between the treatment means

[3] P value below the table represent significance difference across treatments

4.3.2 Soil GHG fluxes and ancillary information

Soil CH_4 fluxes were mostly negative across the four treatments with uptake rates ranging from 0 to 40 µg CH_4-C m^2 h^{-1} throughout the study period (Figure 4.10 a). Emissions as high as 50 µg CH_4-C m^2 h^{-1}, for CH_4 were obtained immediately after harvest (both during Feb 2017 and July 2017) (Figure 4.10 a). However, there was no increase in emissions after the February 2018 harvest. Planting during the SR 2017

season also stimulated emissions with fluxes up to 20 µg CH_4-C m^2 h^{-1} attained in the plots treated with inorganic fertilisers (Figure 4.10 a). This implies that upland soils in the study area predominantly acted as sinks for CH_4 fluxes. These results agree with other studies carried out on East African agricultural soils (Rosenstock et al., 2016; Pelster et al., 2017; Ortiz-Gonzalo et al., 2018). Soil CH_4 emissions depend on the net balance between the activities of methanogens and methanotrophs (Le Mer & Roger, 2001) and which are affected by environmental conditions (Cardenas et al., 2016).

The soil CH_4 fluxes remained relatively low throughout the year of study (Figure 4.10 a) possibly due to most of the months being generally dry which may have hindered the production of methane due to lack of anaerobic conditions. This could be attributed to the location of the study area, whereby it lies in a marginal area with soils being 60% sand, and receiving most (64% for LR 2017 and 96% SR 2017) of the rains in the first month of onset. The semi-arid conditions in the study area may have favoured methane uptake across treatments as was noted by Zona et al. (2013). As was observed by Subke et al. (2018), progressive drying of the soil increases soil pore connectivity and facilitates more rapid transport of CH_4 from the atmosphere to sites of methanotrophic activity.

Similarly, the low fluxes at the onset of the rains could be attributed to a counterbalance between CH_4 production by methanogens (due to increased anaerobic conditions) and CH_4 consumption by methanotrophs (due to soil disturbances during land preparation, manure incorporation and planting). According to Butterbach-Bahl and Papen (2002), low uptakes of CH_4 by the soils particularly during the rainy period could be attributed to high production of CH_4 due to increased soil water content as well as high CH_4 uptake due to increased aerobic activities, counteracting against each

other. As observed in other studies, approximately 80-100% of the CH_4 produced in soil by methanogenic archaea is consumed by methanotrophic bacteria at the soil surface as a source of C and energy (Sun et al., 2016; Serrano-Silva et al., 2014).

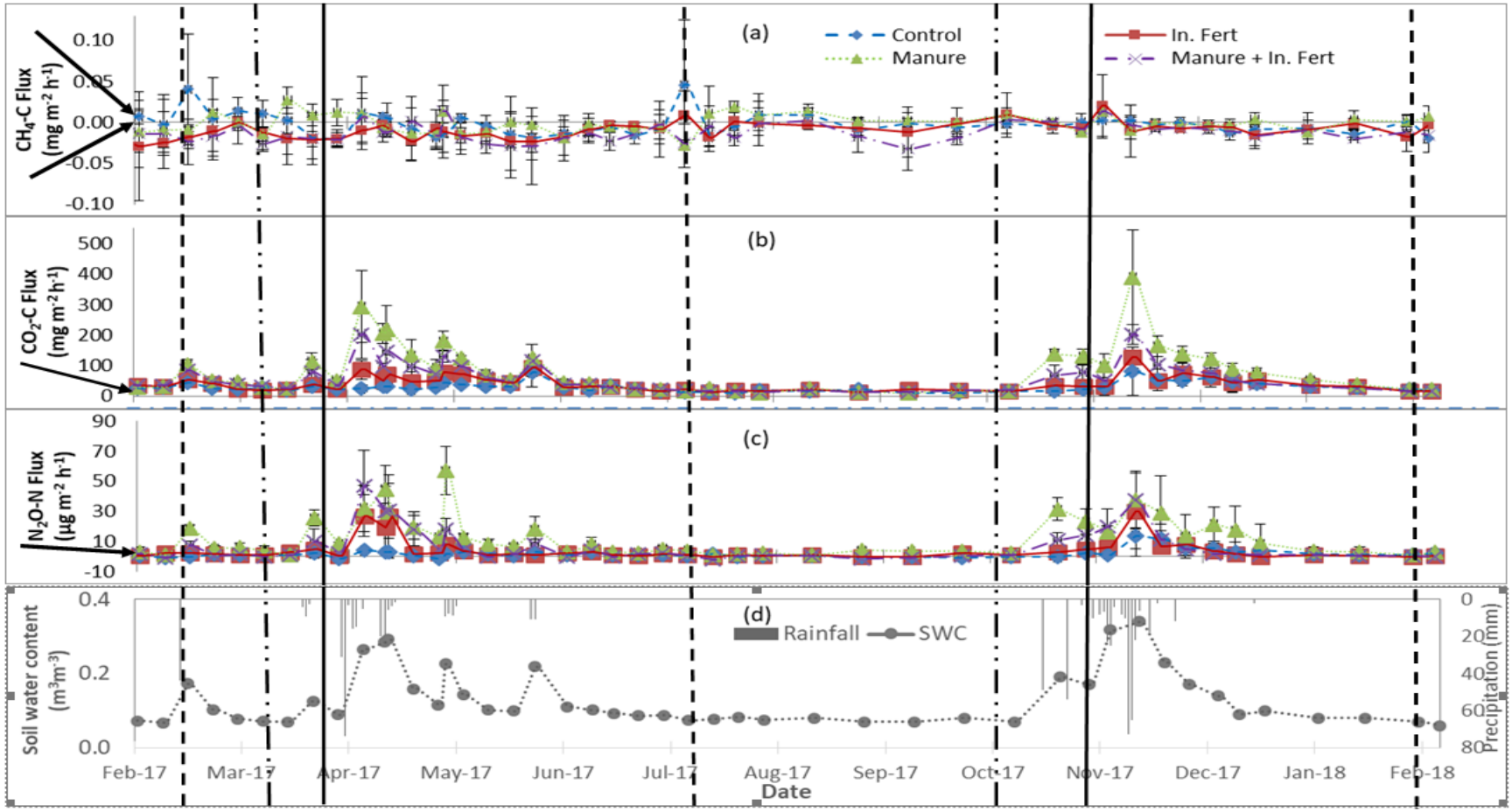

Figure 4.10: Soil GHG fluxes and ancillary information (a) CH_4 (CH_4-C mg m^{-2} h^{-1}), (b) CO_2 (CO_2-C mg m^{-2} h^{-1}), (c) N_2O (N_2O-N mg m^{-2} h^{-1}) fluxes from February 2017 to February 2018 and (d) Soil water content (SWC) at 10 cm depth of soil adjacent to sampling chambers (m^3 m^{-3}) and precipitation (mm). The vertical lines correspond to harvesting of maize (dashed), land preparation and manure incorporation (long-dash dotted line), and planting of maize as well as inorganic fertilisers application (vertical continuous). Arrows beside the vertical axes for figures a, b and c correspond to the minimum detection limits determined following Parkin et al. (2012).

Soil CO_2 emissions ranged from 9 mg CO_2-C m^2 h^{-1} during mid-September 2017 to 390 mg CO_2-C m^2 h^{-1} during mid-November 2017 (Figure 4.10 b). Soil CO_2 emissions remained low (<50 mg CO_2-C m^2 h^{-1}) during the dry periods (June 2017 to October 2017) only increasing after soil rewetting; up to about 294 mg CO_2-C m^2 h^{-1} during the onset of the long rains (April 2017) and up to 390 mg CO_2-C m^2 h^{-1} after the onset of the short rains (Figure 4.10 b). After these peaks, soil CO_2 emissions declined to as low as an average of 18 mg CO_2-C m^2 h^{-1} by February 2018 (Figure 4.10 b). The soil CO_2 emissions were seasonal (Figure 4.10 b) and significantly differed within treatments and across seasons (Table 4.5).

Soil rewetting during the onset of the rains in April and November 2017 (Figure 4.10 b) and which coincided with fertilisation showed a significant increase in CO_2 emissions, possibly due to increased soil respiration rates and carbon availability (Gelfand et al., 2015). These findings agree with other studies carried out on African soils (Predotova et al., 2010; Rosenstock et al., 2016; Pelster et al., 2017; Ortiz-Gonzalo et al., 2018), which identified a clear seasonal pattern of CO_2 emissions based on soil rewetting patterns. Soil wetting increases the diffusion of substrates and the mobility of microorganisms utilising those substrates thus increasing respiration (Barton et al., 2016).

During the dry periods of the year (Figure 4.10 b), the CO_2 emissions remained low and which could be attributed to lower microbial activities and also due to lack of roots respiration when there is no crop growing in the farms (Ortiz-Gonzalo et al., 2018). Plots treated with animal manure emitted the highest amounts of CO_2 emissions possibly due to the decomposition of organic matter applied as animal manure. As was noted by Konda et al. (2010) and Ortiz-Gonzalo et al. (2018), CO_2

emissions depend on combined respirations from plant roots, soil fauna, microbial respiration and decomposition of soil organic matter.

Soil N_2O fluxes remained low for most of the year, with rates typically below 10 µg N_2O-N m^2 h^{-1} (Figure 4.10 c). Emissions peaked (as high as 57 and 37 µg N_2O-N m^2 h^{-1} for the onset of the long and short rains respectively) (Figure 4.10 c). After these peaks, soil N_2O fluxes slowly declined to reach about 2 µg N_2O-N m^2 h^{-1} by early February 2018 (Figure 4.10 c). The soil N_2O fluxes (Figure 4.10 c) in the current study followed the same seasonal pattern as that of soil CO_2 emissions (Figure 4.10 b) with little or no fluxes during the rest of the year (Figure 4.10 b) and cumulative fluxes ranging between 0.12 and 1.15 kg N_2O-N ha^{-1} yr^{-1} (Table 4.7). This initial rise in fluxes after fertilisation could mainly be attributed to increased inorganic N concentrations (Figure 4.11). Most of the newly available IN was likely from the fertiliser or the manure, however there was an increase in IN within the control plots as well, which was likely due to the re-wetting of the soil that is known to cause mineralization of native soil organic N (i.e. the Birch effect: Birch, 1958).

In conjunction with the increase of inorganic nitrogen (IN), there was also an increase in soil water content and high soil respiration rates (Figure 4.10 b), likely caused by a rapid rise in root respiration as well as the release of labile C as root exudates enhancing respiration of the rhizosphere community (Haichar et al., 2014). The rapid respiration and high soil water content would, therefore, provide sufficient anaerobic microsites for denitrification, resulting in high soil N_2O emissions (Pelster et al., 2012; Butterbach-Bahl et al., 2013).

4.3.3 Seasonal GHG fluxes

During the LR 2017 season, cumulative soil CH_4 fluxes (P=0.021), CO_2 emissions (P<0.001) and N_2O fluxes (P=0.002) differed across treatments (Table 4.5). During the SR 2017 season, cumulative soil CH_4 fluxes (P=0.004), CO_2 emissions (P=0.006) and N_2O fluxes (P=0.002) differed across treatments (Table 4.5). In both seasons, animal manure combined with inorganic fertilisers took up the highest amounts of CH_4 while sole animal manure produced the highest amounts of both CO_2 and N_2O emissions (Table 4.5). Overall, cumulative seasonal CO_2 emissions (P=0.008) and N_2O fluxes (P=0.001) significantly differed across the seasons (Table 4.5). Soil CH_4 fluxes were generally taken up by the soils in the study area and differed across the treatments (Table 4.5).

Table 4.5: Mean (±1 SEM) seasonal cumulative GHG fluxes for four different fertiliser treatments to maize (DH 04 variety) crop in Embu County, Kenya

Season[1]	**Treatments[2]**	**CH_4 (kg CH_4-C ha^{-1})**	**CO_2 (Mg CO_2-C ha^{-1})**	**N_2O (kg N_2O-N ha^{-1})**
LR 17	Control	-0.04^{b} [3]±0.03	0.33^{b}±0.04	0.02^{c}±0.02
	In. Fert.	-0.18^{a}±0.06	0.47^{b}±0.06	0.11^{b}±0.03
	Manure	-0.02^{b}±0.03	0.90^{a}±0.07	0.30^{a}±0.03
	Manure + In. Fert.	-0.16^{a}±0.04	0.71^{a}±0.11	0.17^{b}±0.03
	P value[4]	*0.021*	*<0.001*	*0.002*
SR 17	Control	-0.05^{c}±0.02	0.98^{b}±1.17	0.10^{c}±0.05
	In. Fert.	-0.37^{b}±0.10	1.34^{b}±0.18	0.27^{b}±0.04
	Manure	-0.03^{c}±0.10	2.49^{a}±0.20	0.85a±0.05
	Manure + In Fert.	-0.48^{a}±0.09	1.86^{b}±0.27	0.43^{b}±0.08
	P value[4]	*0.04*	*0.006*	*0.002*
Seasonal difference		*0.121*	*0.008*	*0.001*

[1] Season abbreviations: SR 17 = 2017 short rainy season (6th February to 6th July 2017), LR 17= 2017 long rainy season (7th July to 6th February 2018)

[2]Treatment abbreviations: Control = no external input, In. Fert. = inorganic fertiliser (60 kg N ha^{-1} from NPK at N=23%, P=23% K=0%); Manure = animal manure applied at 60 kg N ha^{-1}; Manure + In. Fert. = combination of animal manure at half rate (30 kg N ha^{-1}) and inorganic fertiliser at half rate (30 kg N ha^{-1})

[3] Same superscript letters in the same column denote no significant difference between the treatment means.

[4] P value below the table represent significance difference across treatments

4.3.4 Soil moisture and soil inorganic nitrogen

Soil moisture content (MC) was generally below 0.15 m^3 m^{-3}, although MC did peak at 0.29 and 0.34 during the onset of the long and short rainy seasons, respectively as seen in figure 4.10 d. In the control plot, inorganic nitrogen (IN) concentrations in the top 20 cm of soil remained below 20 mg N kg^{-1} soil throughout the year, while the IN concentrations in the fertilized plots peaked shortly after fertilization but dropped below 20 mg N kg^{-1} soil within approximately 2 months after inorganic fertilization (Figure 4.11). Soil IN consisted primarily of NO_3^--N (approximately 86%) with the rest of the soil IN comprised of NH_4^+-N.

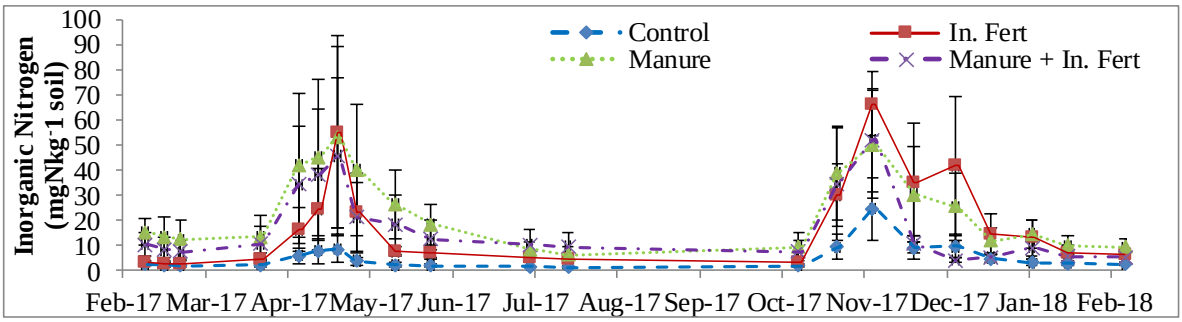

Figure 4.11: Inorganic Nitrogen (mg N kg^{-1} soil) from four different treatments with maize (DH 04 variety) crop in Embu County, Kenya between February 2017 and February 2018**.** Treatment abbreviations are: control = no external input, In. Fert. = Inorganic fertiliser (60 kg N ha^{-1} from NPK at N=23%, P=23% and K=0%) applied at planting); manure = animal manure applied at 60 kg N ha^{-1}; man + In. Fert. = combination of animal manure at half rate (30 kg N ha^{-1}) and inorganic fertiliser at half rate (30 kg N ha^{-1}).

4.3.5 Crop production, leaf area index (LAI) and yield-scaled emissions (YSE)

During the LR 2017 season, mean leaf production (P = 0.018), root production (P = 0.006), and stem production (P = 0.024) significantly differed across treatments. However, grain production and leaf area index (LAI) was similar across treatments

(Table 4.6). Plots treated with animal manure produced the highest leaf (2.38 Mg ha^{-1}), root (0.38 Mg ha^{-1}), and stem (1.77 Mg ha^{-1}) biomass (Table 4.6). Similar to the LR 2017 season, plots treated with animal manure produced the highest amount of leaves (3.25 Mg ha^{-1}), roots (0.61 Mg ha^{-1}), and stems (1.86 Mg ha^{-1}) biomass (Table 4.6) in the SR 2017 season. There was a significant difference in mean root production (P=0.001) and LAI (P=0.009) between the seasons (Table 4.6) with SR 17 having higher root and LAI production.

Table 4.6: Biomass production and Leaf Area Index (LAI) for the long and short rainy 2017 seasons for the different treatments with maize in Embu County, Kenya

Season[1]	Treatment[2]	Leaves (Mg ha^{-1})	Roots (Mg ha^{-1})	Stems (Mg ha^{-1})	Grains (Mg ha^{-1})	LAI (m^2m^{-2})
LR 2017	Control	0.86^{b}±0.26	0.11^{b}±0.03	0.44^{b}±0.21	0.06±0.06	0.35^{a}±0.10
	In. Fert.	1.93^{b}±0.32	0.22^{b}±0.01	1.05^{b}±0.19	0.07±0.05	0.53^{a}±0.14
	Manure	2.38^{a}±0.22	0.38^{a}±0.01	1.77^{a}±0.37	0.09±0.07	0.73^{a}±0.06
	Manure + In. Fert.	1.63^{b}±0.22	0.27^{b}±0.06	0.97^{b}±0.37	0.05±0.05	0.46^{a}±0.26
	P value[3]	*0.018*	*0.006*	*0.024*	*0.124*	*0.195*
SR 2017	Control	1.57^{b}±0.25	0.27±0.03	0.69^{b}±0.15	0.09^{b}±0.07	0.78^{b}±0.11
	In. Fert.	2.10^{b}±0.27	0.46±0.12	1.37^{b}±0.26	0.31^{b}±0.05	1.12^{b}±0.14
	Manure	3.25^{a}±0.45	0.61±0.07	1.86^{a}±0.22	2.41^{a}±0.57	1.53^{a}±0.16
	Manure + In. Fert.	2.20^{b}±0.10	0.43±0.04	1.23^{b}±0.29	0.22^{b}±0.19	1.16^{b}±0.16
	P value[3]	*0.022*	*0.069*	*0.044*	*0.001*	*0.004*
Seasonal P value		*0.342*	*0.001*	*0.80*	*0.258*	*0.009*
Interaction		*0.004*	*0.60*	*0.67*	*0.001*	*0.001*

[1]Season abbreviations: SR 17 = 2017 short rainy season (March-July 2017), LR 17= 2017 long rainy season (October 2017-February 2018)

[2] Treatment abbreviations: Control = no external input, In. Fert. = inorganic fertiliser (60 kg N ha^{-1} from NPK at N=23%, P=23% K=0%); Manure = animal manure applied at 60 kg N ha^{-1}; Manure + In. Fert. = combination of animal manure at half rate (30 kg N ha^{-1}) and inorganic fertiliser at half rate (30 kg N ha^{-1})

[2] Same superscript letters in the same column denote no significant difference between the treatment means

[3] P value below the table represent significance difference across treatments

[4]Effects of fixed factors (treatments) on biomass production with season as random factor

Maize yields were higher in the SR 2017 than in LR 2017 (Table 4.6), though not significantly different. Control plots had the lowest grain yields while animal manure had the highest grain yields (Table 4.6). With no external inputs applied, maize yields from the control plots were low, possibly due to lack of addition of nutrients to replenish the soils. However, most of the fertilised plots also had very low yields that appear to be related to precipitation as the grain yield was consistently (although not significantly) greater during the SR 2017 season, when precipitation was 32% higher than during the LR 2017 season.

For the manure plots, this 32% increase in rainfall caused a 27-fold increase in grain yields. The low crop production during the LR 2017 could be attributed to the low, erratic rainfall, characterised by three dry periods of 13, 20 and 36 days, experienced between 2 weeks after emergence and harvesting (Figure 4.10 d). This agrees with other studies carried out in the study area which noted more reliable rainfall and higher yields during the short rains than in the long rains (Ngetich et al., 2014; Okeyo et al., 2014; Kiboi et al., 2017). The much greater response in grain yield in the manure plot compared to the other treatments to the higher precipitation during the SR 2017 season could be attributed to the build-up of soil organic carbon over time as seen in the high level of soil carbon content (Table 4.3). It can also be as a result of the ability of the soil organic matter to retain moisture into the dry period of the growing season (Rawls et al., 2003; Ankenbauer and Loheide, 2017) as demonstrated by relatively high biomass and LAI throughout the year (Table 4.6).

Yield-scaled emissions (g N_2O-N emitted per kg N exported as grains) were lowest from plots treated with animal manure (0.5 g N_2O-N kg^{-1} N) and highest in plots treated with a combination of animal manure and inorganic fertilisers 2.2 g N_2O-N

kg^{-1} N. (Table 4.7). Yield-scaled N_2O emissions (YSE), expressed as annual emissions per unit grain production, can help evaluate the GHG impacts (van Groenigen et al., 2010; Li et al., 2015). Although yields do not affect farm GHG emissions or removals, they are relevant for standardisation of various prospects (Ortiz-Gonzalo et al., 2017).

For this study, the yield-scaled emissions ranged between 0.5 and 2.2 g N_2O-N kg^{-1} N above ground N uptake across the treatments and which were within the range of other studies in sub-Saharan Africa (Nyamadzawo et al., 2014; Ortiz-Gonzalo et al., 2017; Pelster et al., 2017). Sole application of animal manure had the lowest YSE while manure combined with inorganic fertilisers had the highest YSE (Table 4.7). The low amounts of YSE in a sole application of animal manure could be attributed to the ability of the animal manure to retain more moisture throughout the year than the other treatments under study. Animal manure combined with inorganic fertiliser had the highest YSE due to high fluxes but low grain yield. Leaf area index (LAI) followed seasonality and was high in plots treated with animal manure and least in control treatments. The LAI was higher in the second season (SR 2017) than in the first season (LR 2017) (Figure 4.12).

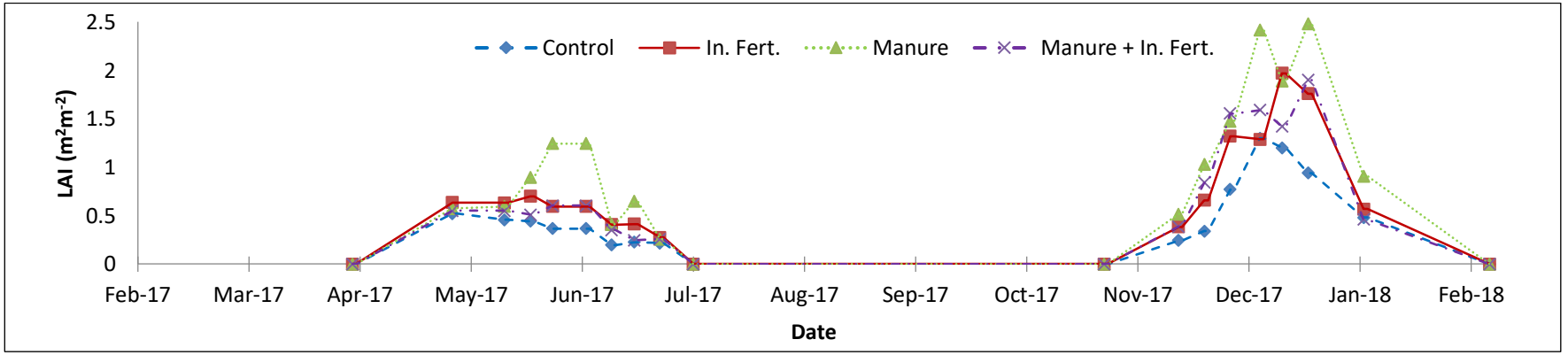

Figure 4.12: Leaf area index (LAI) from four different treatments with maize (DH 04) crop in Embu County, Kenya between February 2017 and February 2018. Treatment abbreviation are control = no external input, fert = Inorganic fertiliser (60 kg N ha^{-1} from NPK at N=23%, P=23% and K=0%) applied at planting); manure = animal manure applied at 60 kg N ha^{-1}; man + fert = combination of animal manure at half rate (30 kg N ha^{-1}) and inorganic fertiliser at half rate (30 kg N ha^{-1}).

4.3.6 GHG budget, global warming potential (GWP), emission factors (EFs) and GHG intensity

Annual cumulative soil CH_4 fluxes differed across treatments ($P<0.001$) and ranged from -0.09±0.04 kg CH_4-C ha^{-1} from control plots to -0.65±0.13 kg CH_4-C ha^{-1} from plots treated with animal manure combined with inorganic fertilisers at half rate (Table 4.7). Cumulative soil CO_2 emissions differed across treatments ($P<0.001$) ranging from 1.31±0.20 Mg CO_2-C ha^{-1} in control plots to 3.39±0.27 Mg CO_2-C ha^{-1} from plots treated with animal manure (Table 4.7). Cumulative soil N_2O fluxes differed across treatments ($P<0.001$) and ranged from 0.12±0.07 kg N_2O-N ha^{-1} from control plots to 1.15±0.08 kg N_2O-N ha^{-1} from plots treated with animal manure (Table 4.7).

The N_2O emission factors (EFs) from this study were slightly lower than the default IPCC Tier 1 of 1% with animal manure treatment having the highest EF (0.9%) while inorganic fertiliser had the lowest EF at 0.2% (Table 4.7). However, the EF values from this study, based on different soil fertility management practices, corroborates the default IPCC Tier 1 emission factors and which ranged between 0.2 – 0.9% (Table 4.7). Direct soil N_2O emissions from agriculture are often estimated using the default IPCC emission factor (EF) of 1% (IPCC, 2006). According to Raut et al. (2015), most of the reported emission factors are usually between 2-8 times higher than the default IPCC Tier 1 EF values. The net global warming potential from the four treatments was 622 kg CO_2-eq. ha^{-1} with manure having the highest contribution (341 kg CO_2-eq. ha^{-1}) while control had the least (33 kg CO_2-eq. ha^{-1}) (Table 4.7). The Greenhouse gas intensity (GHGI) was in the range of 0.1 to 0.6 kg CO_2 eq. kg^{-1} with manure having the least GHGI while manure + fertiliser had the highest GHGI (Table 4.7).

Table 4.7: Mean (± SE) annual cumulative GHG fluxes (between February 2017 and February 2018) for four different fertiliser treatments to a maize (DH 04 variety) crop in Embu County, Kenya

Treatments[1]	CH_4 (kg CH_4-C ha^{-1} yr^{-1})	CO_2 (Mg CO_2-C ha^{-1} yr^{-1})	N_2O (kg N_2O-N ha^{-1} yr^{-1})	Net GWP[3] (kg CO_2-eq. ha^{-1})	GHGI[4] (kg CO_2 eq. kg^{-1} grain[1])	YSE[5] (g N_2O-N kg^{-1} grain[1])	EF[6] (%)
Control	-0.09[d] [2]±0.04	1.31[c]±0.20	0.12[d]±0.07	33 (5)	0.2	0.8	-
In. Fert.	-0.56[b]±0.16	1.81[c]±0.24	0.37[c]±0.08	91 (15)	0.2	1.1	0.2
Manure	-0.05[c]±0.14	3.39[a]±0.27	1.15[a]±0.08	341 (55)	0.1	0.5	0.9
Manure + In. Fert.	-0.65[a]±0.13	2.57[b]±0.38	0.60[b]±0.11	157 (25)	0.6	2.2	0.4
P value	*<0.001*	*<0.001*	*<0.001*				

[1] Treatment abbreviations: Control = no external input, In. Fert. = inorganic fertiliser (60 kg N ha^{-1} from NPK at N=23%, P=23% K=0%); Manure = animal manure applied at 60 kg N ha^{-1}; Manure + In Fert = combination of animal manure at half rate (30 kg N ha^{-1}) and inorganic fertiliser at half rate (30 kg N ha^{-1})

[2] Same superscript letters in the same column denote no significant difference between the treatment means

[3] GWP = Global warming potential, values in parentheses are percentage per treatment of the total carbon dioxide equivalent CO_2-eq - calculated for a time horizon of 100 years, factors 34 for CH_4 and 298 for N_2O (Myhre et al., 2013). Values in parentheses represent column percentages.

[4]GHGI= Greenhouse gas intensity calculated by dividing the net GWP by total grain yield production in a year (kg CO_2 equivalent kg^{-1})

[5] YSE=Yield-scaled emission expressed as g N_2O-N emitted per kg N exported as grains (g N_2O-N kg^{-1})

[6]Emission factors (EF) calculated by dividing the amount of N lost as N_2O-N by the amount of N applied

Cumulative annual CO_2 emissions

The cumulative annual CO_2 emissions for this study (1.31 and 3.39 Mg CO_2-C ha^{-1} yr^{-1}) were well within the range of other studies carried out in East African upland soils (Rosenstock et al., 2016; Pelster et al., 2017; Ortiz-Gonzalo et al., 2018). From these previous studies, carried out on maize fields, CO_2 emissions ranged between 1 and 15.9 Mg CO_2-C ha^{-1} yr^{-1}. It is important to note that the CO_2 emissions from this study were purely from root respiration and microbial decomposition of organic matter and that to obtain the full GHG balance, both photosynthesis and aboveground vegetation respiration should be considered (Pelster et al., 2017).

Cumulative annual CH_4 emissions

The cumulative annual uptake of soil CH_4 fluxes (-0.65 to -0.09 kg CH_4-C ha^{-1} yr^{-1}) (Table 4.7) were within the range of previous studies carried out on managed agricultural soils in East Africa (Rosenstock et al., 2016; Pelster et al., 2017; Ortiz-Gonzalo et al., 2018), and which found upland agricultural soils acting predominantly as sinks of CH_4. With no external inputs applied in the control plots, there was low methane consumption possibly due to low population of methanotrophs. The control plots had relatively low amounts of soil carbon content (Table 4.3) and which may have hindered the production of methanotrophic communities due to lack of a buffer during low CH_4 availability periods (Subke et al., 2018). Methanotrophic bacteria are unique in their ability to utilise methane as a sole carbon and energy source (Hanson & Hanson, 1996).

Plots treated with animal (goat) manure had high CH_4 emissions possibly due to addition of large amounts of methanogens with the application of goat manure.

Among livestock, ruminants produce the highest amounts of enteric methane since methanogens can produce methane freely through the normal process of feed digestion in the rumen and lower digestive tract (Hook et al., 2010; Wanapat et al., 2015; Olijhoek et al., 2016). As a result, the manure produced equally contains a high concentration of methanogens which ends up in the soils. The combination of added methanogens and soils becoming anaerobic during the rains may have promoted the CH_4 production. Also, according to Nyamadzawo et al. (2014), large quantities of C becomes available to methanogens when animal manures are mixed with the soil, which may if the soil is anaerobic and methanogens are present, result in more CH_4 emissions.

Application of inorganic fertilisers enhanced CH_4 oxidation resulting in a high CH_4 uptake. These results agree with Nyamadzawo et al. (2014) who noted that application of N into sandy loam soils reduced CH_4 emissions. Use of N fertilisers may mitigate CH_4 emissions since ammonium-based fertilisation stimulates growth and activity of methane oxidisers (Bodelier et al., 2000). While some studies have identified the ability of Ammonium and CH_4 oxidizers to compete for O_2 to use it as an electron acceptor (Serrano-Silva et al., 2014) and thus acting as an inhibitor of CH_4 oxidation (Bykova et al., 2007) others have contradicted these findings and noted the N fertilisers to stimulate the CH_4 oxidation (Mohanty et al., 2004) based on different soils under different conditions while others have pointed out no effect of Ammonium on CH_4 oxidation (Kiese et al., 2003). For this study, the addition of inorganic fertilisers enhanced CH_4 oxidation thus resulting in CH_4 uptake across treatments. In the combination of animal manure and inorganic fertilisers, the inorganic fertiliser could have increased the oxidation of methane while the labile C from animal manure

could have buffered methanotrophic populations during periods when CH_4 availability was low as observed by Subke et al. (2018), thus resulting to more methane uptake than sole manure and sole inorganic fertilisers.

Cumulative annual N_2O emissions

The cumulative N_2O fluxes from this study (0.12 and 1.15 kg N_2O-N ha^{-1} yr^{-1}) (Table 4.7) were well within the range of other studies carried out on managed agricultural soils in East African soils, whose results ranged between -1 to 4.1 kg N_2O-N ha^{-1} yr^{-1} (Rosenstock et al., 2016; Pelster et al., 2017; Ortiz-Gonzalo et al., 2018). There are significant inconsistencies in the literature on the effect of inorganic fertilisers and animal manure on soil N_2O fluxes. Some studies show higher soil N_2O fluxes from animal manures, such as Ding et al. (2007) on sandy loam in a maize-wheat rotation (Acquic inceptisol) in China, Chantigny et al. (2010) on loam (loamy, mixed, frigid, Typic Dystrocryept) soils in Canada, and Sosulski et al. (2014) on Luvisols - loamy sand in Poland. Other studies show the opposite results (higher N_2O fluxes from inorganic fertilisers) such as Ellert and Janzen (2008) on a loam to clay loam soils with 70% clay (Gleysolic Humic Vertisols) in Canada, Mukumbuta et al. (2017) on Andosols in Japan and Chantigny et al. (2010) on clay (clayey, mixed, frigid, Typic Humaquept) soils in Canada. Others did not identify any significant difference between soil N_2O fluxes from animal manure and inorganic fertilisers such as Shimizu et al. (2013) on Andosols - well-drained soils in Japan. According to Pelster et al. (2012), studies where manure applications caused greater N_2O emissions than mineral fertilisers were generally on coarse-textured, well-drained soils, whereas studies with no differences or greater emissions from mineral N fertilisers tended to be from moderate to fine-textured soils. In the current study, the IN concentrations within the

mineral fertiliser plots were similar to those plots that had manure applied (Figure 4.12).

However, the N_2O fluxes in the mineral fertiliser plots were less than plots treated with manure (Table 5). As these soils were a sandy loam texture with low (0.5-1.5%) C content, we concluded that the differences in the soil N_2O fluxes across fertiliser treatments could be attributed to the differences in available C, consistent with several previous studies (e.g. Chantigny et al., 2010; Rochette et al., 2018). Availability of more labile C in the manure treatments (Table 4.3) may have provided the necessary environment for denitrification to take place. According to Pelster et al. (2012), readily mineralisable C provides the essential electron donor for denitrification, and that addition of C may also increase microbial respiration rates, which may deplete soil oxygen, providing the anaerobic conditions required for denitrification.

4.3.7 Correlations between soil GHG fluxes and crop production (grains and biomass), and other controlling factors

Annual cumulative CH_4 fluxes (Table 4.7) were not correlated with any of the measured factors, however, both the cumulative CO_2 emissions were correlated with soil C content (r=0.997, P=0.023) and soil N content (r=0.990, P=0.010) while N_2O fluxes (Table 4.7) were correlated with soil N content (r=0.957, P=0.043). During the LR 2017 season, cumulative CH_4 fluxes (Table 4.5) were not correlated with any of the measured factors, however, cumulative CO_2 emissions correlated with root biomass (r=0.973, P=0.027) and cumulative seasonal IN (r=0.989, P=0.011) while cumulative seasonal N_2O fluxes (Table 4.5) were correlated with cumulative seasonal IN (r=0.986, P=0.014), root (r=0.991, P=0.009) and stem biomass (r=0.954, P=0.046). During the SR 2017 season, cumulative CH_4 fluxes were not correlated with any of the measured factors, cumulative CO_2 emissions (Table 4.5) correlated with root

biomass (r=0.989, P=0.011) while cumulative seasonal N_2O fluxes were correlated with root biomass (r=0.962, P=0.038) and grain production (r=0.980, P=0.020).

4.4 Simulation of soil GHG fluxes in the semiarid parts of central highlands of Kenya using DNDC model

4.4.1 DNDC model calibration

The DNDC model was calibrated using field observed data from control plots and showed a good agreement between the field observations and model-simulated data (R^2=0.99) (Figure 4.13), which were not statistically different at P=0.05. This indicates that the model was successfully calibrated (García et al., 2014). From the comparisons between observed and simulated data, the biomass increased in the last stage of plant growth - grain filling (Figure 4.13 d). The modelled data tended to start the simulations slightly later than the observed values generally and with higher values compared to the observed. The simulated data also overestimated the amounts of carbon allocated to various maize crop components compared to observed values (Figure 4.13).

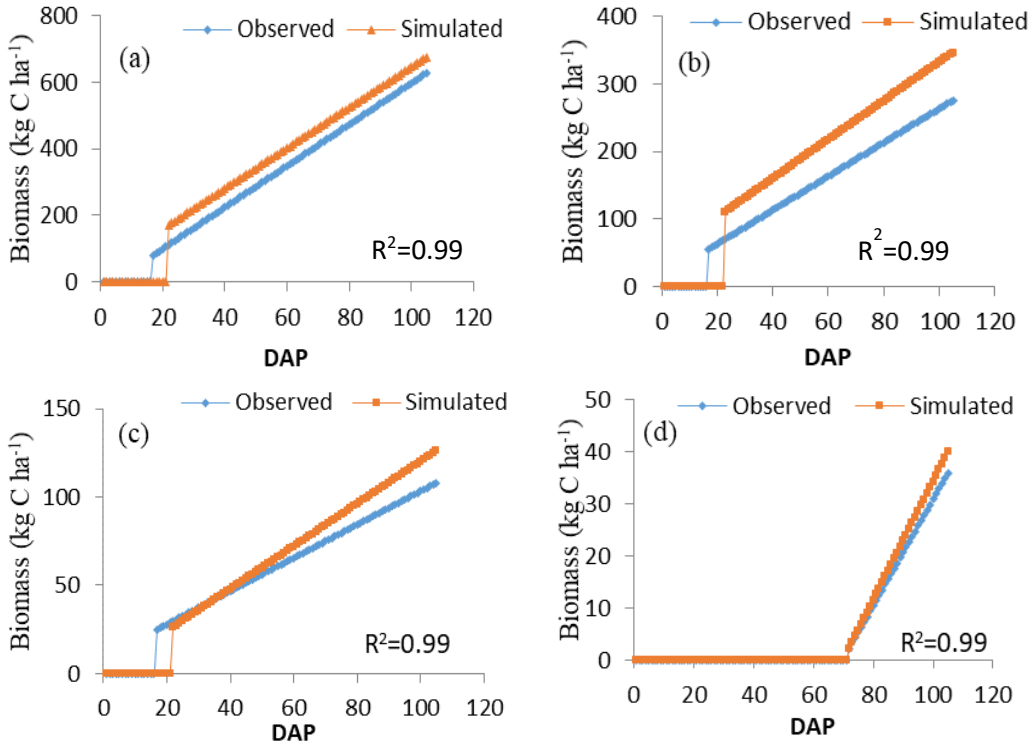

Figure 4.13: Observed and predicted maize plant carbon for a) leaves, b) stems, c) roots and d) grains from a control plot used for DNDC model calibration in the central highlands of Kenya.

4.4.2 DNDC model validation

The DNDC model was validated with field observed data collected through destructive sampling from a maize plot treated with inorganic fertilisers at 60 kg N ha^{-1} and which were linearly interpolated between sampling dates. The calibrated data equally had a high degree of agreement (R^2) between observed and simulated plant carbon across the maize plant components ranging between 0.88 and 0.99 (Figure 4.14). There was no significant difference in yields between observed and calibrated values at P=0.05 (Figure 4.14) an indication that the simulated data can be relied on for other purposes (Simba et al., 2013). The simulated carbon was generally higher than the observed values and which agrees with Kröbel et al. (2011) in Canada using DNDC, García et al. (2014) in Colombia using APSIM model, Simba et al. (2013) in Zimbabwe and Ahmadi et al. (2015) in Iran both using FAO-AquaCrop model who found the modelled values in both calibration and validation being higher than the observed. However, a study by Umair et al. (2017) using CropSyst model showed both overestimation and underestimation of simulated data across the years of calibration and validation.

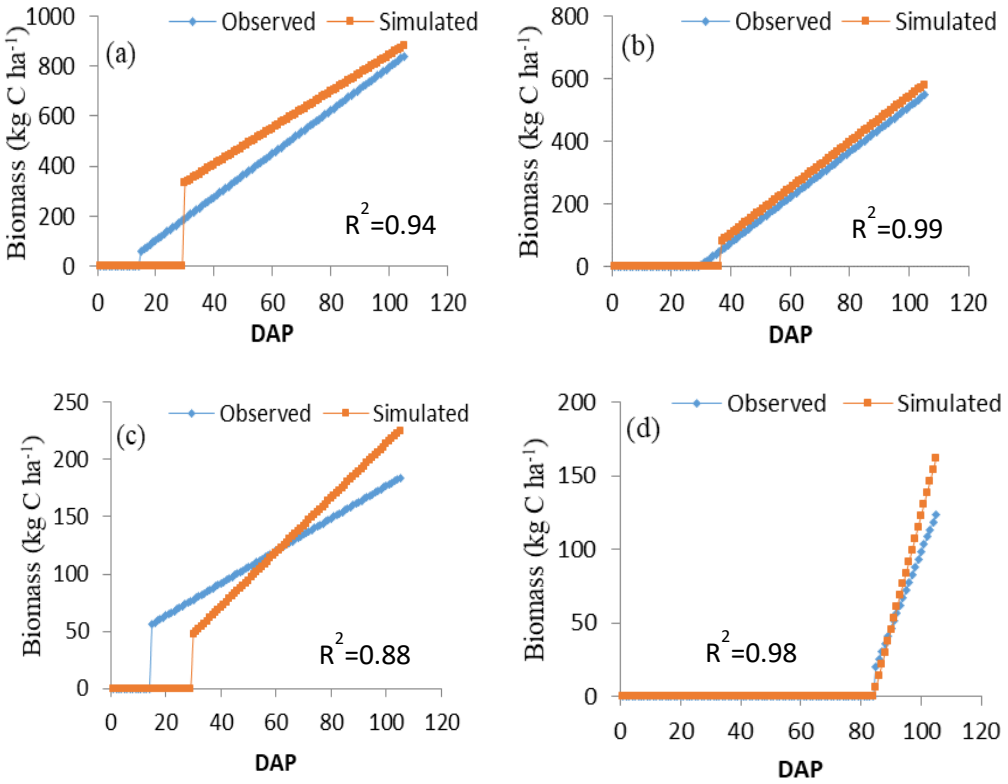

Figure 4.14: Observed and predicted values of maize plant carbon from a) leaves, b) stems, c) roots and d) grains from a control plot used for DNDC model calibration in the central highlands of Kenya.

The relationship between the calibrated and validated data portrayed a narrow range of RMSE (1.3 - 6.4 Mg C ha^{-1}) and low bias (0.68 - 1.03) across the plant components (Table 4.8). The RMSE from this study is well within the range of other studies carried out on simulating maize biomass (Heng et al., 2009; Paredes et al., 2014; Ahmadi et al., 2015), using AquaCrop model and Li et al. (2017) in Canada using DNDC model.

Table 4.8: Summary of the statistics across plant components for control and inorganic fertilisers treatments

Treatments	Component	RSME	Bias
Control	Leaf	4.7	1.00
	Stems	1.5	1.02
	Roots	6.1	0.99
	Grains	2.1	0.84
Inorganic fertilisers	Leaf	6.4	1.03
	Stems	2.3	0.92
	Roots	3.0	0.77
	Grains	1.3	0.68

4.4.3 Observed versus predicted leaf area index (LAI)

There was generally a good agreement between observed and predicted leaf area indices for control plots as well as for plots treated with inorganic fertilisers (R^2=0.99) (Figure 4.15). The modelled data tended to slightly overestimate the LAI for both treatments (Figure 4.15).

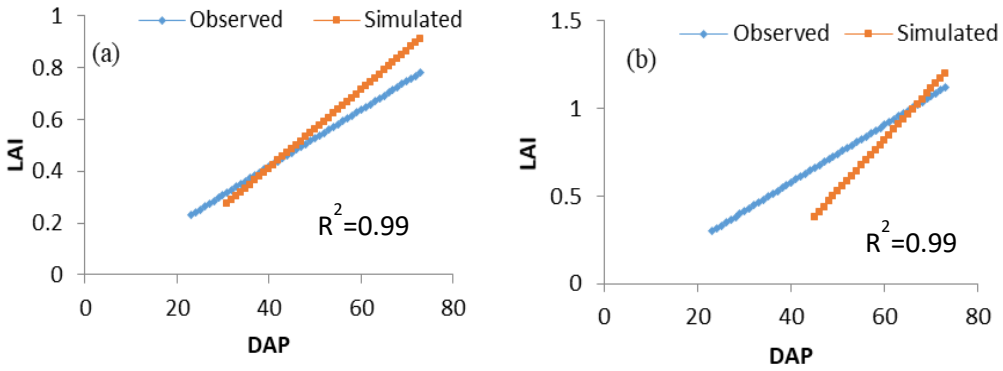

Figure 4.15: Observed and predicted leaf area index (LAI) at physiological maturity from plots treated with (a) control, (b) inorganic fertilisers in the dry parts of central highlands of Kenya

4.4.4 Simulated annual plant carbon

The annual cumulative carbon from various maize crop components significantly differed across treatments (P<0.001) (Table 4.9). Overall, plots treated with animal manure had the highest amounts of carbon allocated along maize crop components while control plots had the least amounts of carbon allocated along the maize plant components (Table 4.9). The simulated data from the DNDC model generally overestimated crop biomass and yields as compared to previous studies carried out in the same study area. For instance, as observed in the second objective on greenhouse gases quantification (Figure 4.10), with a total annual rainfall of 704 mm, using inorganic fertilisers applied at 60 kg N ha-^{1} recorded total biomass of 7.48 Mg ha^{-1} (2.99 Mg C ha^{-1}). Ngetich et al. (2014) in the same study site, which received an

annual total rainfall of approximately 780 mm in the year 2010, recorded an average aboveground biomass (AGB) of 11.51 Mg ha^{-1} (4.60 Mg C ha^{-1}) after application of inorganic fertilisers applied at 60 kg N ha^{-1} under different tillage systems compared with the simulated AGB of 6.73 Mg C ha^{-1}. It could be that the DNDC model assumed an even distribution of rainfall across the maize growing period based on the total rainfall received and that may not have captured the uneven distribution of rainfall thus leading to an overestimation of biomass and yield.

Table 4.9: DNDC simulated carbon allocation along plant components

Treatment	**Leaf (Mg C ha^{-1})**	**Stem (Mg C ha^{-1})**	**Roots (Mg C ha^{-1})**	**Grains (Mg C ha^{-1})**	**Total (Mg C ha^{-1})**
Control	1.61^{d}	1.05^{d}	0.48^{b}	0.03^{b}	3.17^{d}
Inorganic Fertilisers	4.49^{b}	2.22^{b}	0.59a	0.03^{b}	7.32^{b}
Manure	5.13^{a}	2.56^{a}	0.65^{a}	0.06^{a}	8.39^{a}
Manure + Fertilisers	3.87^{c}	1.92^{c}	0.50^{b}	0.02^{b}	6.31^{c}
P value	*<0.001*	*<0.001*	*<0.001*	*<0.001*	*<0.001*

4.4.5 DNDC Simulated greenhouse gas (CO_2 and N_2O) emissions

The DNDC simulated GHG fluxes for both CO_2 and N_2O followed seasonality rising immediately after soil rewetting which coincides with fertilisation and onset of the rains (Figures 4.16 and 4.17). During the dry periods of the year, the fluxes remained relatively low. Generally, the DNDC simulated data tended to overestimate the CO_2 emissions while underestimating the N_2O fluxes (Figures 4.16 and 4.17).

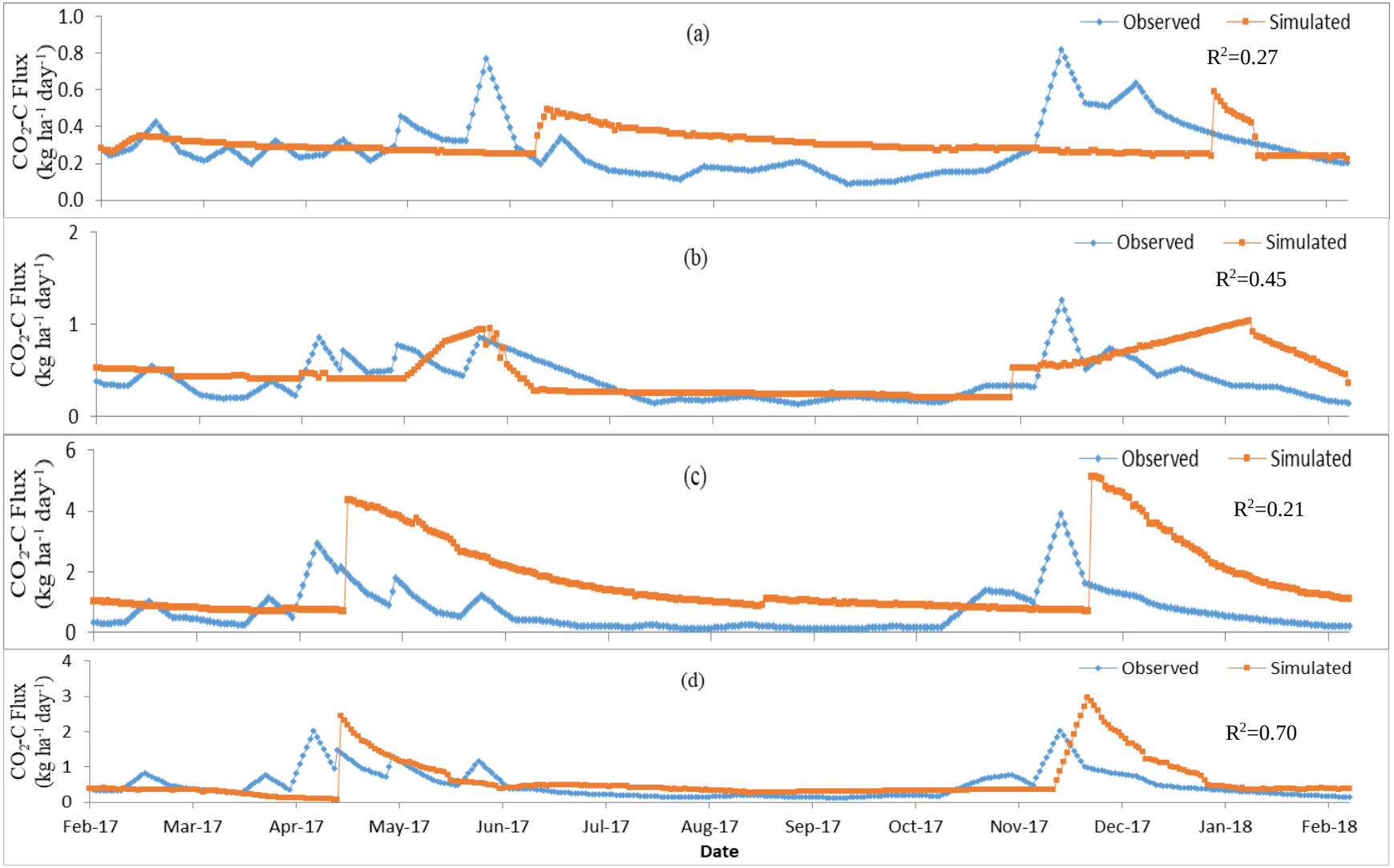

Figure 4.16: Observed and predicted CO_2 fluxes from four different treatments; (a) control, (b) inorganic fertilisers, (c) animal manure and (d) animal manure + inorganic fertilisers in Embu County, Kenya.

According to Lehuger et al. (2011), CO_2 exchanges between the soil-plant system and the atmosphere are modelled via the net photosynthesis and soil organic carbon (SOC) mineralisation processes. Carbon dioxide emissions depend on combined respirations from plant roots, soil fauna, microbial respiration and decomposition of soil organic matter (Ortiz-Gonzalo et al., 2018). The DNDC model-simulated CO_2 emissions compared relatively well with the observed fluxes (Figure 4.16) which followed seasonality as previously reported in (Figure 4.10 b).

Carbon dioxide fluxes' peaks for both observed and simulated fluxes were observed after soil rewetting at the onset of the rains and which coincided with fertilisation implying that the trends in the simulated daily CO_2 emissions could have been influenced by climate, fertilisation and crop growth stage. The modelled results showed that both the autotrophic and heterotrophic respiration is the source of soil CO_2 emission during the maize growing season as earlier observed. However, the simulated peak of CO_2 emissions was generally delayed and recorded slightly late in the season compared with the observed peaks (Figure 4.16) which may be attributed to the model's late estimation of decomposition of organic materials and increased soil respiration, weeks after manure incorporation and fertiliser application. The highest soil respiration peak was recorded in SR 2017 attaining a high of 6 kg CO_2-C ha^{-1} day^{-1} from animal manure treatment (Figure 4.16 c) and which is consistent with (Figure 4.10 b). It was observed that farm management practices (fertilisation and date of application) and crop parameters (biomass fraction) influences soil respiration, thus need for their consideration in future DNDC model applications (Li et al., 2017).

The annual simulated CO_2 emissions differed across treatments ($P<0.001$) with animal manure recording the highest amounts of CO_2 emissions (1.47 Mg CO_2-C ha^{-}

^{1} yr^{-1}) while control recorded the lowest amounts of CO_2 emissions (1.9 Mg CO_2-C ha^{-1} yr^{-1}) (Table 4.10). Overall, the simulated data tended to overestimate the annual CO_2 emissions across the treatments in the range of 12% for control treatment to 2% from animal manure + inorganic fertilisers treatments, though the differences were not significant at P=0.05. The low prediction from control treatment could be attributed to low amounts of substrates for microorganism thus leading to low CO_2 emissions while the high amounts of fluxes from animal manure treatment could be associated with readily available substrates from the decomposition of organic materials applied as goat manure.

The overestimation in the simulated data could be attributed to the ability of DNDC model to factor in more dynamics of C fluxes occurring at the interface between the terrestrial ecosystems and the atmosphere compared with the observed CO_2 emissions which are mainly from root respiration and soil microbial heterotrophic respiration as collected using static chambers. According to Li et al. (2010), the modelled CO_2 emissions include photosynthesis, plant autotrophic respiration, soil microbial heterotrophic respiration, and dissolved organic carbon (DOC) leaching.

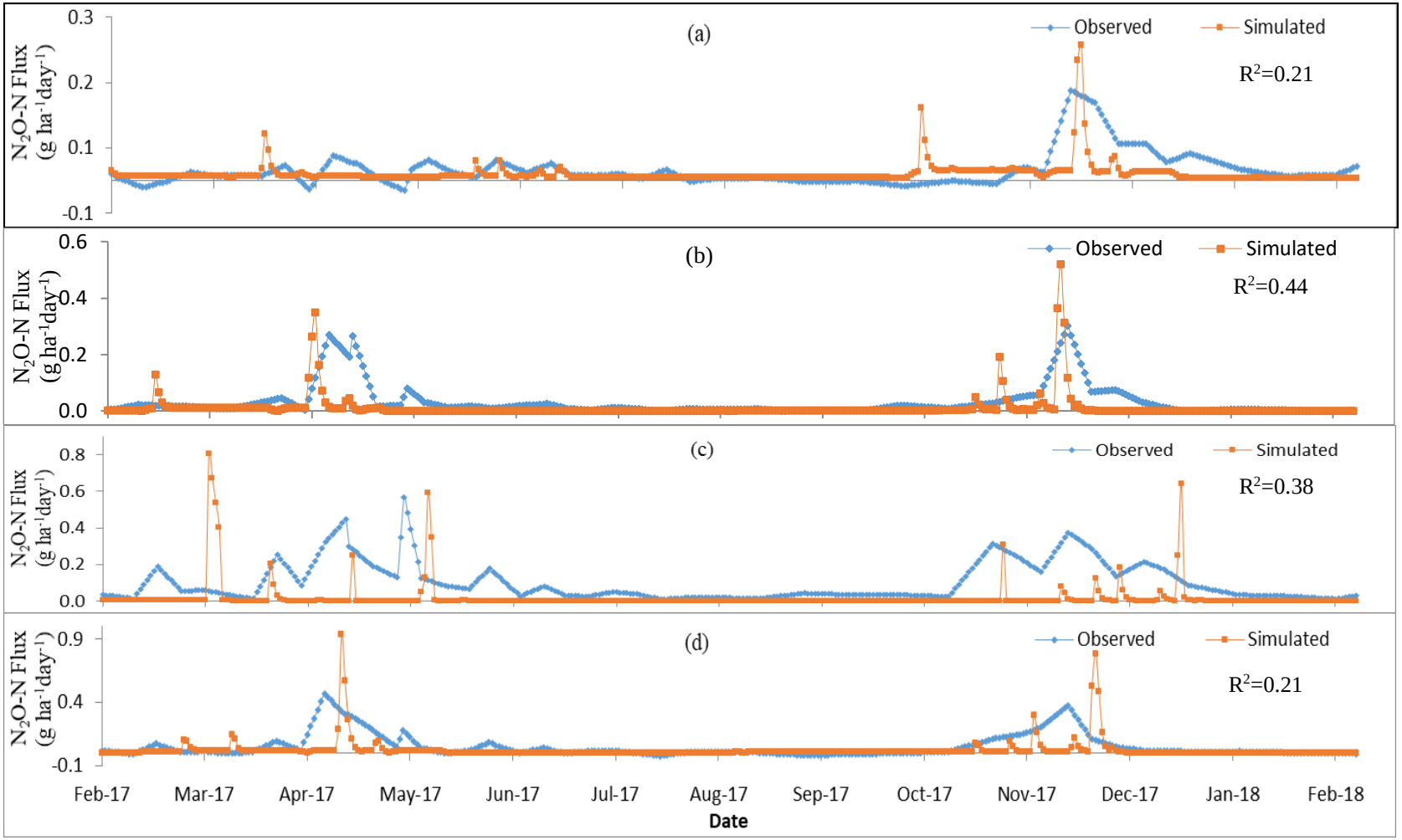

Figure 4.17: Observed and predicted N_2O fluxes from four different treatments; (a) control, (b) inorganic fertilisers, (c) animal manure and (d) animal manure + inorganic fertilisers in Embu County, Kenya.

The N_2O emissions provided by the biogeochemical simulation models are mostly generated by denitrification and nitrification (78%), mainly based (i.e. <70% of the models) on a soil N pools (e.g. nitrate pool, NH_4 pool) with soil water and temperature acting as primary drivers of change on mineral N pools (Brilli et al., 2017). In DNDC, net soil N_2O flux is the result of the balance between production and transformation through nitrification and denitrification reactions and losses through diffusion (Gaillard et al., 2017). The model simulated daily N_2O fluxes from the current study (Figure 4.17) followed the same seasonal pattern as the observed daily N_2O fluxes as previously reported in Figure 4.10 c. All daily simulations described temporal dynamics in N_2O fluxes (Figure 4.17) with an R^2 between 0.21 and 0.48 and which significantly correlated with observed (P=0.01).

The simulated annual N_2O fluxes differed considerably (P<0.001) across treatments with control recording the least amounts (0.09 kg N_2O-N ha^{-1} yr^{-1}) while animal manure recorded the highest amounts of N_2O fluxes (0.98 kg N_2O-N ha^{-1} yr^{-1}) (Table 4.10). In control plots, the low amounts of N_2O fluxes could be attributed to low quantities of substrates while the high quantities of N_2O fluxes could be attributed to the availability of more labile C in the manure treatments providing the necessary environment for denitrification to take place. According to Li et al. (2010), manure amendment and elevated residue incorporation both increases SOC content that provides more substrates to stimulate N_2O emissions through nitrification and denitrification in the soil.

Overall, the simulated data generally underestimated the N_2O fluxes with the highest underestimations (24%) recorded in the control treatments and the least from the animal manure + Inorganic fertiliser treatments (5%) (Table 4.10). The results agree

with Uzoma et al. (2015) in a study in Canada who noted that the DNDC model generally underestimated cumulative N_2O fluxes from corn fields. Gaillard et al. (2017) identified a clear tendency across all models (EPIC, DNDC, DayCent, Ensemble) to increasingly underestimate N_2O flux as observed flux increases.

The underestimation of N_2O fluxes from the current study could be attributed to the fact that the semiarid soils in the study area remains dry most of the year and dries up very fast after a rainfall event, and so the model is unable to accurately capture the abrupt changes in the soil water content, which doesn't last long before drying up. According to Smith et al. (2008), the DNDC model underestimations of N_2O fluxes may be a result of soil draining too quickly following rainfall, un-simulated lateral flow, or inaccurate model calculation of porosity. Further, Uzoma et al. (2015) and Congreves et al. (2016) noted that the soil hydrology sub-model in DNDC, have a cascade flow routine which drains the profile to field capacity, which likely underestimated soil water content and denitrification events during a period of high rainfall shortly after fertilizer application at onset, resulting to underestimation of N_2O fluxes.

The daily DNDC-simulated N_2O is in the form of peak emissions, mainly coming from both nitrification and denitrification (Wang et al., 2011). For this study, the simulated peaks for N_2O fluxes were well aligned for the timing of the peaks which followed rainfall events and a slight difference in the magnitude of the simulated N_2O peaks (Figure 4.17). This is because the model has a capacity to utilise daily weather data such as rainfall and in return simulate daily N_2O peaks. These results are consistent with finding of other studies who identified the DNDC model to generally capture the peaks of daily N_2O flux induced by heavy precipitation, although slight

discrepancies remained between the magnitude of the modelled N_2O peaks and the corresponding observations (Chen et al., 2015; Uzoma et al., 2015; Deng et al., 2018).

The simulated data also predicted more frequent N_2O peaks after rainfall events than the field observations (e.g. mid October to end of Dec 2017) and which is consistent with observations by Deng et al. (2018) who noted more frequent N_2O peaks after rainfall events during the rainy season, and which were not always observed in the field studies. As was observed by other N_2O modelling studies, accurate simulation of timing and daily N_2O flux variability possess a significant challenge (Smith et al., 2008; Fitton et al. 2014; Uzoma et al., 2015). However, where models are unable to simulate the timing of peak daily fluxes, comparisons might favour cumulative flux totals (Gaillard et al., 2017).

4.4.6 Comparison between annual observed and simulated CO_2 and N_2O fluxes

The simulated CO_2 emissions were slightly higher than the observed emissions while N_2O fluxes were marginally lower than the observed fluxes (Table 4.10). For the simulated CO_2 emissions, the overestimations were highest in control plots (12%) and least in plots treated with animal manure combined with inorganic fertilisers (2%). For N_2O fluxes, the highest underestimation of the simulated fluxes was highest in control plots (24%) and lowest in the plot as treated with manure combined with fertilisers (5%) (Table 4.10).

Table 4.10: Comparison between annual observed and simulated CO_2 and N_2O fluxes

	CO_2 (Mg CO_2-C ha^{-1} yr^{-1})			N_2O (Kg N_2O-N ha^{-1} yr^{-1})		
Treatment	**Observed**	**Simulated**	**Difference**	**Observed**	**Simulated**	**Difference**
Control	1.31^{c}	1.47c	0.16(12)	0.12^{d}	0.09^{c}	-0.03(24)
In. Fert	1.81^{c}	1.90^{c}	0.09(10)	0.37^{c}	0.34^{b}	-0.03(8)
Animal manure	3.39^{a}	3.66^{a}	0.27(8)	1.15^{a}	0.98^{a}	-0.17(15)
Manure + In. Fert	2.57^{b}	2.61^{b}	0.04(2)	0.6^{b}	0.57^{a}	-0.03(5)
P value	*<0.001*	*<0.001*		*<0.001*	*<0.001*	

Note: Values in parentheses represent column percentages

4.5 Length of growing season, rainfall onset and cessation dates in the agricultural potential zones of Kenya

4.5.1 Number of rainy seasons in Kenyan agricultural potential zones

Based on the analysis done in this study, Kenya's potential agricultural zones can be classified into two major regions. The first region, containing a majority of the agricultural potential zones, has two distinct seasons, i.e. Long rains (LR) majorly spanning between March to June and short rains (SR) spanning between October and December (Figures 4.18, 4.19, 4.21 and 4.22). The second category portrays one distinct season per year, spanning from March to December (Figures 4.20 and 4.23).

4.5.2 Rainfall onset date

The mean rainfall onset date for the LR season portrays a high temporal variability with the earliest onset across the region received in mid-February (13th February) while the latest onset date is received in mid-April (17th February) (Figure 4.18). Most parts of the country generally receive their LR onset in March and which agrees with other studies carried on rainfall in Kenya (Mugalavai et al., 2008; Ngetich et al., 2014; Yang et al., 2015). The rainfall onset dates tend to start from South West (high elevation) and gradually move towards the North East (low elevation) parts of Kenya (Figure 4.18). This direction of the onset was also observed by other studies carried

out in the region (Mugalavai et al., 2008; Dunning et al., 2016). During this period, the influence is majorly from the ITCZ which is usually overhead at the equator (Anyah & Semazzi, 2006) and which results to orographic rains beginning in the high altitude and gradually progressing towards the low altitude areas (Ngetich et al., 2014). According to Dunning et al. (2016), the seasonal progression of the ITCZ is the primary driver of the seasonal cycle of precipitation for the majority of Africa.

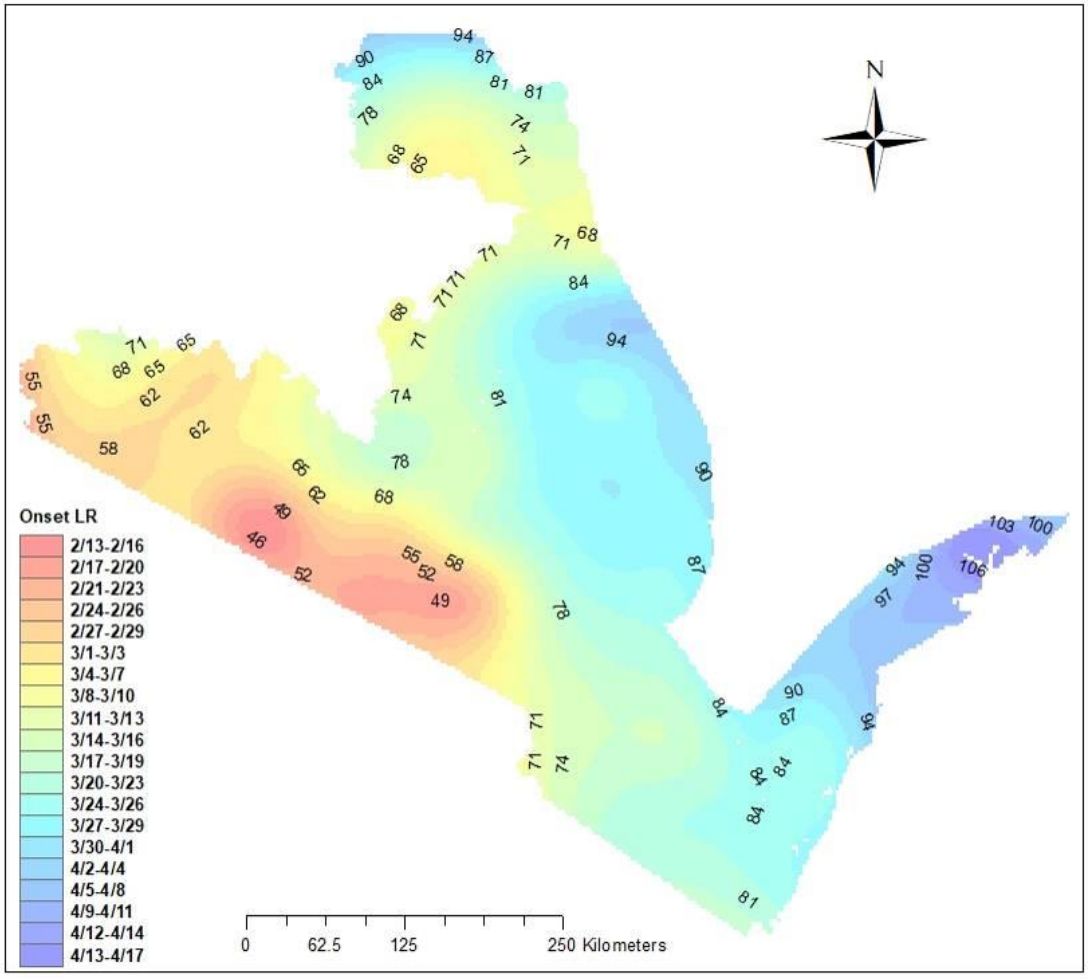

Figure 4.18: Rainfall onset dates for long rain season in Kenya (Source: Author, 2018)

For the SR season, the mean rainfall onset dates portray a temporal variation with part of Kenya experiencing onset in early-August while other zones experience onset as late as mid-November (Figure 4.19). The Coastal stretch and parts of Central Kenya

experiences late SR onset while parts of the lower Central and South West Kenya experience early onset (Figure 4.19). The direction of the onset days tends to move from Western to Eastern parts of Kenya gradually. This agrees with Ngetich et al. (2014) and Mugalavai et al. (2008) who noted the direction of early and late cessation generally moving from Western parts towards the Eastern direction in SR season. During this period, the rainfall onset could be associated with the Westerly influx of moisture from the Atlantic Ocean and moist Congo air masses. As was noted by Mugalavai et al. (2008) the Congo air mass influences on the short rain season.

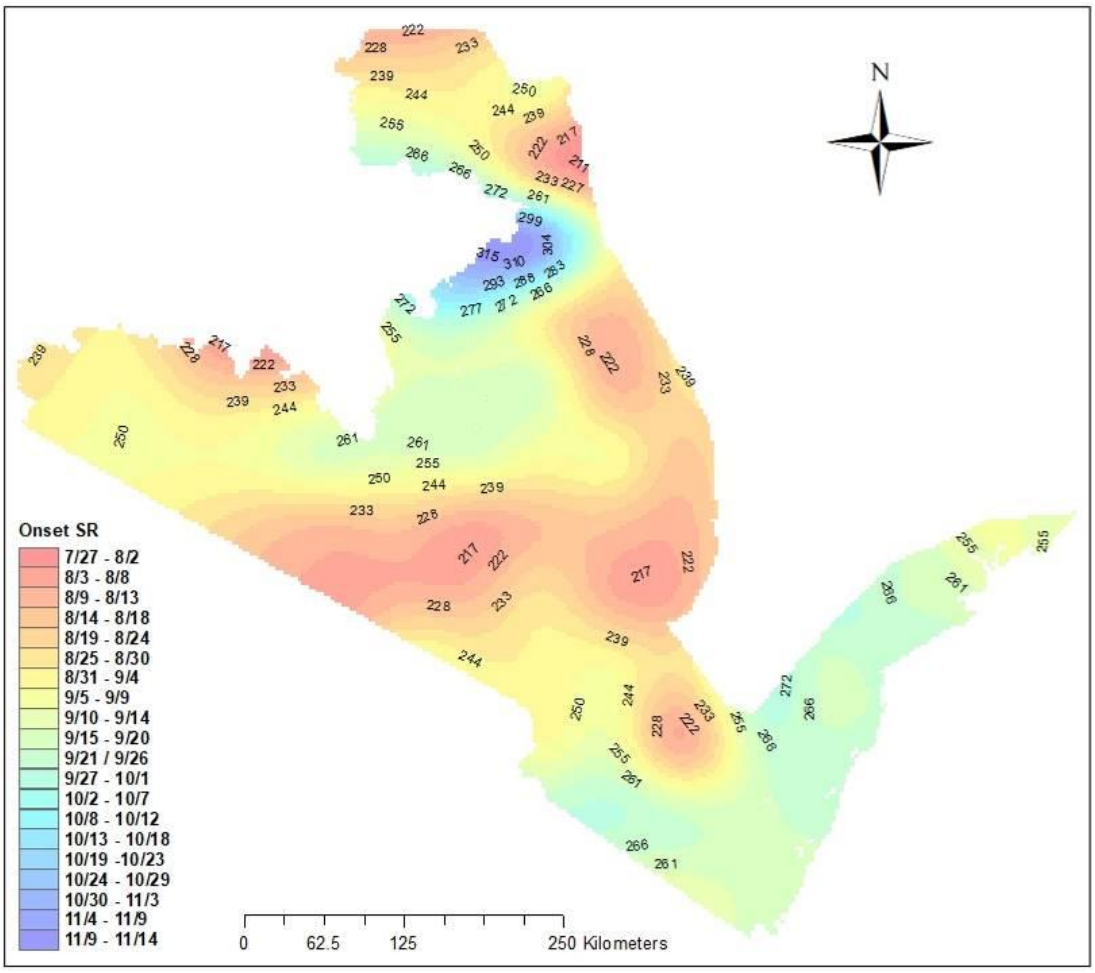

Figure 4.19: Rainfall onset dates for short rain season in Kenya (Source: Author, 2018)

For the one season region, the rainfall onset exhibited some slight temporal variations with the earliest onset being experienced around mid-February and the latest onset experienced in late March (Figure 4.20). The rainfall onset tends to move from West to East with regions in the Western part of Kenya experiencing early onset while the areas in the East experienced late onset. The Northern parts of this area also experience late onset (Figure 4.20). Most parts of this area receive their onset in March (Figure 4.20). This region of Kenya tends to exhibit characteristics of both the LR and SR seasons. For instance, the direction of the onset dates resembles that of SR while the actual onset dates resemble those of LR season. From the results, it could be that both the ITCZ and the Congo air mass have a significant influence on the rainfall patterns in this region and which results to areas adjacent the lake experiencing early onset as compared to zones away from the lake (Figure 4.20).

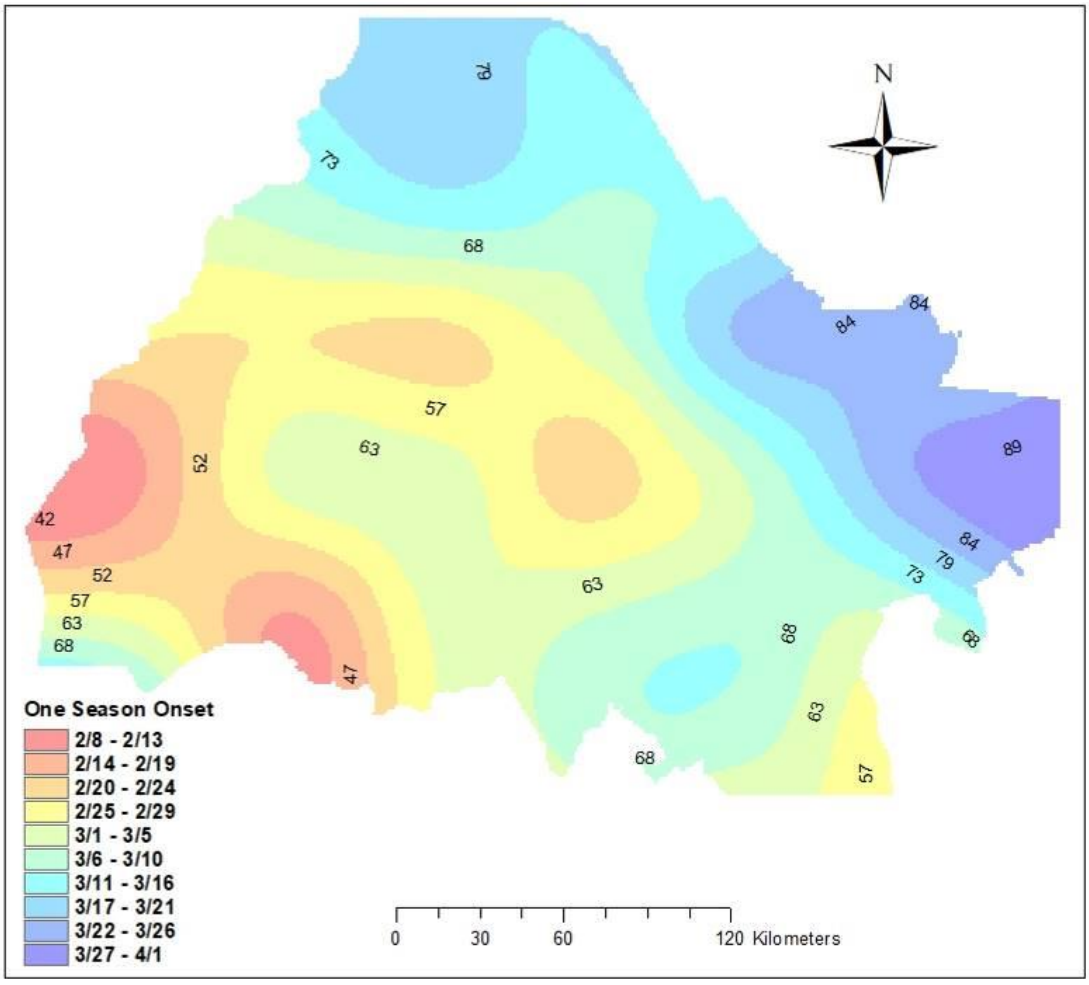

Figure 4.20: Rainfall onset for one season in Kenya (Source: Author, 2018)

4.5.3 Rainfall cessation date

The mean rainfall cessation date for the LR season also portrays a distinct temporal variability across the country with the earliest cessation being experienced in some parts of Kenya as early as mid-April and the latest in early July (Figure 4.21). Most parts of the country generally experience rainfall cessation in May (Figure 4.21), which is approximately a month after the mean onset date. The LR cessation also tends to follow the same direction as that of the LR onset which starts from the Western parts (high elevation) and gradually progresses towards the Eastern parts (low elevation) of Kenya (Figure 4.21). The cessation also tends to be experienced

early in the high altitude zones compared to the low altitude zones (Figure 4.21) and which seems to depend on localised influence as noted by Mugalavai et al. (2008).

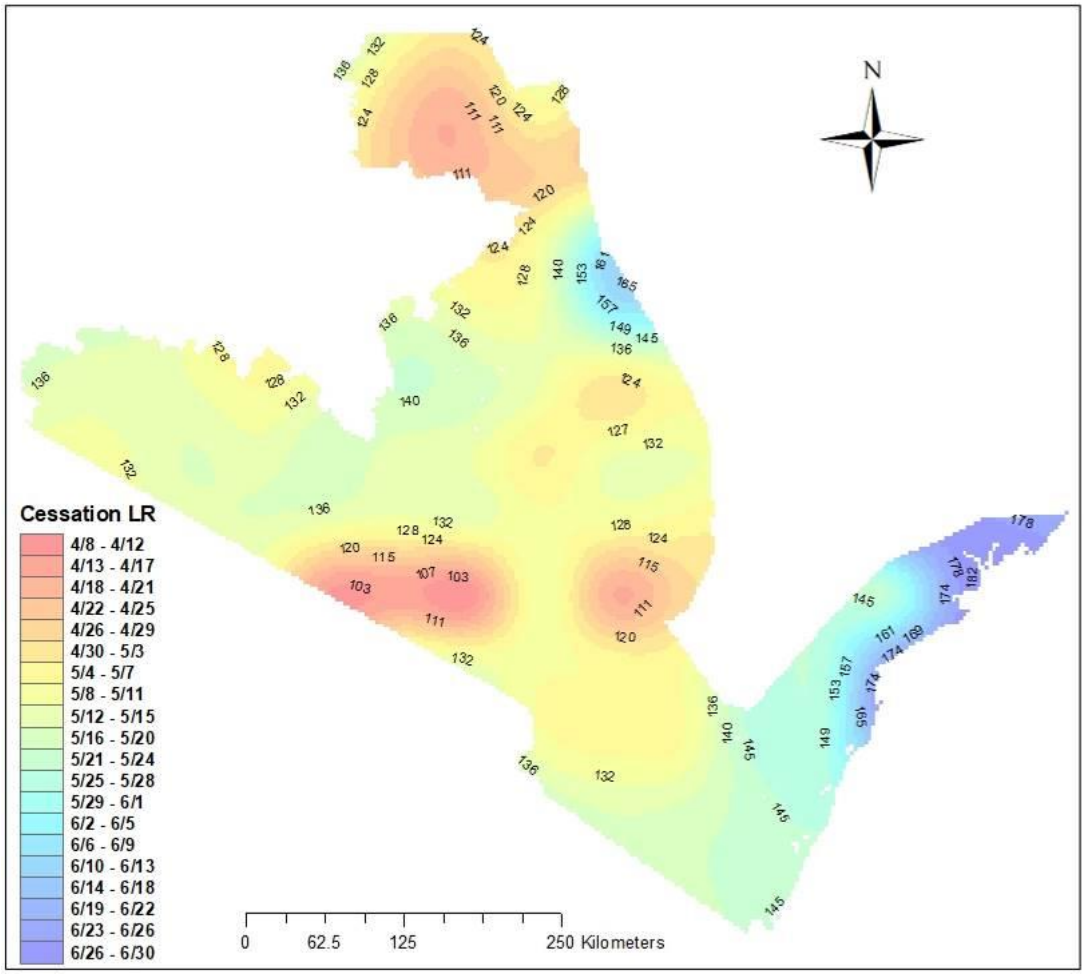

Figure 4.21: Rainfall cessation dates for long rain season in Kenya (Source: Author, 2018)

For the SR mean cessation date, there is relatively low temporal variation in most parts of Kenya with most of the zones majorly experiencing a cessation in October (Figure 4.22). The distinct difference in mean SR cessation dates is identified in the Northern part of Kenya and which tends to experience early cessations (Figure 4.22) generally. The direction of the mean rainfall cessation dates followed that of the SR onset, which is usually from the Western to Eastern parts of Kenya (Figure 4.22). These results are in agreement with other studies carried out in the region on onset

and cessation and who identified the significant impact of the Congo air mass to influence the SR season (Mugalavai et al., 2008; Ngetich et al., 2014; Dunning et al., 2016).

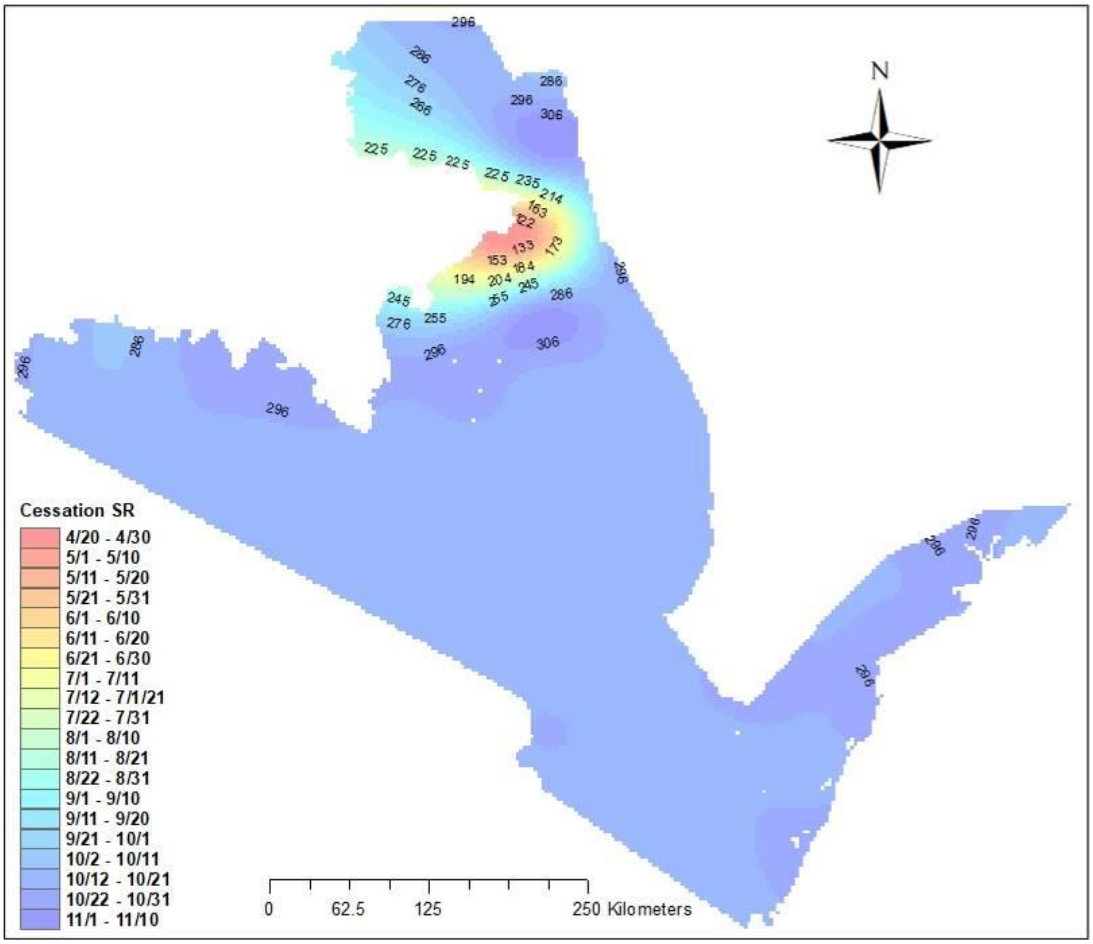

Figure 4.22: Rainfall cessation dates for short rain season in Kenya (Source: Author, 2018)

Rainfall cessation during the one season also exhibits slight temporal variations ranging between late-September and early-November (Figure 4.23). The cessation tends to move from North East to South West (Figure 4.23) and which is the inverse of the one season onset. Most of the regions during the one season experienced a cessation in October (Figure 4.23). The areas adjacent to Lake Victoria experiences late cessation compared to areas away from the lake (Figure 4.23).

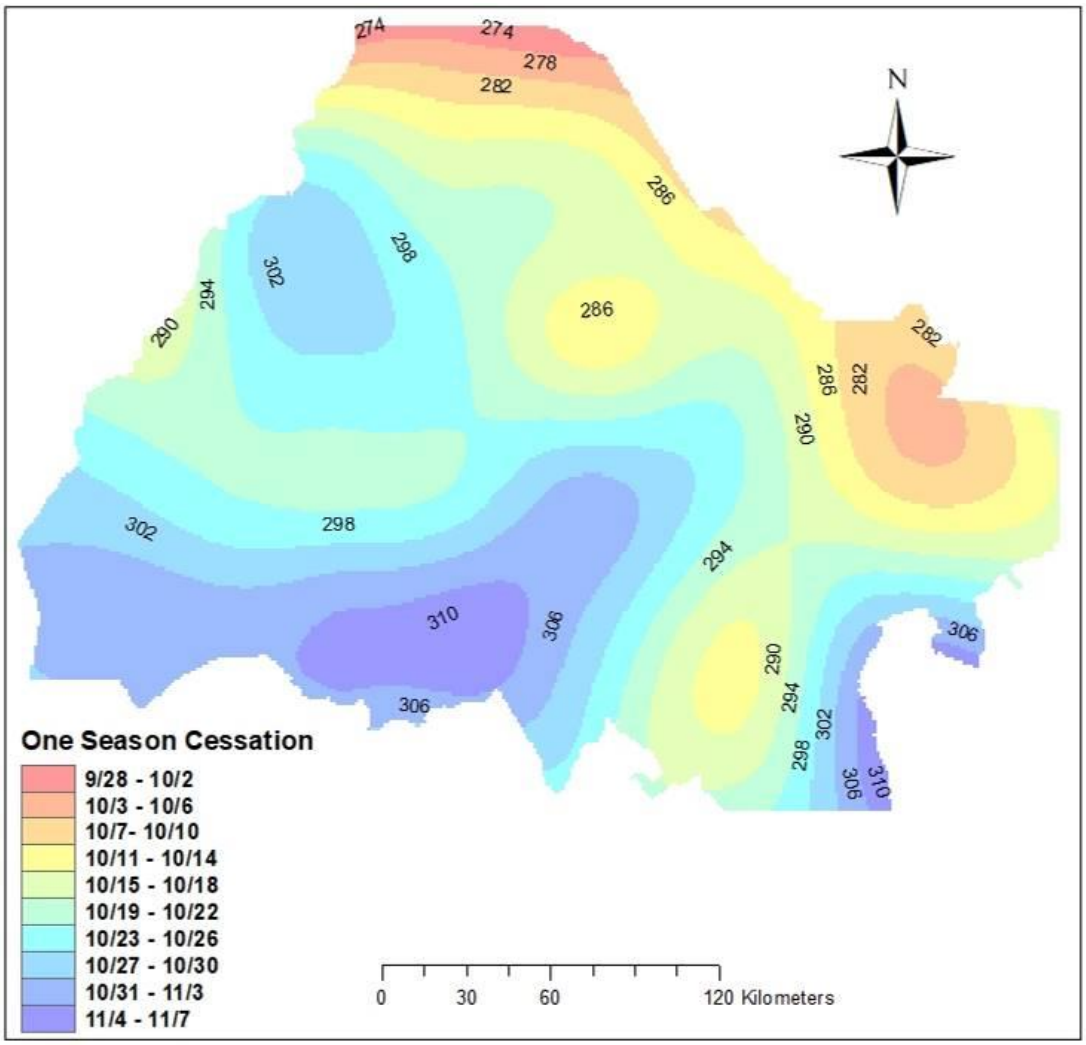

Figure 4.23: One season rainfall cessation in Kenya (Source: Author, 2018)

4.5.4 Length of growing season

During the LR season, the length of growing season equally portrays a temporal variation with the shortest experienced growing season being 23 days and the most extended growing season being 90 days (Figure 4.24). Most of the Western, Southern and Coastal (South eastern) parts of Kenya experience relatively longer growing seasons compared to parts of the Central and Northern part of Kenya (Figure 4.24). The zones that experience relatively longer growing season experience rainfall onset relatively early. As was noted by Sivakumar (1990), early onset of the rains gives a longer growing season while a delayed onset may lead to a short growing season.

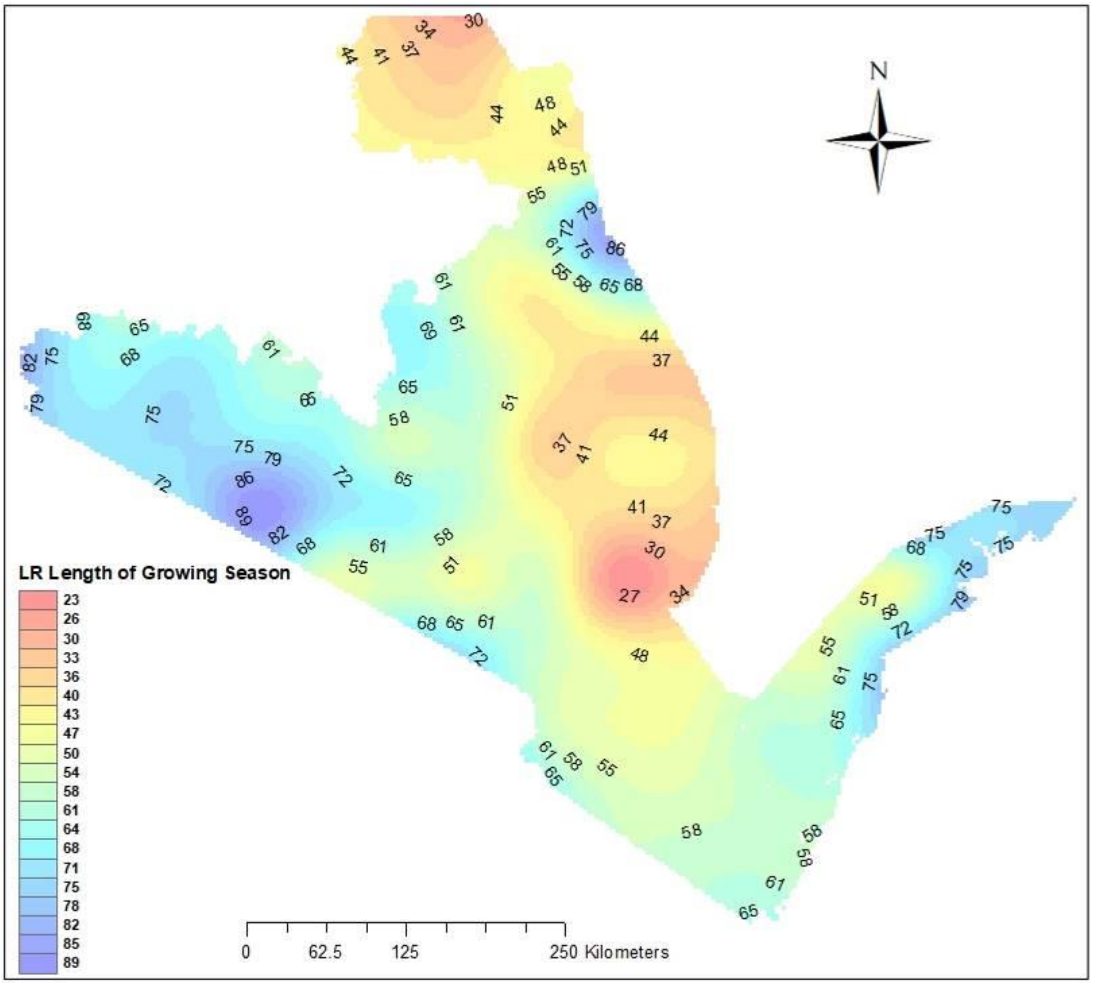

Figure 4.24: Long rains length of growing season (Source: Author, 2018)

For the SR season, the length of growing season portrayed a distinct temporal variation across the country. The SR season exhibited an inverse of the long rains with the Coastal, Western and Central regions of Kenya experiencing the shortest duration of growing season while parts of south Eastern Kenya experienced the most extended length of growing season (Figure 4.25). The direction of the length of the growing season was from the Eastern to Western parts of Kenya and which could have been influenced by the westerly influx of moisture from the Atlantic Ocean and moist Congo air masses (Mugalavai et al., 2008). As was observed in the SR onset, the Western parts of the country received the onsets slightly early and which could have

led to the long growing season during the SR in these zones compared to the zones in the Eastern side of Kenya.

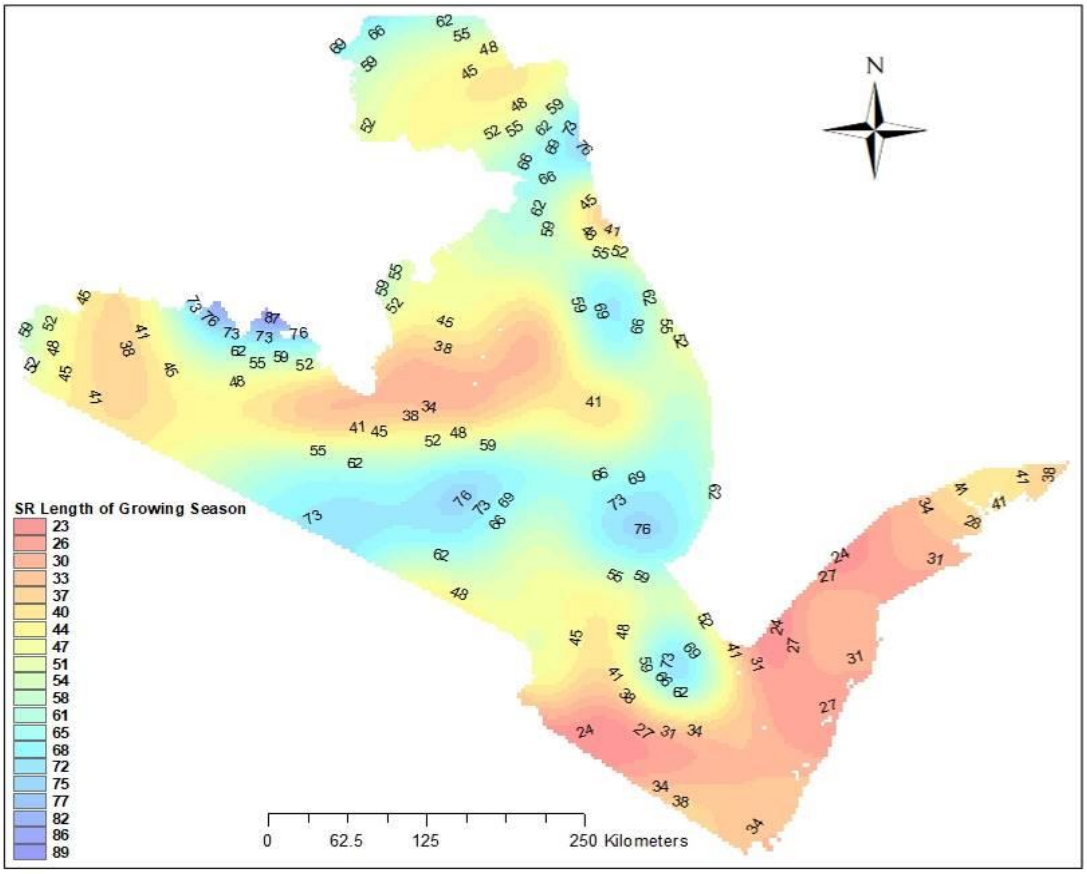

Figure 4.25: Long rains length of growing season (Source: Author, 2018)

The length of growing season for the one season zone exhibit a slight temporal variation with some areas having the shortest growing period of 192 days while others exhibit the most extended length of growing season of 259 days of sufficient rainfall (Figure 4.26). The direction of the length of the growing season moved from North East to South Western parts of Kenya (Figure 4.26). The zones adjacent the lake experienced the longest season and which could be attributed to the same regions experiencing the earliest onset and latest cessation as had earlier been noted due to the influence of the lake to this region.

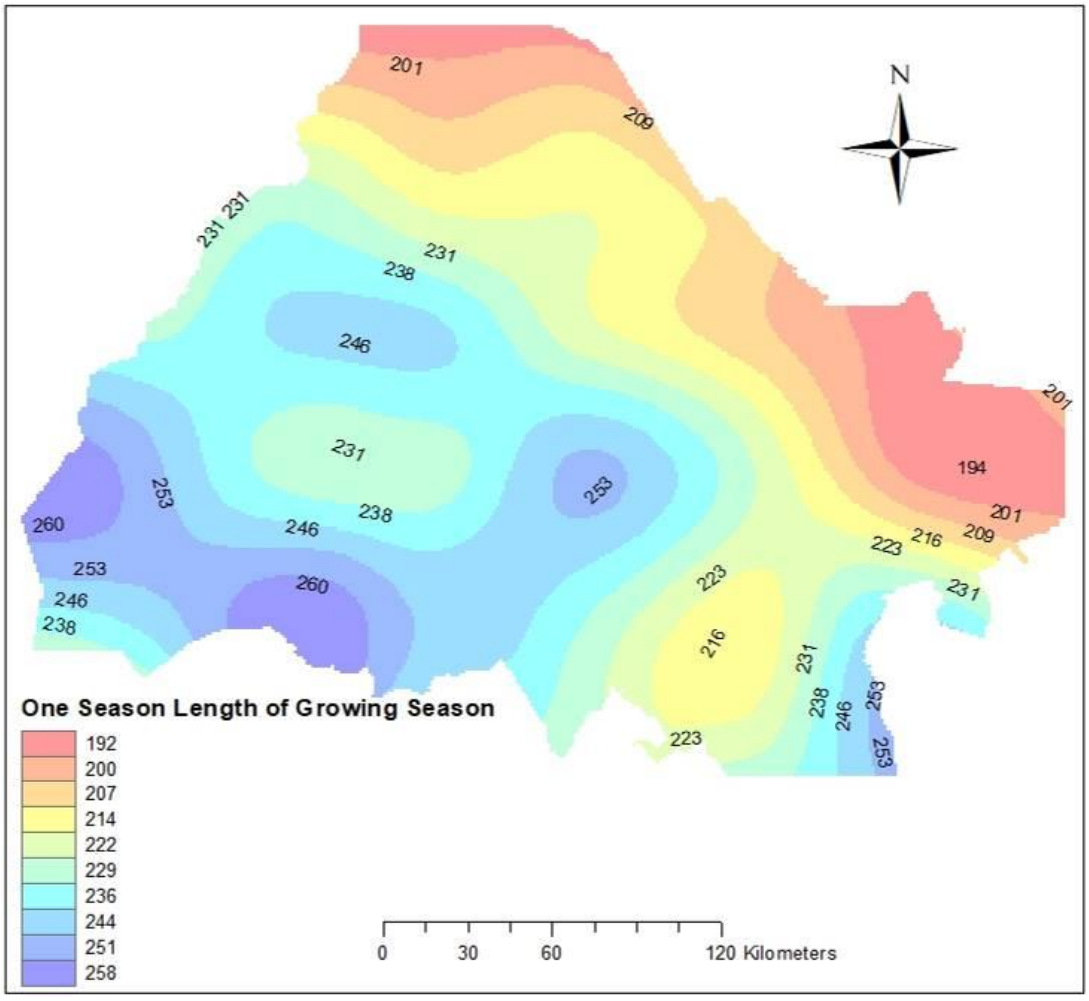

Figure 4.26: Length of growing season for the one season zones (Source: Author, 2018)

4.5.5 Cropping calendar

The Kenyan cropping calendar generally starts in mid-February for both the one season region and the region receiving both LR and SR rains (Figure 4.27 a). For one season region, the cropping calendar progresses almost the whole year until November when cessation occurs (Figure 4.27 b and d). For the region receiving two seasons, the cropping calendar starts with LR onset in February each year and progresses until around mid-June when the LR cessation is experienced (Figure 4.27 d). Later on, around August, the SR onset (Figure 4.27 c) is experienced and

progresses until November when the SR cessation is experienced (Figure 4.27 b), which is the same time when the one season cessation is also experienced.

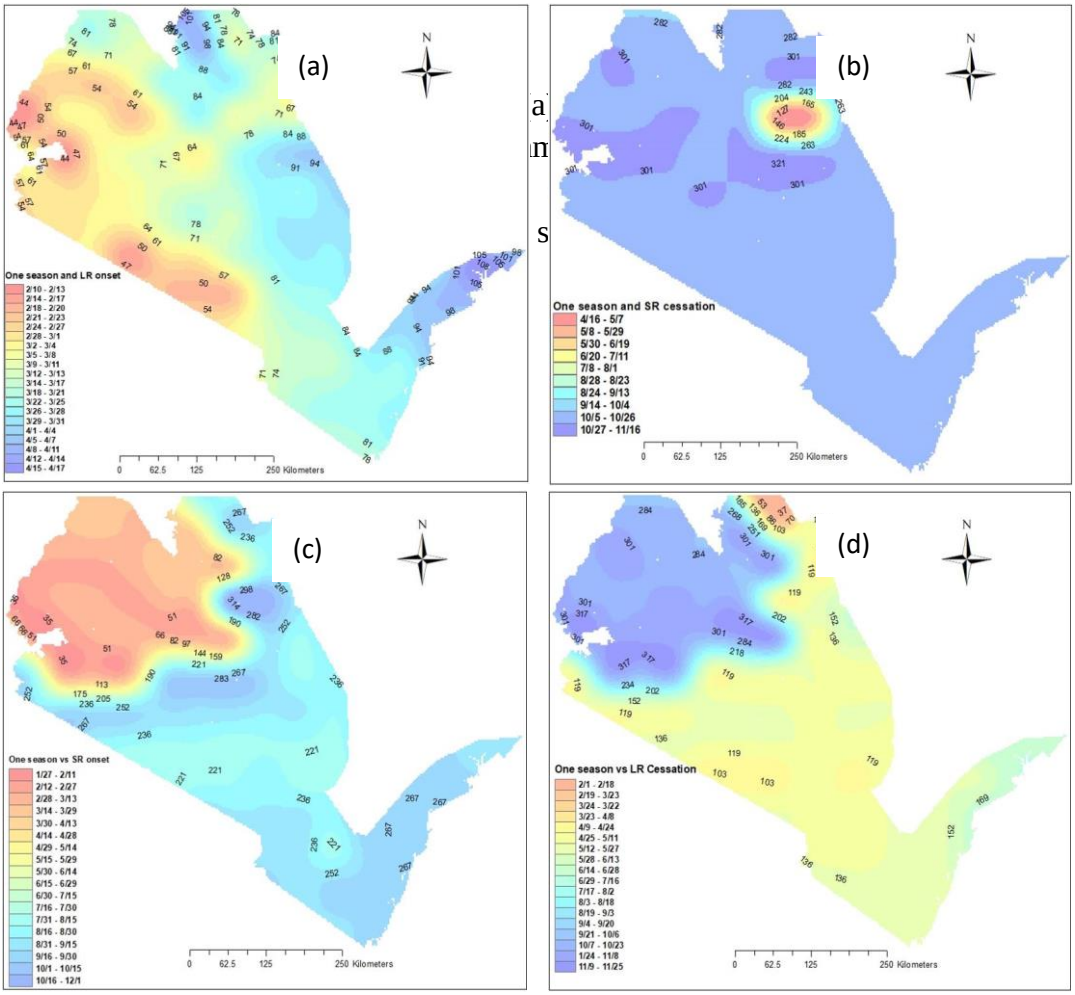

CHAPTER FIVE

SUMMARY OF FINDINGS, CONCLUSIONS AND RECOMMENDATIONS

5.1: Overview

This chapter presents the summary of the findings, conclusions and recommendations based on the objectives of this study. Based on the findings and recommendations from this study, areas of further research have been outlined.

5.2 Summary of the findings

Based on the results observed, all the satellite products overestimated and also underestimated the rainfall amounts based on the pixel to pixel differences (ME). The TRMM product was identified as the best-suited satellite product to predict rainfall in the humid zones and particularly tropical cool humid (TCH), tropical cool sub-humid (TCSH) and tropical warm, humid (TWH) zones. The GPCC product was found suited for predicting rainfall in the tropical warm semiarid (TWSA) and tropical warm sub-humid (TWSH). The LARC-POWER product was found suited for predicting rainfall in the arid zones; tropical cool arid (TCA) and tropical cool semiarid (TCSA). The CHIRPS 2.0 precipitation product was best suited for predicting rainfall in the tropical warm arid (TWA).

The findings of this study indicate variations in GHG (CO_2, CH_4 and N_2O) fluxes based on types of soil amendments applied in semiarid soils in central highlands of Kenya. The GHG fluxes from this study were well within the range of other studies carried out on GHG in the managed upland soils in East Africa. This study fills the gap on the quantities of GHG fluxes and the key factors controlling GHG emissions from a long-term managed on-station research in the drier parts of central Kenya with

high management intensities. Based on the emission factors (EFs) observed from this study, compared with the default IPCC EFs, there is general agreement especially if reporting for the low potential areas and which may differ based on the annual variability.

The DNDC model was able to simulate daily GHG fluxes and notably CO_2 and N_2O for a whole year. The simulated GHG data followed seasonality with an increase in fluxes following the onset of the rains and fertilisation. Plots treated with animal manure had the highest amounts of both CO_2 and N_2O fluxes while control plots had the least amounts of both CO_2 and N_2O fluxes. The simulated data captured the magnitude of the CO_2 peaks though they were delayed coming a few weeks after the observed peaks. The simulated data captured well the timing of the fluxes, mainly the N_2O fluxes, with a slight variation in the magnitude of the N_2O fluxes.

Most of the potential agricultural zones of Kenya during the LR season receive their onset in March and cessation in May translating to a season length of between 23 and 90 days of sufficient rainfall. During the SR season, most of the zones in Kenya experience their onset in September and cessation in October translating to a growing season length of between 23 and 90 days of sufficient rainfall. For the one season, most zones experience their onset in March, similar to the LR onset, and cessation in October, similar to SR cessation, translating to a length of growing season of between 192 and 259 days of sufficient rainfall. Across the country, there are distinct temporal and spatial variations in the onset dates and the length of growing season from one zone to another. This portrays a definite challenge as faced by the smallholder farmers in planning rainfed agricultural cropping calendar; including when to till, incorporate inputs, sow and harvest.

5.3 Conclusions

From this study, it was concluded that;

i. The freely available SRS products provide an accurate alternative source of rainfall data over Kenya for agricultural advisory services and other climate related studies
ii. Animal (goat) manure demonstrates a potential to increase both yields and reduce yield-scaled N_2O emissions simultaneously.
iii. The DNDC model cheaply and accurately simulates GHG from different soil amendment inputs
iv. The derived cropping calendar (length of growing season, rainfall onset and cessation dates) provides a guide on the current status of Kenyan cropping calendar

5.4: Recommendations

From the findings of this study, the following recommendations were derived:

i. The available satellite precipitation products provide a reliable alternative source of precipitation data in low rainfall data prone zones and should be used based on accuracy determined per the agro-ecological zones of Kenya.
ii. Use of animal manure should be emphasised for smallholder farmers to achieve both food security and simultaneously lower GHG emissions thus promoting climate smart agriculture.
iii. The DNDC provides a cheaper reliable alternative method of quantifying the greenhouse gases from the different soil amendment inputs and which can be used to input in the national GHG inventories thus contributing to accurate assessments and reporting to the UNFCCC on GHG emissions from

agricultural soils as well as to identify valuable mitigation and adaptation measures.

iv. The smallholder farmers should be encouraged to follow the observed cropping calendar from this study to determine the right timing for land preparation, sowing and harvesting with the aim of maximising the rainfed agricultural production.

5.5. Areas for further research

Based on the findings of this study, the following areas for further research were identified

i. There is need to evaluate more available long-term satellite precipitation products, spanning a longer period than this study, based on the various agro-ecological zones of Kenya and especially using daily observed data to ascertain their accuracy.

ii. There is need for establishment of more similar empirical studies on GHG carried out mainly in high agricultural potential zones with differing environmental conditions, to capture the influence of farmers' practice on GHG fluxes and to establish similar studies for more extended periods of time (>1 year) to capture the influence of annual weather variations on GHG fluxes.

iii. There is need to evaluate the DNDC model in simulating GHG from various soil amendment inputs in other regions particularly the high potential agricultural zones of Kenya with more long-term observed data.

iv. There is the need for more studies on evaluating the length of the growing season, onset and cessation dates based on other available long-term daily

observed satellite products, based on the different agro-ecological zones to capture their differences in accuracy in predicting precipitation estimations.

REFERENCES

Abiola, F., Mohd-mokhtar, R., Ismail, W., Mohamad, N., & Mandeep, J. S. (2012). Ground validation of space-borne satellite rainfall products in Malaysia. *Advances in Space Research*, *50*(9), 1241–1249. https://doi.org/10.1016/j.asr.2012.06.031

Ahmadi, S. H., Mosallaeepour, E., Kamgar-Haghighi, A. A., & Sepaskhah, A. R. (2015). Modeling Maize Yield and Soil Water Content with AquaCrop Under Full and Deficit Irrigation Management. *Water Resources Management*, *29*(8), 2837–2853. https://doi.org/10.1007/s11269-015-0973-3

Alazzy, A., Lü, H., Chen, R., Ali, A. B., Zhu, Y., & Su, J. (2017). Evaluation of Satellite Precipitation Products and Their Potential Influence on Hydrological Modeling over the Ganzi River Basin of the Tibetan Plateau. *Advances in Meteorology*, *2017*. https://doi.org/10.1155/2017/3695285

Ali, A., & Erenstein, O. (2017). Assessing farmer use of climate change adaptation practices and impacts on food security and poverty in Pakistan. *Climate Risk Management*, *16*, 183–194. https://doi.org/10.1016/j.crm.2016.12.001

Amekudzi, L., Yamba, E., Preko, K., Asare, E., Aryee, J., Baidu, M., & Codjoe, S. (2015). Variabilities in Rainfall Onset, Cessation and Length of Rainy Season for the Various Agro-Ecological Zones of Ghana. *Climate*, *3*(2), 416–434. https://doi.org/10.3390/cli3020416

Ankenbauer, K. J., & Loheide, S. P. (2017). The effects of soil organic matter on soil water retention and plant water use in a meadow of the Sierra Nevada, CA. *Hydrological Processes*, *31*(4), 891–901. https://doi.org/10.1002/hyp.11070

Anyah, R. O., & Semazzi, F. H. M. (2006). Climate variability over the Greater Horn of Africa based on NCAR AGCM ensemble, *62*, 39–62. https://doi.org/10.1007/s00704-005-0203-7

Arias-Navarro, C., Díaz-Pinés, E., Kiese, R., Rosenstock, T. S., Rufino, M. C., Stern, D., & Butterbach-Bahl, K. (2013). Gas pooling: A sampling technique to overcome spatial heterogeneity of soil carbon dioxide and nitrous oxide fluxes. *Soil Biology and Biochemistry*, *67*, 20–23. https://doi.org/10.1016/j.soilbio.2013.08.011

Arvor, D., Funatsu, B. M., Michot, V., & Dubreui, V. (2017). Monitoring rainfall patterns in the southern Amazon with PERSIANN-CDR data: Long-term characteristics and trends. *Remote Sensing*, *9*(9). https://doi.org/10.3390/rs9090889

As-syakur, A. R., Osawa, T., Miura, F., Nuarsa, I. W., Wayan, N., Bagus, I. G., & Tanaka, T. (2016). Maritime Continent rainfall variability during the TRMM era : Modoki. The role of monsoon, topography and El Nino. *Dynamics of Atmospheres and Oceans*, *75*, 58–77. https://doi.org/10.1016/j.dynatmoce.2016.05.004

Asfaw, A., Simane, B., Hassen, A., & Bantider, A. (2017). Variability and time series trend analysis of rainfall and temperature in northcentral Ethiopia: A case study in Woleka sub-basin. *Weather and Climate Extremes*, 1–13. https://doi.org/10.1016/j.wace.2017.12.002

Awange, J., Ferreira, V. G., Forootan, E., Khandu, Andam-Akorful, S. A., Agutu, N. O., & He, X. F. (2016). Uncertainties in remotely sensed precipitation data over Africa. *International Journal of Climatology*, *36*(1), 303–323. https://doi.org/10.1002/joc.4346

Bai, L., Shi, C., Li, L., Yang, Y., & Wu, J. (2018). Accuracy of CHIRPS Satellite-Rainfall Products over Mainland China. *Remote Sensing*, *10*(3), 362. https://doi.org/10.3390/rs10030362

Baidu, M., Amekudzi, L., Aryee, J., & Annor, T. (2017). Assessment of Long-term Spatio-temporal Rainfall Variability over Ghana using Wavelet Analysis. *Climate*, *5*(30), 1–24. https://doi.org/10.3390/cli5020030

Balsamo, G., Albergel, C., Beljaars, A., Boussetta, S., Brun, E., Cloke, H., & Vitart, F. (2015). ERA-Interim/Land: A global land surface reanalysis data set. *Hydrology and Earth System Sciences*, *19*(1), 389–407. https://doi.org/10.5194/hess-19-389-2015

Barton, L., Hoyle, F. C., Stefanova, K. T., & Murphy, D. V. (2016). Incorporating organic matter alters soil greenhouse gas emissions and increases grain yield in a semi-arid climate. *Agriculture, Ecosystems and Environment*, *231*(3), 320–330. https://doi.org/10.1016/j.agee.2016.07.004

Bateman, E. J., & Baggs, E. M. (2005). Contributions of nitrification and denitrification to N_2O emissions from soils at different water-filled pore space. *Biology and Fertility of Soils*, *41*(6), 379–388. https://doi.org/10.1007/s00374-005-0858-3

Bieber, N., Ker, J. H., Wang, X., Triantafyllidis, C., van Dam, K. H., Koppelaar, R. H. E. M., & Shah, N. (2018). Sustainable planning of the energy-water-food nexus using decision making tools. *Energy Policy*, *113*, 584–607. https://doi.org/10.1016/j.enpol.2017.11.037

Birch, H. (1958). The effect of soil drying on humus decomposition and nitrogen availability. *Plant and Soil*, (1), 9–10.

Blacutt, L. A., Herdies, D. L., de Gonçalves, L. G. G., Vila, D. A., & Andrade, M. (2015). Precipitation comparison for the CFSR, MERRA, TRMM3B42 and Combined Scheme datasets in Bolivia. *Atmospheric Research*, *163*, 117–131. https://doi.org/10.1016/j.atmosres.2015.02.002

Blaney, H., & Criddle, W. (1962). Determining Consumptive Use and Irrigation Water Requirements. *USDA Technical Bulletin 1275, Beltsville*.

Bodelier, P., Hahn, A., Arth, I., & Frenzel, P. (2000). Effects of ammonium-based fertilisation on microbial processes involved in methane emission from soils planted with rice. *Biogeochemistry*, (Neue 1997), 225–257. https://doi.org/10.1023/A:1006438802362

Boyard-Micheau, J., Camberlin, P., Philippon, N., & Moron, V. (2013). Regional-scale rainy season onset detection: A new approach based on multivariate analysis. *Journal of Climate*, *26*(22), 8916–8928. https://doi.org/10.1175/JCLI-D-12-00730.1

Brilli, L., Bechini, L., Bindi, M., Carozzi, M., Cavalli, D., Conant, R., & Bellocchi, G. (2017). Review and analysis of strengths and weaknesses of agro-ecosystem models for simulating C and N fluxes. *Science of the Total Environment*, *598*, 445–470. https://doi.org/10.1016/j.scitotenv.2017.03.208

Burton, D. L., Zebarth, B. J., Gillam, K. M., & MacLeod, J. A. (2008). Effect of fertilizer nitrogen management on N_2O emissions in commercial corn fields. *Canadian Journal of Soil Science*, *88*(2), 189–195. https://doi.org/10.4141/CJSS06010

Butterbach-Bahl, K., Baggs, E. M., Dannenmann, M., Kiese, R., & Zechmeister-Boltenstern, S. (2013). Nitrous oxide emissions from soils: how well do we understand the processes and their controls? *Philosophical Transactions of the Royal Society B: Biological Sciences*, *368*(1621), 20130122–20130122. https://doi.org/10.1098/rstb.2013.0122

Butterbach-Bahl, K., & Papen, H. (2002). Four years continuous record of CH_4-exchange between the atmosphere and untreated and limed soil of a N-saturated spruce and beech forest ecosystem in Germany. *Plant and Soil*, *240*(1), 77–90. https://doi.org/10.1023/A:1015856617553

Byakatonda, J., Parida, B. P., Kenabatho, P. K., & Moalafhi, D. B. (2018). Prediction of onset and cessation of austral summer rainfall and dry spell frequency analysis in semiarid Botswana. *Theoretical and Applied Climatology*, 1–17. https://doi.org/10.1007/s00704-017-2358-4

Bykova, S., Boeckx, P., Kravchenko, I., Galchenko, V., & Van Cleemput, O. (2007). Response of CH_4 oxidation and methanotrophic diversity to NH_4^+ and CH_4 mixing ratios. *Biology and Fertility of Soils*, *43*(3), 341–348. https://doi.org/10.1007/s00374-006-0114-5

Campbell, B. M., Vermeulen, S. J., Aggarwal, P. K., Corner-Dolloff, C., Girvetz, E., & Wollenberg, E. (2016). Reducing risks to food security from climate change. *Global Food Security*, 0–1. https://doi.org/10.1016/j.gfs.2016.06.002

Cardenas, L. M., Misselbrook, T. M., Hodgson, C., Donovan, N., Gilhespy, S., Smith, K. A., & Chadwick, D. (2016). Effect of the application of cattle urine with or without the nitrification inhibitor DCD, and dung on greenhouse gas emissions from a UK grassland soil. *Agriculture, Ecosystems and Environment*, *235*, 229–241. https://doi.org/10.1016/j.agee.2016.10.025

Chantigny, M. H., Rochette, P., Angers, D. A., Bittman, S., Buckley, K., Massé, D., & Gasser, M.O. (2010). Soil Nitrous Oxide Emissions Following Band-Incorporation of Fertilizer Nitrogen and Swine Manure. *Journal of Environment Quality*, *39*(5), 1545. https://doi.org/10.2134/jeq2009.0482

Chen, C., Chen, D., & Lam, S. K. (2015). Simulation of nitrous oxide emission and mineralized nitrogen under different straw retention conditions using a denitrification-decomposition model. *Clean - Soil, Air, Water*, *43*(4), 577–583. https://doi.org/10.1002/clen.201400318

Chen, C., Yu, Z., Li, L., & Yang, C. (2011). Adaptability evaluation of TRMM satellite rainfall and its application in the Dongjiang River Basin. *Procedia Environmental Sciences*, *10*, 396–402. https://doi.org/10.1016/j.proenv.2011.09.065

Chen, M., Shi, W., Xie, P., Silva, V. B. S., Kousky, V. E., Higgins, R. W., & Janowiak, J. E. (2008). Assessing objective techniques for gauge-based analyses of global daily precipitation. *Journal of Geophysical Research Atmospheres*, *113*(4), 1–13. https://doi.org/10.1029/2007JD009132

Chen, S., Liu, H., You, Y., Mullens, E., Hu, J., Yuan, Y., & Hong, Y. (2014). Evaluation of high-resolution precipitation estimates from satellites during July 2012 Beijing flood event using dense rain gauge observations. *PLoS ONE*, *9*(4), 1–7. https://doi.org/10.1371/journal.pone.0089681

Chi, J., Waldo, S., Pressley, S., O'Keeffe, P., Huggins, D., Stöckle, C., & Lamb, B. (2016). Assessing carbon and water dynamics of no-till and conventional tillage cropping systems in the inland Pacific Northwest US using the eddy covariance method. *Agricultural and Forest Meteorology*, *218–219*, 37–49. https://doi.org/10.1016/j.agrformet.2015.11.019

Ciais, P., Bombelli, A., Williams, M., Piao, S. L., Chave, J., Ryan, C. M., & Valentini, R. (2011). The carbon balance of Africa: synthesis of recent research studies. *Philosophical Transactions of the Royal Society A: Mathematical, Physical and Engineering Sciences*, *369*(1943), 2038–2057. https://doi.org/10.1098/rsta.2010.0328

Congreves, K. A., Grant, B. B., Dutta, B., Smith, W. N., Chantigny, M. H., Rochette, P., & Desjardins, R. L. (2016). Predicting ammonia volatilization after field application of swine slurry: DNDC model development. *Agriculture, Ecosystems and Environment*, *219*, 179–189. https://doi.org/10.1016/j.agee.2015.10.028

Conti, F., Hsu, K. L., Noto, L. V., & Sorooshian, S. (2014). Evaluation and comparison of satellite precipitation estimates with reference to a local area in the Mediterranean Sea. *Atmospheric Research*, *138*, 189–204. https://doi.org/10.1016/j.atmosres.2013.11.011

Deng, J., Li, C., Burger, M., Horwath, W. R., Smart, D., Six, J., & Frolking, S. (2018). Assessing data-induced uncertainty of N_2O emissions from arable soils in Europe using a process-based biogeochemical model. *Journal of Geophysical Research: Biogeosciences*, *13*, 12971.

Deng, Q., Hui, D., Wang, J., Yu, C. L., Li, C., Reddy, K. C., & Dennis, S. (2016). Assessing the impacts of tillage and fertilization management on nitrous oxide emissions in a cornfield using the DNDC model. *Journal of Geophysical Research: Biogeosciences*, *121*(2), 337–349. https://doi.org/10.1002/2015JG003239

Dhib, S., Mannaerts, C. M., Bargaoui, Z., Retsios, V., & Maathuis, B. H. P. (2017). Evaluating the MSG satellite Multi-Sensor Precipitation Estimate for extreme rainfall monitoring over northern Tunisia. *Weather and Climate Extremes*, *16*, 14–22. https://doi.org/10.1016/j.wace.2017.03.002

Ding, W., Meng, L., Cai, Z., & Han, F. (2007). Effects of long-term amendment of organic manure and nitrogen fertilizer on nitrous oxide emission in a sandy loam soil. *Journal of Environmental Sciences (China)*, *19*(2), 185–193. https://doi.org/10.1016/S1001-0742(07)60030-8

Dinku, T., Ceccato, P., & Connor, S. J. (2011). Challenges of satellite rainfall estimation over mountainous and arid parts of east Africa. *International Journal of Remote Sensing*, *32*(21), 5965–5979. https://doi.org/10.1080/01431161.2010.499381

Dinku, T., Ruiz, F., Connor, S. J., & Ceccato, P. (2010). Validation and intercomparison of satellite rainfall estimates over Colombia. *Journal of Applied Meteorology and Climatology*, *49*(5), 1004–1014. https://doi.org/10.1175/2009JAMC2260.1

Dourte, D. R., Fraisse, C. W., & Bartels, W. L. (2015). Exploring changes in rainfall intensity and seasonal variability in the Southeastern U.S.: Stakeholder engagement, observations, and adaptation. *Climate Risk Management*, *7*, 11–19. https://doi.org/10.1016/j.crm.2015.02.001

Duan, Z., & Bastiaanssen, W. G. M. (2013). First results from Version 7 TRMM 3B43 precipitation product in combination with a new downscaling-calibration procedure. *Remote Sensing of Environment*, *131*, 1–13. https://doi.org/10.1016/j.rse.2012.12.002

Duan, Z., Liu, J., Tuo, Y., Chiogna, G., & Disse, M. (2016). Evaluation of eight high spatial resolution gridded precipitation products in Adige Basin (Italy) at multiple temporal and spatial scales. *Science of the Total Environment*, *573*, 1536–1553. https://doi.org/10.1016/j.scitotenv.2016.08.213

Dunning, C. M., Black, E. C. L., & Allan, R. P. (2016). The onset and cessation of seasonal rainfall over Africa. *Journal of Geophysical Research*, *121*(19), 11405–11424. https://doi.org/10.1002/2016JD025428

Dutta, B., Grant, B. B., Campbell, C. A., Lemke, R. L., Desjardins, R. L., & Smith, W. N. (2017). A multi model evaluation of long-term effects of crop management and cropping systems on nitrogen dynamics in the Canadian semi-arid prairie. *Agricultural Systems*, *151*, 136–147. https://doi.org/10.1016/j.agsy.2016.12.003

Ellert, B. H., & Janzen, H. H. (2008). Nitrous oxide, carbon dioxide and methane emissions from irrigated cropping systems as influenced by legumes, manure and fertilizer. *Canadian Journal of Soil Science*, *88*(2), 207–217. https://doi.org/10.4141/CJSS06036

ESRI, (2016). ArcGIS Desktop: Release 10.4 (February 18, 2016)

Eugster, W., & Merbold, L. (2015). Eddy covariance for quantifying trace gas fluxes from soils. *Soil*, *1*(1), 187–205. https://doi.org/10.5194/soil-1-187-2015

FAO. (1996). Agro-Ecological Zoning Guidelines. *FAO Soils Bulletin 76*, 3–5.

FAO. (2009). The state of food and agriculture. Viale Delle Terme di Caracalla, 00153 Rome, Italy. Retrieved from http://www.fao.org/docrep/012/i0680e/i0680e.pdf

FAO. (2010). The State of Food Insecurity in the World Addressing food insecurity in protracted crises 2010 Key messages. Notes. https://doi.org/10.1519/JSC.0b013e3181b8666e

Fitton, N., Datta, A., Hastings, A., Kuhnert, M., Topp, C. F. E., Cloy, J. M., & Smith, P. (2014). The challenge of modelling nitrogen management at the field scale: Simulation and sensitivity analysis of N_2O fluxes across nine experimental sites using Daily DayCent. *Environmental Research Letters*, *9*(9). https://doi.org/10.1088/1748-9326/9/9/095003

Funk, C., Dettinger, M. D., Michaelsen, J. C., Verdin, J. P., Brown, M. E., Barlow, M., & Hoell, A. (2008). Warming of the Indian Ocean threatens eastern and southern African food security but could be mitigated by agricultural development. *Proceedings of the National Academy of Sciences*, *105*(32), 11081–11086. https://doi.org/10.1073/pnas.0708196105

Funk, C., Peterson, P., Landsfeld, M., Pedreros, D., Verdin, J., Shukla, S., & Michaelsen, J. (2015). The climate hazards infrared precipitation with stations - A new environmental record for monitoring extremes. *Scientific Data*, *2*, 1–21. https://doi.org/10.1038/sdata.2015.66

Gaillard, R. K., Jones, C. D., Ingraham, P., Collier, S., Izaurrald, R. C., Jokela, W., & Salas, W. (2017). Underestimation of N_2O emissions in a comparison of the DayCent, DNDC, and EPIC models. *Ecological Applications: Ecological Society of America*, *12*(10), 3218–3221. https://doi.org/10.1002/eap.01674

García, Á., Riaño, H., & Magnitskiy, S. (2014). Simulation of corn (Zea mays L.) production in different agricultural zones of Colombia using the AquaCrop model. *Agronomia Colombiana*, *32*(3), 358–366. https://doi.org/10.15446/agron.colomb.v32n3.45939

Giltrap, D. L., Li, C., & Saggar, S. (2010). DNDC: A process-based model of greenhouse gas fluxes from agricultural soils. *Agriculture, Ecosystems and Environment*, *136*(3–4), 292–300. https://doi.org/10.1016/j.agee.2009.06.014

GoK. (2012). Availability and Accessibility to Climate Data for Kenya. *Adaptation Technical Analysis, Technical*, 1–47.

Gourdji, S., Läderach, P., Valle, A. M., Martinez, C. Z., & Lobell, D. B. (2015). Historical climate trends, deforestation, and maize and bean yields in Nicaragua. *Agricultural and Forest Meteorology*, *200*, 270–281. https://doi.org/10.1016/j.agrformet.2014.10.002

Guest, G., Kröbel, R., Grant, B., Smith, W., Sansoulet, J., Pattey, E., & Tremblay, G. (2017). Model comparison of soil processes in eastern Canada using DayCent, DNDC and STICS. *Nutrient Cycling in Agroecosystems*, *109*(3), 211–232. https://doi.org/10.1007/s10705-017-9880-8

Haichar, F. el Z., Santaella, C., Heulin, T., & Achouak, W. (2014). Root exudates mediated interactions below ground. *Soil Biology and Biochemistry*, *77*, 69–80. https://doi.org/10.1016/j.soilbio.2014.06.017

Hanson, R. S., & Hanson, T. E. (1996). Methanotrophic bacteria. *Microbiological Reviews*, *60*(2), 439–471.

Harris, I., Jones, P. D., Osborn, T. J., & Lister, D. H. (2014). Updated high-resolution grids of monthly climatic observations - the CRU TS3.10 Dataset. *International Journal of Climatology*, *34*(3), 623–642. https://doi.org/10.1002/joc.3711

Harvey, C. A., Rakotobe, Z. L., Rao, N. S., Dave, R., Razafimahatratra, H., Rabarijohn, H., & Mackinnon, J. L. (2014). Extreme vulnerability of smallholder farmers to agricultural risks and climate change in Madagascar Extreme vulnerability of smallholder farmers to agricultural risks and climate change in Madagascar Author for correspondence : *Phil. Trans. R. Soc.*, *369*(1639), 1–12. https://doi.org/10.1098/rstb.2013.0089

He, Z., Yang, L., Tian, F., Ni, G., Hou, A., & Lu, H. (2017). Intercomparisons of Rainfall Estimates from TRMM and GPM Multisatellite Products over the Upper Mekong River Basin. *Journal of Hydrometeorology*, *18*(2), 413–430. https://doi.org/10.1175/JHM-D-16-0198.1

Heng, L. K., Hsiao, T., Evett, S., Howell, T., & Steduto, P. (2009). Validating the FAO aquacrop model for irrigated and water deficient field maize. *Agronomy Journal*, *101*(3), 488–498. https://doi.org/10.2134/agronj2008.0029xs

Hickman, J. E., Palm, C. A., Mutuo, P., Melillo, J. M., & Tang, J. (2014). Nitrous oxide (N_2O) emissions in response to increasing fertilizer addition in maize (Zea mays L.) agriculture in western Kenya. *Nutrient Cycling in Agroecosystems*, *100*(2), 177–187. https://doi.org/10.1007/s10705-014-9636-7

Hobouchian, M. P., Salio, P., García Skabar, Y., Vila, D., & Garreaud, R. (2017). Assessment of satellite precipitation estimates over the slopes of the subtropical Andes. *Atmospheric Research*, *190*, 43–54. https://doi.org/10.1016/j.atmosres.2017.02.006

Hook, S. E., Wright, A. D. G., & McBride, B. W. (2010). Methanogens: Methane producers of the rumen and mitigation strategies. *Hindawi Publishing Corporation; Archaea*, *2010*, 50–60. https://doi.org/10.1155/2010/945785

Hossain, M., Roy, K., & Datta, D. (2014). Spatial and Temporal Variability of Rainfall over the South-West Coast of Bangladesh. *Climate*, *2*(2), 28–46. https://doi.org/10.3390/cli2020028

Hsu, K., Gao, X., Sorooshian, S., & Gupta, H. V. (1997). Precipitation Estimation from Remotely Sensed Information Using Artificial Neural Networks. *Journal of Applied Meteorology*, *36*(9), 1176–1190. https://doi.org/10.1175/1520-0450(1997)036

Hu, Q., Yang, D., Li, Z., Mishra, A. K., Wang, Y., & Yang, H. (2014). Multi-scale evaluation of six high-resolution satellite monthly rainfall estimates over a humid region in China with dense rain gauges. *International Journal of Remote Sensing*, *35*(4), 1272–1294. https://doi.org/10.1080/01431161.2013.876118

Huffman, G. J., Bolvin, D. T., Nelkin, E. J., Wolff, D. B., Adler, R. F., Gu, G., & Stocker, E. F. (2007). The TRMM Multisatellite Precipitation Analysis (TMPA): Quasi-Global, Multiyear, Combined-Sensor Precipitation Estimates at Fine Scales. *Journal of Hydrometeorology*, *8*(1), 38–55. https://doi.org/10.1175/JHM560.1

Huho, J. M., & Mugalavai, E. M. (2010). The Effects of Droughts on Food Security in Kenya. *The International Journal of Climate Change: Impacts and Responses*, *2*(2), 61–72. https://doi.org/10.18848/1835-7156/CGP/v02i02/37312

Ioannidou, M. P., Kalogiros, J. A., & Stavrakis, A. K. (2016). Comparison of the TRMM Precipitation Radar rainfall estimation with ground-based disdrometer and radar measurements in South Greece. *Atmospheric Research*, *181*, 172–185. https://doi.org/10.1016/j.atmosres.2016.06.023

IPCC. (2007). IPCC (Intergovernmental Panel on Climate Change) Climate Change 2007 : An Assessment of the Intergovernmental Panel on Climate Change. *Climate Change 2007: Synthesis Report*, (Valencia, Spain), 12–17.

IPCC. (2014). Summary for Policymakers. In: Climate Change 2014: Mitigation of Climate Change. *Summary for Policymakers. In: Climate Change 2014: Mitigation of Climate Change. Contribution of Work- Ing Group III to the Fifth Assessment Report of the Intergovernmental Panel on Climate Change. Edenhofer, O., R. Pichs-Madruga, Y. Sokona, E. Farahani*, Cambridge University Press, Cambridge, United King.

Jaetzold, R., Schmidt, H., Hornetz, B., & Shisanya, C. (2007). Farm Management Handbook of Kenya Subpart C1, *II*, 1–573.

Jarecki, M., Grant, B., Smith, W., Deen, B., Drury, C., VanderZaag, A., & Wagner-Riddle, C. (2018). Long-term Trends in Corn Yields and Soil Carbon under Diversified Crop Rotations. *Journal of Environment Quality*, *0*(0), 0. https://doi.org/10.2134/jeq2017.08.0317

Jovani-Sancho, A. J., Brosnan, S., & Byrne, K. A. (2017). Partitioning of soil respiration in a first rotation beech plantation. *Biology and Environment*, *117B*(2), 91–105. https://doi.org/10.3318/BIOE.2017.09

Joyce, R., Janowiak, J. E., Arkin, P. A., & Xie, P. (2004). CMORPH: A Method that Produces Global Precipitation Estimates from Passive Microwave and Infrared Data at High Spatial and Temporal Resolution. *Journal of Hydrometeorology*, *5*(3), 487–503. https://doi.org/10.1175/1525-7541(2004)005

Jury, M. R. (2017). Evaluation of satellite-model proxies for hydro-meteorological services in the upper Zambezi. *Journal of Hydrology: Regional Studies*, *13*(August 2016), 91–109. https://doi.org/10.1016/j.ejrh.2017.08.003

Kalnay, E., Kanamitsu, M., Kistler, R., Collins, W., Deaven, D., Gandin, L., & Joseph, D. (1996). NCAR 40-year reanalysis project. *Bull Amer Meteor Soc*, *77 SRC-*, 437–470.

Kassie, B. T., Hengsdijk, H., Rötter, R., Kahiluoto, H., Asseng, S., & Van Ittersum, M. (2013). Adapting to climate variability and change: Experiences from cereal-based farming in the central rift and kobo valleys, Ethiopia. *Environmental Management*, *52*(5), 1115–1131. https://doi.org/10.1007/s00267-013-0145-2

Katiraie-Boroujerdy, P.-S., Nasrollahi, N., Hsu, K. lin, & Sorooshian, S. (2013). Evaluation of satellite-based precipitation estimation over Iran. *Journal of Arid Environments*, *97*, 205–219. https://doi.org/10.1016/j.jaridenv.2013.05.013

Katsanos, D., Retalis, A., & Michaelides, S. (2016). Validation of a high-resolution precipitation database (CHIRPS) over Cyprus for a 30-year period. *Atmospheric Research*, *169*, 459–464. https://doi.org/10.1016/J.ATMOSRES.2015.05.015

Khatri-Chhetri, A., Aggarwal, P. K., Joshi, P. K., & Vyas, S. (2017). Farmers' prioritization of climate-smart agriculture (CSA) technologies. *Agricultural Systems*, *151*, 184–191. https://doi.org/10.1016/j.agsy.2016.10.005

Kiboi, M. N., Ngetich, K. F., Diels, J., Mucheru-Muna, M., Mugwe, J., & Mugendi, D. N. (2017). Minimum tillage, tied ridging and mulching for better maize yield and yield stability in the Central Highlands of Kenya. *Soil and Tillage Research*, *170*(April), 157–166. https://doi.org/10.1016/j.still.2017.04.001

Kiese, R., Hewett, B., Graham, A., & Butterbach-Bahl, K. (2003). Seasonal variability of N_2O emissions and CH_4 uptake by tropical rainforest soils of Queensland , Australia, *17*(2), 1–13. https://doi.org/10.1029/2002GB002014

Kipkorir, E. (2005). RAIN : A Software Package for Determination of Rainfall Parameters and Relative Yield Forecast. *Moi University, Eldoret, Kenya*, 22.

Kirschke, S., Bousquet, P., Ciais, P., Saunois, M., Canadell, J. G., Dlugokencky, E. J., & Zeng, G. (2013). Three decades of global methane sources and sinks. *Nature Geoscience*, *6*(10), 813–823. https://doi.org/10.1038/ngeo1955

Kisaka, M. O., Mucheru-Muna, M., Ngetich, F. K., Mugwe, J., Mugendi, D., Mairura, F., & Makokha, G. L. (2015). Potential of deterministic and geostatistical rainfall interpolation under high rainfall variability and dry spells : Case of Kenya ' s Central Highlands. *Theor Appl Climatol*. https://doi.org/10.1007/s00704-015-1413-2

Kisaka, M. O., Mucheru-Muna, M., Ngetich, F. K., Mugwe, J. N., Mugendi, D., & Mairura, F. (2015). Rainfall variability, drought characterization, and efficacy of rainfall data reconstruction: Case of Eastern Kenya. *Advances in Meteorology*, *2015*. https://doi.org/10.1155/2015/380404

Kolawole, O. D., Wolski, P., Ngwenya, B., & Mmopelwa, G. (2014). Ethno-meteorology and scientific weather forecasting: Small farmers and scientists' perspectives on climate variability in the Okavango Delta, Botswana. *Climate Risk Management*, *4*, 43–58. https://doi.org/10.1016/j.crm.2014.08.002

Konda, R., Ohta, S., Ishizuka, S., Heriyanto, J., & Wicaksono, A. (2010). Seasonal changes in the spatial structures of N_2O, CO_2, and CH_4 fluxes from Acacia mangium plantation soils in Indonesia. *Soil Biology and Biochemistry*, *42*(9), 1512–1522. https://doi.org/10.1016/J.SOILBIO.2010.05.022

Krakauer, N., Pradhanang, S., Panthi, J., Lakhankar, T., & Jha, A. (2015). Probabilistic Precipitation Estimation with a Satellite Product. *Climate*, *3*(2), 329–348. https://doi.org/10.3390/cli3020329

Kröbel, R., Smith, W. N., Grant, B. B., Desjardins, R. L., Campbell, C. A., Tremblay, N., & Mcconkey, B. G. (2011). Development and evaluation of a new Canadian spring wheat sub-model for DNDC. *Canadian Journal of Soil Science*, *91*, 503–520. https://doi.org/10.4141/CJSS2010-059

Le Mer, J., & Roger, P. (2001). Production, oxidation, emission and consumption of methane by soils: A review. *European Journal of Soil Biology*, *37*(1), 25–50. https://doi.org/10.1016/S1164-5563(01)01067-6

Lehuger, S., Gabrielle, B., Laville, P., Lamboni, M., Loubet, B., & Cellier, P. (2011). Predicting and mitigating the net greenhouse gas emissions of crop rotations in Western Europe. *Agricultural and Forest Meteorology*, *151*(12), 1654–1671. https://doi.org/10.1016/j.agrformet.2011.07.002

Lenz-Wiedemann, V. I. S., Schneider, K., Miao, Y., & Bareth, G. (2012). Development of a regional crop growth model for Northeast China. *Procedia Environmental Sciences*, *13*(2011), 1946–1955. https://doi.org/10.1016/j.proenv.2012.01.188

Li, B., Fan, C. H., Zhang, H., Chen, Z. Z., Sun, L. Y., & Xiong, Z. Q. (2015). Combined effects of nitrogen fertilization and biochar on the net global warming potential, greenhouse gas intensity and net ecosystem economic budget in intensive vegetable agriculture in southeastern China. *Atmospheric Environment*, *100*, 10–19. https://doi.org/10.1016/j.atmosenv.2014.10.034

Li, C. (2007). Quantifying greenhouse gas emissions from soils: Scientific basis and modeling approach. *Soil Science and Plant Nutrition*, *53*(4), 344–352. https://doi.org/10.1111/j.1747-0765.2007.00133.x

Li, C., Frolking, S., & Tod, F. (1992). A Model of Nitrous Oxide Evolution From soil by Rainfall Events: 1. Model Structure and Sensitivity. *Journal of Geophysical Research (Atmospheres)*, *97*(D5), 9759–9776.

Li, H., Qiu, J., Wang, L., Tang, H., Li, C., & Van Ranst, E. (2010). Modelling impacts of alternative farming management practices on greenhouse gas emissions from a winter wheat-maize rotation system in China. *Agriculture, Ecosystems and Environment*, *135*(1–2), 24–33. https://doi.org/10.1016/j.agee.2009.08.003

Li, Z., Yang, J. Y., Drury, C. F., Yang, X. M., Reynolds, W. D., Li, X., & Hu, C. (2017). Evaluation of the DNDC model for simulating soil temperature, moisture and respiration from monoculture and rotational corn, soybean and winter wheat in Canada. *Ecological Modelling*, *360*(October), 230–243. https://doi.org/10.1016/j.ecolmodel.2017.07.013

Macharia, J., Mugwe, J., Mucheru-Muna, M., & Mugendi, D. (2014). Socioeconomic Factors Influencing Levels of Knowledge in Soil Fertility Management in the Central Highlands of Kenya. *Journal of Agricultural Science and Technology B*, *4*, 701–711. https://doi.org/10.17265/2161-6264/2014.09.003

MacLeod, D. (2018). Seasonal predictability of onset and cessation of the East African rains. *Weather and Climate Extremes*, 0–1. https://doi.org/10.1016/j.wace.2018.05.003

Manzanas, R., Amekudzi, L. K., Preko, K., Herrera, S., & Gutiérrez, J. M. (2014). Precipitation variability and trends in Ghana: An intercomparison of observational and reanalysis products. *Climatic Change*, *124*(4), 805–819. https://doi.org/10.1007/s10584-014-1100-9

Martinez, C., Alberti, G., Cotrufo, M. F., Magnani, F., Zanotelli, D., Camin, F., & Rodeghiero, M. (2016). Belowground carbon allocation patterns as determined by the in-growth soil core13C technique across different ecosystem types. *Geoderma*, *263*, 140–150. https://doi.org/10.1016/j.geoderma.2015.08.043

Masaka, J., Nyamangara, J., & Wuta, M. (2014). Nitrous oxide emissions from wetland soil amended with inorganic and organic fertilizers. *Archives of Agronomy and Soil Science*, *60*(10), 1363–1387. https://doi.org/10.1080/03650340.2014.890707

McDowell, J. Z., & Hess, J. J. (2012). Accessing adaptation: Multiple stressors on livelihoods in the Bolivian highlands under a changing climate. *Global Environmental Change*, *22*(2), 342–352. https://doi.org/10.1016/j.gloenvcha.2011.11.002

Meng, J., Li, L., Hao, Z., Wang, J., & Shao, Q. (2014). Suitability of TRMM satellite rainfall in driving a distributed hydrological model in the source region of Yellow River, *509*, 320–332. https://doi.org/10.1016/j.jhydrol.2013.11.049

Midega, C. A. O., Murage, A. W., Pittchar, J. O., & Khan, Z. R. (2016). Managing storage pests of maize: Farmers' knowledge, perceptions and practices in western Kenya. *Crop Protection*, *90*, 142–149. https://doi.org/10.1016/j.cropro.2016.08.033

Midega, C. A. O., Pittchar, J. O., Pickett, J. A., Hailu, G. W., & Khan, Z. R. (2018). A climate-adapted push-pull system effectively controls fall armyworm, Spodoptera frugiperda (J E Smith), in maize in East Africa. *Crop Protection*, *105*, 10–15. https://doi.org/10.1016/j.cropro.2017.11.003

Moazami, S., Golian, S., Hong, Y., Sheng, C., & Reza, M. (2016). Comprehensive evaluation of four high-resolution satellite precipitation products under diverse climate conditions in Iran. *Hydrological Sciences Journal*, *61*(2), 420–440. https://doi.org/10.1080/02626667.2014.987675

Mohanty, S. R., Nayak, D. R., Babu, Y. J., & Adhya, T. K. (2004). Butachlor inhibits production and oxidation of methane in tropical rice soils under flooded condition. *Microbiological Research*, *159*(3), 193–201. https://doi.org/10.1016/j.micres.2004.03.004

Montazerolghaem, M., Vervoort, W., Minasny, B., & McBratney, A. (2016). Long-term variability of the leading seasonal modes of rainfall in south-eastern Australia. *Weather and Climate Extremes*, *13*, 1–14. https://doi.org/10.1016/j.wace.2016.04.001

Mourtzinis, S., Rattalino Edreira, J. I., Conley, S. P., & Grassini, P. (2017). From grid to field: Assessing quality of gridded weather data for agricultural applications. *European Journal of Agronomy*, *82*, 163–172. https://doi.org/10.1016/j.eja.2016.10.013

Mucheru-Muna, M., Mugendi, D., Mugwe, J., Kung'u, J., Merckx, R., & Vanlauwe, B. (2009). Soil Mineral N Dynamics in a Maize Crop Following Different Soil Fertility Amendments in Different Soil Fertility Status in Sub-humid and Semi-arid Regions in Central Kenya. *Agriculture and Biological Sciences*, *5*(6), 978–993.

Mucheru-Muna, M., Mugendi, D., Pypers, P., Mugwe, J., Kung'U, J., Vanlauwe, B., & Merckx, R. (2014). Enhancing maize productivity and profitability using organic inputs and mineral fertilizer in central Kenya small-hold farms. *Experimental Agriculture*, *50*(2), 250–269. https://doi.org/10.1017/S0014479713000525

Mugalavai, E. M., Kipkorir, E. C., Raes, D., & Rao, M. S. (2008). Analysis of rainfall onset, cessation and length of growing season for western Kenya. *Agricultural and Forest Meteorology*, *148*(6–7), 1123–1135. https://doi.org/10.1016/j.agrformet.2008.02.013

Mugi-Ngenga, E. W., Mucheru-Muna, M. W., Mugwe, J. N., Ngetich, F. K., Mairura, F. S., & Mugendi, D. N. (2016). Household's socio-economic factors influencing the level of adaptation to climate variability in the dry zones of Eastern Kenya. *Journal of Rural Studies*, *43*, 49–60. https://doi.org/10.1016/j.jrurstud.2015.11.004

Mugwe, J., Mucheru-Muna, M., Mugendi, D., Kung'u, J., Bationo, A., & Mairura, F. (2009). Adoption potential of selected organic resources for improving soil fertility in the central highlands of Kenya. *Agroforestry Systems*, *76*(2), 467–485. https://doi.org/10.1007/s10457-009-9217-y

Mugwe, J., Mugendi, D., Mucheru-Muna, M., Merckx, R., Chianu, J., & Vanlauwe, B. (2009). Determinants of the decision to adopt integrated soil fertility management practices by smallholder farmers in the central highlands of Kenya. *Experimental Agriculture*, *45*(1), 61–75. https://doi.org/10.1017/S0014479708007072

Mukumbuta, I., Shimizu, M., & Hatano, R. (2017). Mitigating Global Warming Potential and Greenhouse Gas Intensities by Applying Composted Manure in Cornfield: A 3-Year Field Study in an Andosol Soil. *Agriculture*, *7*(2), 13. https://doi.org/10.3390/agriculture7020013

Mulianga, B., Bégué, A., Simoes, M., & Todoroff, P. (2013). Forecasting regional sugarcane yield based on time integral and spatial aggregation of MODIS NDVI. *Remote Sensing*, *5*(5), 2184–2199. https://doi.org/10.3390/rs5052184

Müller, M. F., & Thompson, S. E. (2013). Advances in Water Resources Bias adjustment of satellite rainfall data through stochastic modeling : Methods development and application to Nepal. *Advances in Water Resources*, *60*, 121–134. https://doi.org/10.1016/j.advwatres.2013.08.004

Myhre, G., Shindell, D., Bréon, F.-M., Collins, W., Fuglestvedt, J., Huang, J., & Zhang, H. (2013). Anthropogenic and Natural Radiative Forcing. *Anthropogenic and Natural Radiative Forcing. In: Climate Change 2013: The Physical Science Basis. Contribution of Working Group I to the Fifth Assessment Report of the Intergovernmental Panel on Climate Change. Stocker, T.F., D. Qin, G.-K. Plattner, M.*, (Cambridge University Press, Cambridge, United Kingdom and New York, NY, USA. 659), 659–740. https://doi.org/10.1017/CBO9781107415324.018

Mzezewa, J., Misi, T., & Rensburg, L. D. Van. (2010). Characterisation of rainfall at a semi-arid ecotope in the Limpopo Province (South Africa) and its implications for sustainable crop production. *Http://www.wrc.org.za*, *36*(1), 19–26.

Nastos, P., Kapsomenakis, J., & Philandras, K. M. (2015). Evaluation of the TRMM 3B43 gridded precipitation estimates over Greece. *Atmospheric Research*. https://doi.org/10.1016/j.atmosres.2015.08.008

Negrón Juárez, R. I., Li, W., Fu, R., Fernandes, K., & de Oliveira Cardoso, A. (2009). Comparison of Precipitation Datasets over the Tropical South American and African Continents. *Journal of Hydrometeorology*, *10*(1), 289–299. https://doi.org/10.1175/2008JHM1023.1

NEMA. (2015). Government of Kenya (GoK); Second National Communication to the United Nations Framework Convention on Climate Change (UNFCCC). *Government printers*. Nairobi, Kenya

Ngetich, K. F., Diels, J., Shisanya, C. A., Mugwe, J. N., Mucheru-Muna, M., & Mugendi, D. N. (2014). Effects of selected soil and water conservation techniques on runoff, sediment yield and maize productivity under sub-humid and semi-arid conditions in Kenya. *Catena*, *121*, 288–296. https://doi.org/10.1016/j.catena.2014.05.026

Ngetich, K. F., Mucheru-Muna, M., Mugwe, J. N., Shisanya, C. A., Diels, J., & Mugendi, D. N. (2014). Length of growing season, rainfall temporal distribution, onset and cessation dates in the Kenyan highlands. *Agricultural and Forest Meteorology*, *188*, 24–32. https://doi.org/10.1016/j.agrformet.2013.12.011

Nhemachena, C., & Hassan, R. (2007). Micro-Level Analysis of Farmers ' Adaptation to Climate Change in Southern Africa. *IFPRI Discussion*, *714*, Paper No. 00714. International Food Policy Researc. Retrieved from http://www.ifpri.org/publication/micro-level-analysis-farmers-adaptation-climate-change-southern-africa-0

Njenga, N., Mucheru-Muna, M., & Muriuki, J. (2014). Assessing Perceived Impacts of Climate Change and How Small-Scale Farmers Adapt In North Kinangop Location, Nyandarua County, Kenya ISSN 2319-9725. *International Journal of Innovative Research & Studies*.

Nogueira, S. M. C., Moreira, M. A., & Volpato, M. M. L. (2018). Evaluating Precipitation Estimates from Eta, TRMM and CHRIPS Data in the South-Southeast Region of Minas Gerais State-Brazil. *Remote Sensing*, *10*(2), 313. https://doi.org/10.3390/rs10020313

Nyamadzawo, G., Wuta, M., Nyamangara, J., Smith, J. L., & Rees, R. M. (2014). Nitrous oxide and methane emissions from cultivated seasonal wetland (dambo) soils with inorganic, organic and integrated nutrient management. *Nutrient Cycling in Agroecosystems*, *100*(2), 161–175. https://doi.org/10.1007/s10705-014-9634-9

Nyćkowiak, J., Leśny, J., Olejnik, J., Merbold, L., & Niu, S. (2018). Regional carbon uptake of croplands in Poland between 1960 and 2009. *Meteorology Hydrology and Water Management*, *6*(1), 67–76. https://doi.org/10.26491/mhwm/80505

Ochoa, A., Pineda, L., Crespo, P., & Willems, P. (2014). Evaluation of TRMM 3B42 precipitation estimates and WRF retrospective precipitation simulation over the Pacific-Andean region of Ecuador and Peru. *Hydrology and Earth System Sciences*, *18*(8), 3179–3193. https://doi.org/10.5194/hess-18-3179-2014

Odekunle, T. O. (2006). Determining rainy season onset and retreat over Nigeria from precipitation amount and number of rainy days. *Theoretical and Applied Climatology*, *83*(1–4), 193–201. https://doi.org/10.1007/s00704-005-0166-8

Oertel, C., Matschullat, J., Zurba, K., Zimmermann, F., & Erasmi, S. (2016). Greenhouse gas emissions from soils-A review. *Chemie Der Erde - Geochemistry*, *76*(3), 327–352. https://doi.org/10.1016/j.chemer.2016.04.002

Okeyo, A. I., Mucheru-Muna, M., Mugwe, J., Ngetich, K. F., Mugendi, D. N., Diels, J., & Shisanya, C. A. (2014). Effects of selected soil and water conservation technologies on nutrient losses and maize yields in the central highlands of Kenya. *Agricultural Water Management*, *137*, 52–58.

Olayide, O. E., Tetteh, I. K., & Popoola, L. (2016). Differential impacts of rainfall and irrigation on agricultural production in Nigeria: Any lessons for climate-smart agriculture? *Agricultural Water Management*, *178*, 30–36. https://doi.org/10.1016/j.agwat.2016.08.034

Olijhoek, D. W., Hellwing, A. L. F., Brask, M., Weisbjerg, M. R., Højberg, O., Larsen, M. K., & Lund, P. (2016). Effect of dietary nitrate level on enteric methane production, hydrogen emission, rumen fermentation, and nutrient digestibility in dairy cows. *Journal of Dairy Science*, *99*(8), 6191–6205. https://doi.org/10.3168/jds.2015-10691

Ortiz-Gonzalo, D., Andreas, de N., Philippe, V., Víctor, S.-V., Myles, O., & Rosenstock, T. S. (2018). Multi-scale measurements show limited soil greenhouse emissions in Kenyan smallholder coffee-dairy systems. *Science of the Total Environment*, *626*, 328–339. https://doi.org/10.1016/j.scitotenv.2017.12.247

Ortiz-Gonzalo, D., Vaast, P., Oelofse, M., de Neergaard, A., Albrecht, A., & Rosenstock, T. S. (2017). Farm-scale greenhouse gas balances, hotspots and uncertainties in smallholder crop-livestock systems in Central Kenya. *Agriculture, Ecosystems and Environment*, *248*, 58–70. https://doi.org/10.1016/j.agee.2017.06.002

Osman-Elasha, B. (2007). Africa's vulnerability to environmental stress and climate change. *Tiempo*, *63*, 3–9.

Otolo, J. R. A., & Wakhungu, J. (2013). Factors Influencing Livelihood Zonation in Kenya. *International Journal of Education and Research*, *1*(12), 1–10.

Ouatiki, H., Boudhar, A., Tramblay, Y., Jarlan, L., Benabdelouhab, T., Hanich, L., & Chehbouni, A. (2017). Evaluation of TRMM 3B42 V7 Rainfall Product over the Oum Er Rbia Watershed in Morocco. *Climate*, *5*(1), 1. https://doi.org/10.3390/cli5010001

Oyoshi, K., Sobue, S., & Takeuchi, W. (2013). Development of complicated rice crop calendar in Southeast Asia with time-series MODIS data. *2013 2nd International Conference on Agro-Geoinformatics: Information for Sustainable Agriculture, Agro-Geoinformatics 2013*, (February), 444–447. https://doi.org/10.1109/Argo-Geoinformatics.2013.6621960

Paredes-Trejo, F. J., Barbosa, H. A., Peñaloza-Murillo, M. A., Alejandra Moreno, M., & Farías, A. (2016). Intercomparison of improved satellite rainfall estimation with CHIRPS gridded product and rain gauge data over Venezuela. *Atmosfera*, *29*(4), 323–342. https://doi.org/10.20937/ATM.2016.29.04.04

Paredes, P., de Melo-Abreu, J. P., Alves, I., & Pereira, L. S. (2014). Assessing the performance of the FAO AquaCrop model to estimate maize yields and water use under full and deficit irrigation with focus on model parameterization. *Agricultural Water Management*, *144*, 81–97. https://doi.org/10.1016/j.agwat.2014.06.002

Parkin, T. B., Venterea, R. T., & Hargreaves, S. K. (2012). Calculating the detection limits of chamber- based soil greenhouse gas flux measurements. Journal of environmental quality, 41, 705–715.

Pelster, D., Chantigny, M. H., Rochette, P., Angers, D. A., Rieux, C., & Vanasse, A. (2012). Nitrous Oxide Emissions Respond Differently to Mineral and Organic Nitrogen Sources in Contrasting Soil Types. *Journal of Environment Quality*, *41*(2), 427. https://doi.org/10.2134/jeq2011.0261

Pelster, D. E., Larouche, F., Rochette, P., Chantigny, M. H., Allaire, S., & Angers, D. A. (2011). Nitrogen fertilization but not soil tillage affects nitrous oxide emissions from a clay loam soil under a maize-soybean rotation. *Soil and Tillage Research*, *115–116*, 16–26. https://doi.org/10.1016/j.still.2011.06.001

Pelster, D., Rufino, M., Rosenstock, T., Mango, J., Saiz, G., Diaz-Pines, E., & Butterbach-Bahl, K. (2017). Smallholder farms in eastern African tropical highlands have low soil greenhouse gas fluxes. *Biogeosciences*, *14*(1), 187–202. https://doi.org/10.5194/bg-14-187-2017

Place, F., Barrett, C. B., Freeman, H. A., Ramisch, J. J., & Vanlauwe, B. (2003). Prospects for integrated soil fertility management using organic and inorganic inputs: Evidence from smallholder African agricultural systems. *Food Policy*, *28*(4), 365–378. https://doi.org/10.1016/j.foodpol.2003.08.009

Prakash, S., Mitra, A. K., Pai, D. S., & AghaKouchak, A. (2016). From TRMM to GPM: How well can heavy rainfall be detected from space? *Advances in Water Resources*, *88*, 1–7. https://doi.org/10.1016/j.advwatres.2015.11.008

Predotova, M., Gebauer, J., Diogo, R. V. C., Schlecht, E., & Buerkert, A. (2010). Emissions of ammonia, nitrous oxide and carbon dioxide from urban gardens in Niamey, Niger. *Field Crops Research*, *115*(1), 1–8. https://doi.org/10.1016/j.fcr.2009.09.010

Quirino, D. T., Casaroli, D., Jucá Oliveira, R. A., Mesquita, M., Pego Evangelista, A. W., & Alves Júnior, J. (2017). Evaluation of TRMM satellite rainfall estimates (algorithms 3B42 V7 & RT) over the Santo Antônio county (Goiás, Brazil). *Revista Facultad Nacional de Agronomía*, *70*(3), 8251–8261. https://doi.org/10.15446/rfna.v70n3.61805

Raut, N., Sitaula, B. K., Bakken, L. R., Bajracharya, R. M., & Dörsch, P. (2015). Higher N2O emission by intensified crop production in South Asia. *Global Ecology and Conservation*, *4*, 176–184. https://doi.org/10.1016/j.gecco.2015.06.004

Rawls, W. J., Pachepsky, Y. A., Ritchie, J. C., Sobecki, T. M., & Bloodworth, H. (2003). Effect of soil organic carbon on soil water retention. *Geoderma*, *116*(1–2), 61–76. https://doi.org/10.1016/S0016-7061(03)00094-6

Recha, C. W., Makokha, G. L., Traore, P. S., Shisanya, C., Lodoun, T., & Sako, A. (2012). Determination of seasonal rainfall variability, onset and cessation in semi-arid Tharaka district, Kenya. *Theoretical and Applied Climatology*, *108*(3–4), 479–494. https://doi.org/10.1007/s00704-011-0544-3

Reidsma, P., Ewert, F., Lansink, A. O., & Leemans, R. (2010). Adaptation to climate change and climate variability in European agriculture: The importance of farm level responses. *European Journal of Agronomy*, *32*(1), 91–102. https://doi.org/10.1016/j.eja.2009.06.003

Rezaei, E., Webber, H., Gaiser, T., Naab, J., & Ewert, F. (2015). Heat stress in cereals: Mechanisms and modelling. *European Journal of Agronomy*, *64*, 98–113. https://doi.org/10.1016/j.eja.2014.10.003

Richards, M., Metzel, R., Chirinda, N., Ly, P., Nyamadzawo, G., Duong Vu, Q., & Rosenstock, T. S. (2016). Limits of agricultural greenhouse gas calculators to predict soil N_2O and CH_4 fluxes in tropical agriculture. *Scientific Reports*, *6*(April), 1–8. https://doi.org/10.1038/srep26279

Rienecker, M.M., Suarez, M.J., Gelaro, R., Todling, R., Bacmeister, J., Liu, E., Bosilovich, M.G., Schubert, S.D., Takacs, L., Kim, G.K., Bloom, S., Chen, J., Collins, D., Conaty, A., Da Silva, A., Gu, W., Joiner, J., Koster, R.D., Lucchesi, R., Molod, A., Owens, T., Pawson, S., Pegion, P., Redder, C.R., Reichle, R., Robertson, F.R., Ruddick, A.G., Sienkiewicz, M., Woollen, J., (2011). MERRA: NASA's modern-era retrospective analysis for research and applications. J. Clim. 24, 3624–3648. https://doi.org/10.1175/JCLI-D-11-00015.1

Rientjes, T., Haile, A. T., & Fenta, A. A. (2012). Diurnal rainfall variability over the Upper Blue Nile Basin: A remote sensing based approach. *International Journal of Applied Earth Observation and Geoinformation*, *21*(1), 311–325. https://doi.org/10.1016/j.jag.2012.07.009

Robbins, J. C. (2016). A probabilistic approach for assessing landslide-triggering event rainfall in Papua New Guinea, using TRMM satellite precipitation estimates. *Journal of Hydrology*, *541*, 296–309. https://doi.org/10.1016/j.jhydrol.2016.06.052

Rochette, P., Liang, C., Pelster, D., Bergeron, O., Lemke, R., Kroebel, R., & Flemming, C. (2018). Soil nitrous oxide emissions from agricultural soils in Canada: Exploring relationships with soil, crop and climatic variables. *Agriculture, Ecosystems and Environment*, *254*, 69–81. https://doi.org/10.1016/j.agee.2017.10.021

Rockström, J., Karlberg, L., Wani, S. P., Barron, J., Hatibu, N., Oweis, T., & Qiang, Z. (2010). Managing water in rainfed agriculture: The need for a paradigm shift. *Agricultural Water Management*, *97*(4), 543–550. https://doi.org/10.1016/j.agwat.2009.09.009

Rojas-Downing, M., Nejadhashemi, A. P., Harrigan, T., & Woznicki, S. A. (2017). Climate change and livestock: Impacts, adaptation, and mitigation. *Climate Risk Management*, *16*, 145–163. https://doi.org/10.1016/j.crm.2017.02.001

Rosenstock, T., Mpanda, M., Pelster, D. E., Butterbach-Bahl, K., Rufino, M. C., Thiong'o, M., & Neufeldt, H. (2016). Greenhouse gas fluxes from agricultural soils of Kenya and Tanzania. *Journal of Geophysical Research: Biogeosciences*, *121*(6), 1568–1580. https://doi.org/10.1002/2016JG003341

Rossi, M., Kirschbaum, D., Valigi, D., Mondini, A., & Guzzetti, F. (2017). Comparison of Satellite Rainfall Estimates and Rain Gauge Measurements in Italy, and Impact on Landslide Modeling. *Climate*, *5*(4), 90. https://doi.org/10.3390/cli5040090

Rötter, R. P., Palosuo, T., Pirttioja, N. K., Dubrovsky, M., Salo, T., Fronzek, S., & Carter, T. R. (2011). What would happen to barley production in Finland if global warming exceeded 4°C? A model-based assessment. *European Journal of Agronomy*, *35*(4), 205–214. https://doi.org/10.1016/j.eja.2011.06.003

Rui, J., Tong-tong, W., Jin, S., Sheng, G. U. O., Wei, Z. H. U., Ya-jun, Y. U., & Shao-lin, C. (2017). Modeling the biomass of energy crops : Descriptions, strengths and prospective. *Journal of Integrative Agriculture*, *16*(6), 1197–1210. https://doi.org/10.1016/S2095-3119(16)61592-7

Salio, P., Hobouchian, M. P., García Skabar, Y., & Vila, D. (2015). Evaluation of high-resolution satellite precipitation estimates over southern South America using a dense rain gauge network. *Atmospheric Research*, *163*, 146–161. https://doi.org/10.1016/J.ATMOSRES.2014.11.017

Sansoulet, J., Pattey, E., Kröbel, R., Grant, B., Smith, W., Jégo, G., & Tremblay, G. (2014). Comparing the performance of the STICS, DNDC, and DayCent models for predicting N uptake and biomass of spring wheat in Eastern Canada. *Field Crops Research*, *156*, 135–150. https://doi.org/10.1016/j.fcr.2013.11.010

Sari, D. K., Ismullah, I. H., Sulasdi, W. N., & Harto, A. B. (2013). Estimation of Water Consumption of Lowland Rice in Tropical Area based on Heterogeneous Cropping Calendar Using Remote Sensing Technology. *Procedia Environmental Sciences*, *17*, 298–307. https://doi.org/10.1016/j.proenv.2013.02.042

Satgé, F., Bonnet, M., Gosset, M., Molina, J., Hernan, W., Lima, Y., & Garnier, J. (2016). Assessment of satellite rainfall products over the Andean plateau. *Atmospheric Research*, *167*, 1–14. https://doi.org/10.1016/j.atmosres.2015.07.012

Schneider, U., Becker, A., Finger, P., Meyer-christoffer, A., Ziese, M., & Rudolf, B. (2014). GPCC a new land surface precipitation climatology based on quality-controlled in situ data and its role in quantifying the global water cycle. *Theor Appl Climatol*, *115*, 15–40. https://doi.org/10.1007/s00704-013-0860-x

Schroeder, C., K'Oloo, O., Ranabhat, N., Jick, N., Parzies, H., & Gemenet, D. (2013). Potentials of Hybrid Maize Varieties for Small-Holder Farmers in Kenya: A Review Based on Swot Analysis. *African Journal of Food, Agriculture, Nutrition and Development*, *13*(2), 7357–7371.

Serrano-Silva, N., Sarria-Guzmán, Y., Dendooven, L., & Luna-Guido, M. (2014). Methanogenesis and Methanotrophy in Soil: A Review. *Pedosphere*, *24*(3), 291–307. https://doi.org/10.1016/S1002-0160(14)60016-3

Shaojuna, B., Long, L., & Xunc, M. (2011). A study on the net greenhouse gas emissions under intensive high-yielding cropland in North China-a case study of winter wheat-summer maize rotation system in Huantai County. *Energy Procedia*, *5*, 785–792. https://doi.org/10.1016/j.egypro.2011.03.138

Shapiro, A. S. S., & Wilk, M. B. (1965). Biometrika Trust An Analysis of Variance Test for Normality (Complete Samples) Published by: Oxford University Press on behalf of Biometrika Trust Stable URL: http://www.jstor.org/stable/2333709. *Biometrika*, *52*(3), 591–611.

Sharma, S., & Singh, P. (2017). Long Term Spatio-temporal Variability in Rainfall Trends over the State of Jharkhand, India. *Climate*, *5*(1), 18. https://doi.org/10.3390/cli5010018

Shiferaw, B., Tesfaye, K., Kassie, M., Abate, T., Prasanna, B. M., & Menkir, A. (2014). Managing vulnerability to drought and enhancing livelihood resilience in sub-Saharan Africa: Technological, institutional and policy options. *Weather and Climate Extremes*, *3*, 67–79. https://doi.org/10.1016/j.wace.2014.04.004

Shimizu, M., Hatano, R., Arita, T., Kouda, Y., Mori, A., Matsuura, S., & Miyata, A. (2013). The effect of fertilizer and manure application on CH_4 and N_2O emissions from managed grasslands in Japan. *Soil Science and Plant Nutrition*, *59*(1), 69–86. https://doi.org/10.1080/00380768.2012.733926

Shrestha, N. K., Qamer, F. M., Pedreros, D., Murthy, M. S. R., Wahid, S. M., & Shrestha, M. (2017). Evaluating the accuracy of Climate Hazard Group (CHG) satellite rainfall estimates for precipitation based drought monitoring in Koshi basin, Nepal. *Journal of Hydrology: Regional Studies*, *13*(February), 138–151. https://doi.org/10.1016/j.ejrh.2017.08.004

Shrivastava, R., Dash, S. K., Hegde, M. N., Pradeepkumar, K. S., & Sharma, D. N. (2014). Validation of the TRMM Multi Satellite Rainfall Product 3B42 and estimation of scavenging coefficients for 131 I and 137 Cs using TRMM 3B42 rainfall data. *Journal of Environmental Radioactivity*, *138*, 132–136. https://doi.org/10.1016/j.jenvrad.2014.08.011

Shukla, S., McNally, A., Husak, G., & Funk, C. (2014). A seasonal agricultural drought forecast system for food-insecure regions of East Africa. *Hydrology and Earth System Sciences*, *18*(10), 3907–3921. https://doi.org/10.5194/hess-18-3907-2014

Simba, F. M., Mubvuma, M., Murwendo, T., & Chikodzi, D. (2013). Prediction of yield and biomass productions: A remedy to climate change in semi-arid regions of Zimbabwe. *Ijaar*, *1*, 14–21.

Sivakumar, M. V. K. (1990). Exploiting rainy season potential from the onset of rains in the Sahelian zone of West Africa. *Agricultural and Forest Meteorology*, *51*, 321–332.

Smith, P., Bustamante, M., Ahammad, H., Clark, H., Dong, H., Elsiddi, E. A., & Tubiello, F. (2014). Agriculture, forestry and other land use. *Climate Change 2014: Mitigation of Climate Change*, 811–922. https://doi.org/10.1104/pp.900074

Smith, W. N., Grant, B. B., Desjardins, R. L., Rochette, P., Drury, C. F., & Li, C. (2008). Evaluation of two process-based models to estimate soil N_2O emissions in Eastern Canada. *Canadian Journal of Soil Science*, *88*(2), 251–260. https://doi.org/10.4141/CJSS06030

Sommer, R., Paul, B. K., Mukalama, J., & Kihara, J. (2017). Reducing losses but failing to sequester carbon in soils – the case of Conservation Agriculture and Integrated Soil Fertility Management in the humid tropical agro-ecosystem of Western Kenya. *Agriculture, Ecosystems and Environment*, *254*, 82–91. https://doi.org/10.1016/j.agee.2017.11.004

Sosulski, T., Szara, E., Stepien, W., & Szymanska, M. (2014). Nitrous oxide emissions from the soil under different fertilization systems on a long-term experiment. *Plant, Soil and Environment*, *60*(11), 481–488.

Stoof, C. R., Ferreira, A. J. D., Mol, W., Van den Berg, J., De Kort, A., Drooger, S., & Ritsema, C. J. (2015). Soil surface changes increase runoff and erosion risk after a low-moderate severity fire. *Geoderma*, *239*, 58–67. https://doi.org/10.1016/j.geoderma.2014.09.020

Subke, J. A., Moody, C. S., Hill, T. C., Voke, N., Toet, S., Ineson, P., & Teh, Y. A. (2018). Rhizosphere activity and atmospheric methane concentrations drive variations of methane fluxes in a temperate forest soil. *Soil Biology and Biochemistry*, *116*, 323–332. https://doi.org/10.1016/j.soilbio.2017.10.037

Sun, Q., Miao, C., Duan, Q., Ashouri, H., Sorooshian, S., & Hsu, K.-L. (2017). A review of global precipitation datasets: data sources, estimation, and intercomparisons. *Reviews of Geophysics*, 1–29. https://doi.org/10.1002/2017RG000574

Sungmin, O., Foelsche, U., Kirchengast, G., & Fuchsberger, J. (2016). Validation and correction of rainfall data from the WegenerNet high density network in southeast Austria. *Journal of Hydrology*. https://doi.org/10.1016/j.jhydrol.2016.11.049

Sunilkumar, K., Rao, T. N., Saikranthi, K., & Rao, M. P. (2015). Journal of Geophysical Research : Atmospheres. *Journal of Geophysical Research: Atmospheres*, *120*, 8987–9005. https://doi.org/10.1002/2015JD023437.Received

Tan, M. L., Ibrahim, A. L., Duan, Z., Cracknell, A. P., & Chaplot, V. (2015). Evaluation of six high-resolution satellite and ground-based precipitation products over Malaysia. *Remote Sensing*, *7*(2), 1504–1528. https://doi.org/10.3390/rs70201504

Taxak, A. K., Murumkar, A. R., & Arya, D. S. (2014). Long term spatial and temporal rainfall trends and homogeneity analysis in Wainganga basin, Central India. *Weather and Climate Extremes*, *4*, 50–61. https://doi.org/10.1016/j.wace.2014.04.005

Teixeira, E., Fischer, G., van Velthuizen, H., van Dingenen, R., Dentener, F., Mills, G., & Ewert, F. (2011). Limited potential of crop management for mitigating surface ozone impacts on global food supply. *Atmospheric Environment*, *45*(15), 2569–2576. https://doi.org/10.1016/j.atmosenv.2011.02.002

Tesfaye, G., Tadesse, T., Gessesse, B., & Dinku, T. (2017). Validation of new satellite rainfall products over the Upper Blue Nile Basin, Ethiopia. *Atmospheric Measurement Techniques Discussions*, *294*, 1–24. https://doi.org/10.5194/amt-2017-294

Tesfaye, K., Kruseman, G., Cairns, J. E., Zaman-Allah, M., Wegary, D., Zaidi, P. H., & Erenstein, O. (2017). Potential benefits of drought and heat tolerance for adapting maize to climate change in tropical environments. *Climate Risk Management*, 1–14. https://doi.org/10.1016/j.crm.2017.10.001

Tippett, M. K., Almazroui, M., & Kang, I.-S. (2015). Extended-Range Forecasts of Areal-Averaged Rainfall over Saudi Arabia. *Weather and Forecasting*, *30*(4), 1090–1105. https://doi.org/10.1175/WAF-D-15-0011.1

Toté, C., Patricio, D., Boogaard, H., Raymond, van der W., Elena, T., & Chris, F. (2015). Evaluation of Satellite Rainfall Estimates for Drought and Flood Monitoring in Mozambique. *Remote Sensing*, *7*, 1758–1776. https://doi.org/10.3390/rs70201758

Tuo, Y., Duan, Z., Disse, M., & Chiogna, G. (2016). Evaluation of precipitation input for SWAT modeling in Alpine catchment: A case study in the Adige river basin (Italy). *Science of The Total Environment*, *573*, 66–82. https://doi.org/10.1016/j.scitotenv.2016.08.034

Umair, M., Shen, Y., Qi, Y., Zhang, Y., Ahmad, A., Pei, H., & Liu, M. (2017). Evaluation of the CropSyst Model during Wheat-Maize Rotations on the North China Plain for Identifying Soil Evaporation Losses. *Frontiers in Plant Science*, *8*(September). https://doi.org/10.3389/fpls.2017.01667

Uzoma, K. C., Smith, W., Grant, B., Desjardins, R. L., Gao, X., Hanis, K., & Li, C. (2015). Assessing the effects of agricultural management on nitrous oxide emissions using flux measurements and the DNDC model. *Agriculture, Ecosystems and Environment*, *206*, 71–83. https://doi.org/10.1016/j.agee.2015.03.014

Valentini, R., Arneth, A., Bombelli, A., Castaldi, S., Cazzolla Gatti, R., Chevallier, F., & Scholes, R. J. (2014). A full greenhouse gases budget of Africa: Synthesis, uncertainties, and vulnerabilities. *Biogeosciences*, *11*(2), 381–407. https://doi.org/10.5194/bg-11-381-2014

Van Groenigen, J. W., Velthof, G. L., Oenema, O., Van Groenigen, K. J., & Van Kessel, C. (2010). Towards an agronomic assessment of N_2O emissions: A case study for arable crops. *European Journal of Soil Science*, *61*(6), 903–913. https://doi.org/10.1111/j.1365-2389.2009.01217.x

Vanlauwe, B., Descheemaeker, K., Giller, K. E., Huising, J., Merckx, R., Nziguheba, G., & Zingore, S. (2014). Integrated soil fertility management in sub-Saharan Africa: unravelling local adaptation. *SOIL Discussions*, *1*(1), 1239–1286. https://doi.org/10.5194/soild-1-1239-2014

Venhari, A., Tenpierik, M., & Mahdizadeh Hakak, A. (2017). Heat mitigation by greening the cities, a review study. *Environment, Earth and Ecology*, *1*(1), 5–32. https://doi.org/10.24051/eee/67281

Vetter, S. H., Sapkota, T. B., Hillier, J., Stirling, C. M., Macdiarmid, J. I., Aleksandrowicz, L., & Smith, P. (2017). Greenhouse gas emissions from agricultural food production to supply Indian diets: Implications for climate change mitigation. *Agriculture, Ecosystems & Environment*, *237*, 234–241. https://doi.org/10.1016/j.agee.2016.12.024

Wan, G., Yang, M., Liu, Z., Wang, X., & Liang, X. (2017). The precipitation variations in the Qinghai-Xizang (Tibetan) Plateau during 1961-2015. *Atmosphere*, *8*(5). https://doi.org/10.3390/atmos8050080

Wanapat, M., Cherdthong, A., Phesatcha, K., & Kang, S. (2015). Dietary sources and their effects on animal production and environmental sustainability. *Animal Nutrition*, *1*(3), 96–103. https://doi.org/10.1016/j.aninu.2015.07.004

Wang, Y., Sun, G. J., Zhang, F., Qi, J., & Zhao, C. Y. (2011). Modeling impacts of farming management practices on greenhouse gas emissions in the oasis region of China. *Biogeosciences*, *8*(8), 2377–2390. https://doi.org/10.5194/bg-8-2377-2011

Waongo, M., Laux, P., & Kunstmann, H. (2015). Adaptation to climate change: The impacts of optimized planting dates on attainable maize yields under rainfed conditions in Burkina Faso. *Agricultural and Forest Meteorology*, *205*, 23–39. https://doi.org/10.1016/j.agrformet.2015.02.006

Wassmann, R., Jagadish, S. V. K., Sumfleth, K., Pathak, H., Howell, G., Ismail, A., & Heuer, S. (2009). *Chapter 3 Regional Vulnerability of Climate Change Impacts on Asian Rice Production and Scope for Adaptation*. *Advances in Agronomy* (1st ed., Vol. 102). Elsevier Inc. https://doi.org/10.1016/S0065-2113(09)01003-7

White, J. W., Hoogenboom, G., Stackhouse, P. W., & Hoell, J. M. (2008). Evaluation of NASA satellite- and assimilation model-derived long-term daily temperature data over the continental US, *148*, 1574–1584. https://doi.org/10.1016/j.agrformet.2008.05.017

Yang, W., Richard, S., Mark A., C., & Lyon, B. (2015). The Annual Cycle of East African Precipitation. *American Meteorological Society*, *5*, 2385–2404. https://doi.org/10.1175/JCLI-D-14-00484.1

Yang, W., Seager, R., Cane, M. A., & Lyon, B. (2014). The East African Long Rains in Observations and Models Wenchang Yang Bradfield Lyon. *International Research Institute for Climate and Society*, *Lamont-Doh*, 1–42. https://doi.org/10.1175/JCLI-D-13-00447.1

Yegbemey, R. N., Kabir, H., Awoye, O. H. R., Yabi, J. A., & Paraïso, A. A. (2014). Managing the agricultural calendar as coping mechanism to climate variability: A case study of maize farming in northern Benin, West Africa. *Climate Risk Management*, *3*, 13–23. https://doi.org/10.1016/j.crm.2014.04.001

Yegbemey, R. N., Yabi, J. A., Tovignan, S. D., Gantoli, G., & Haroll Kokoye, S. E. (2013). Farmers' decisions to adapt to climate change under various property rights: A case study of maize farming in northern Benin (West Africa). *Land Use Policy*, *34*, 168–175. https://doi.org/10.1016/j.landusepol.2013.03.001

Yong, B., Liu, D., Gourley, J. J., Tian, Y., Huffman, G. J., Ren, L., & Hong, Y. (2015). Global view of real-time TRMM multisatellite precipitation analysis: Implications for its successor global precipitation measurement mission. *Bulletin of the American Meteorological Society*, *96*(2), 283–296. https://doi.org/10.1175/BAMS-D-14-00017.1

Yu, C., Li, C., Xin, Q., Chen, H., Zhang, J., Zhang, F., & Gong, P. (2014). Dynamic assessment of the impact of drought on agricultural yield and scale-dependent return periods over large geographic regions. *Environmental Modelling and Software*, *62*, 454–464. https://doi.org/10.1016/j.envsoft.2014.08.004

Zambrano, F., Wardlow, B., Tadesse, T., Lillo-Saavedra, M., & Lagos, O. (2017). Evaluating satellite-derived long-term historical precipitation datasets for drought monitoring in Chile. *Atmospheric Research*, *186*, 26–42. https://doi.org/10.1016/j.atmosres.2016.11.006

Zhang, F., Zhang, W., Qi, J., & Li, F. M. (2018). A regional evaluation of plastic film mulching for improving crop yields on the Loess Plateau of China. *Agricultural and Forest Meteorology*, *248*, 458–468. https://doi.org/10.1016/j.agrformet.2017.10.030

Zhang, Y., Li, C., Zhou, X., & Moore III, B. (2002). A simulation model linking crop growth and soil biogeochemistry for sustainable agriculture. *Ecological Modelling*, *151*, 75–108. https://doi.org/10.1016/s0304-3800(01)00527-0

Zhang, Y., Wang, H., Liu, S., Lei, Q., Liu, J., He, J., & Liu, H. (2015). Identifying critical nitrogen application rate for maize yield and nitrate leaching in a Haplic Luvisol soil using the DNDC model. *Science of the Total Environment*, *514*, 388–398. https://doi.org/10.1016/j.scitotenv.2015.02.022

Zhao, H., Yang, S., You, S., Huang, Y., Wang, Q., & Zhou, Q. (2018). Comprehensive evaluation of two successive V3 and V4 IMERG final run precipitation products over Mainland China. *Remote Sensing*, *10*(1), 1–23. https://doi.org/10.3390/rs10010034

Zhou, Z., Zheng, X., Baohua, X., Han, S., & Liu, C. (2010). A Process-based Model of N_2O Emission from a Rice-Winter Wheat Rotation Agro-Ecosystem : *ADVANCES IN ATMOSPHERIC SCIENCES*, *27*(1), 137–150. https://doi.org/10.1007/s00376-009-8191-7.1.Introduction

Zona, D., Janssens, I. A., Aubinet, M., Gioli, B., Vicca, S., Fichot, R., & Ceulemans, R. (2013). Fluxes of the greenhouse gases (CO_2, CH_4 and N_2O) above a short-rotation poplar plantation after conversion from agricultural land. *Agricultural and Forest Meteorology*, *169*, 100–110. https://doi.org/10.1016/j.agrformet.2012.10.008

Zulkafli, Z., Buytaert, W., Onof, C., Manz, B., Tarnavsky, E., Lavado, W., & Guyot, J.-L. (2014). A Comparative Performance Analysis of TRMM 3B42 (TMPA) Versions 6 and 7 for Hydrological Applications over Andean–Amazon River Basins. *Journal of Hydrometeorology*, *15*(2), 581–592. https://doi.org/10.1175/JHM-D-13-094.1

Annex 1: List of weather station in Kenya used in the study

S/No	County	Station	Latitude	Longitude	Elevation (m)
1.	Turkana	Lodwar	35.6	3.1	505
2.	Kericho	Kericho	35.3	-0.4	1976
3.	Machakos	Machakos	37.2	-1.6	1600
4.	Kisumu	Kisumu	34.8	-0.1	1149
5.	Kisii	Kisii	34.8	-0.7	1771
6.	Taita-Taveta	Voi	38.6	-3.4	558
7.	Makueni	Makindu	37.8	-2.3	1000
8.	Marsabit	Marsabit	38	2.3	1345
9.	Narok	Narok	35.9	-1.1	1585
10.	Kakamega	Kakamega	34.8	0.3	1582
11.	Kiambu	Thika	37.1	-1	1463
12.	Kilifi	Mtwapa	39.7	-3.9	21
13.	Mombasa	Mombasa	39.6	-4	5
14.	Embu	Embu	37.5	-0.5	1494
15.	Nyeri	Nyeri	37	-0.4	1798
16.	Kiambu	Dagoretti	36.8	-1.3	1798
17.	Meru	Meru	37.7	0.1	1524
18.	Trans-Nzoia	Kitale	35	1	1840
19.	Nakuru	Nakuru	36.1	-0.3	1836
20.	Laikipia	Nyahururu	36.4	0	2392
21.	Wajir	Wajir	40.1	1.8	244
22.	Marsabit	Moyale	39.1	3.5	1110
23.	Kilifi	Malindi	40	-3.2	20
24.	Uasin Gichu	Eldoret	35.3	0.5	2079
25.	Mandera	Mandera	41.87	3.9	330
26.	Garissa	Garissa	39.6	-0.5	128
27.	Lamu	Lamu	40.9	-2.3	6
28.	Mombasa	Msabaha	39.4	-4.3	91
29.	Nairobi	Wilson	36.8	-1.3	1679
30.	Nairobi	JKIA	36.92	-1.32	1624
31.	Laikipia	Nanyuki	37.03	0.05	1890
32.	Nakuru	Naivasha	36.38	-0.7	1899